Democratic and Popular Republic of Algeria
Ministry of Higher Education and Scientific Research
University Mohamed Khider of Biskra

Faculty of Exact Sciences and Science of Nature and Life
Department of Matter Sciences

Ref : ……..

Thesis Presented to obtain the degree of

Doctorate in Chemistry

Option: Materials Chemistry

Entitled:

Elaboration and characterization of PZT-type ceramics

Presented by:

Ben Makhlouf Aymen

Publicly defended on: 15/10/2023

In front of the Jury committee composed of:

Mr. DJANI Fayçal	Professor	University of Biskra	President
Mr. MAKHLOUFI Rachid	MCA	University of Biskra	Supervisor
Mr. BEN MYA Omar	Professor	University of Oued Souf	Examiner
Mr. CHADLI Abdelhakim	MCA	University of Biskra	Examiner

Democratic and Popular Republic of Algeria
Ministry of Higher Education and Scientific Research
University Mohamed Khider of Biskra

Faculty of Exact Sciences and Science of Nature and Life
Department of Matter Sciences

Ref : ……..

Thesis Presented to obtain the degree of

Doctorate in Chemistry

Option: Materials Chemistry

Entitled:

Elaboration and characterization of PZT-type ceramics

Presented by:

Ben Makhlouf Aymen

Publicly defended on: 15/10/2023

In front of the Jury committee composed of:

Mr. DJANI Fayçal	Professor	University of Biskra	President
Mr. MAKHLOUFI Rachid	MCA	University of Biskra	Supervisor
Mr. BEN MYA Omar	Professor	University of Oued Souf	Examiner
Mr. CHADLI Abdelhakim	MCA	University of Biskra	Examiner

Dedication

I dedicate this modest work to:

To my dear parents,

Your unwavering love, support, and encouragement have been the foundation of my 5 years in Biskra. Your sacrifices and belief in me have shaped my dreams and propelled me forward. This thesis is a testament to your endless dedication and the values you instilled in me. Thank you for being my guiding light.

To my beloved brother Oussama, his wife, and my adorable nephews Sadjed and Baraa, Your constant presence and unwavering faith in me have inspired me. Your love and encouragement have pushed me to strive for excellence. I am grateful for your support throughout this journey.

To my brothers Islam and Mohammed

Your unwavering support and belief in my abilities have been invaluable. Your presence in my life has made a significant impact, motivating me to push boundaries and strive for excellence. Thank you for always being there for me.

To my beloved sister Douaa.

Your love, kindness, and unwavering belief in me have been a driving force. Your encouragement and words of wisdom have filled my path with light. Thank you for being my source of inspiration.

To my dearest cousin Ilyes

Words cannot express the depth of gratitude and admiration I have for you. Your unwavering support, encouragement, and belief in me have been a constant source of inspiration throughout my journey. You have been more than a cousin; you have been a true friend and a guiding light.

I dedicate this thesis to all of you, my beloved family. Your love, support, and presence have been the pillars of my success. I am forever grateful for your unwavering belief in me.

Acknowledgements

أولاً وقبل كل شيء، أود أن أحمد لله وأشكره على توفيقي ومنحني القوة والإرادة والمثابرة طوال مساري البحثي.

I would like to express my sincere gratitude to my current supervisor and thesis director, Dr. Rachid Makhloufi. His constant support, availability and encouragement over the last 5 years have been essential to the success of my research. I am very lucky to have had the opportunity to work under their supervision.

I would like also to remember and honor my former supervisor Pr. Ahmed Boutarfia, who unfortunately is no longer with us (may God rest his soul in heaven). His guidance, direction, and experiences have shaped me as a researcher, and I am forever grateful for their contributions to my academic development.

I would like to thank the members of the jury who devoted their time and expertise to evaluating my doctoral research, each by name: the president Pr. DJANI Fayçal from Biskra University, the examinators Pr. BEN MYA Omar from Oued Souf University and Dr. CHADLI Abdelhakim from Biskra University, their constructive comments and valuable suggestions undoubtedly improved the quality of my research.

I would like to thank my lab director, Pr. Ahmed Meghazzi, and express my gratitude for his guidance, assistance, and resources that he provided me throughout my research journey. His experience and commitment to the lab was a critical factor in facilitating my work.

Special mention to my dear friends Fawzi Hadji and Hamza Chlelli, whose unwavering support and assistance have been instrumental in overcoming challenges and achieving success. Their friendship and cooperation made this research journey much more rewarding, and I am truly grateful for their presence. I would also like to express my gratitude to my colleague Bahia Messai for her collaboration and insightful discussions. Her friendship has contributed to making the laboratory a conducive and pleasant environment.

I would like to acknowledge the support and resources provided by Dr. Mourad Nouiri and their laboratory. The use of their facilities and the characteristics conducted in their laboratory have been instrumental in the successful execution of my experiments. Lastly, I would like to

express my gratitude to Pr. Mohamed Toufik Soltani, the head of the Research Laboratory of Photonics and Multifunctional Nanomaterials at the University of Biskra.

To each individual mentioned above, I extend my heartfelt thanks for their contributions, support, and dedication throughout my research journey. Their presence has been instrumental in shaping my academic and personal growth, and I am truly grateful for their unwavering support.

Abstract

In this study, PZT type ceramics with a general formula $Pb_{1-x}Ba_x(Zr_{0.52}Ti_{0.43}(Al_{0.5}Sb_{0.5})_{0.05})O_3$ where (x = 0.00, 0.02, 0.04, 0.06, 0.08, and 0.10) were elaborated by the solid-state reaction method. The main objectives of this study focus on the evolution of structural and electrical properties in the region of the Morphotropic Phase Boundary MPB, the effect of barium substitution, the temperature, and the frequency on electrical properties are also investigated. Different techniques were used to characterize the obtained samples such as X-ray diffraction XRD which shows that the results confirm the high purity of prepared samples without any secondary phase and also indicate the coexistence of both the tetragonal and rhombohedral phases. All the absorption bands corresponding to the perovskite structure are exhibited by The Fourier Transform Infrared spectroscopy FTIR. The Curie temperature TC decreased with increasing Ba^{2+} content. Furthermore, the effect of the temperature, frequency, and composition on the AC conductivity and dielectric properties demonstrated interesting values

Keywords: PZT, Curie temperature, Structural, Morphotropic phase boundary, Dielectric properties, AC conductivity.

Résumé

Dans cette étude, des céramiques de type PZT de formule générale $Pb_{1-x}Ba_x(Zr_{0.52}Ti_{0.43}(Al_{0.5}Sb_{0.5})_{0.05})O_3$ où (x = 0.00, 0.02, 0.04, 0.06, 0.08, et 0.10) ont été élaborées par la méthode de réaction à l'état solide. Les principaux objectifs de cette étude se concentrent sur l'évolution des propriétés structurelles et électriques dans la région de la frontière morphotropique de phase FMP, l'effet de la substitution du baryum, la température et la fréquence sur les propriétés électriques sont également étudiés. Différentes techniques ont été utilisées pour caractériser les échantillons obtenus, telles que la diffraction des rayons X XRD, dont les résultats confirment la grande pureté des échantillons préparés, sans phase secondaire, et indiquent également la coexistence des phases tétragonale et rhomboédrique. Toutes les bandes d'absorption correspondant à la structure de la pérovskite sont mises en évidence par la spectroscopie infrarouge à transformée de Fourier FTIR. La température de Curie TC diminue avec l'augmentation de la teneur en Ba^{2+}. De plus, l'effet de la température, de la fréquence et de la composition sur la conductivité AC et les propriétés diélectriques ont montré des valeurs intéressantes.

Mots-clés : PZT, température de Curie, structure, frontière de phase morphotropique, propriétés diélectriques, conductivité AC.

ملخص

في هذه الدراسة، تم تطوير السيراميك من نوع PZT مع الصيغة العامة $Pb_{1-x}Ba_x (Zr_{0.52}Ti_{0.43} (Al_{0.5}Sb_{0.5})_{0.05}) O_3$.

حيث x= 0.00 ،0.02 ،0.04 ،0.06 ،0.08 و 0.10 طريقة تفاعل الحالة الصلبة. تركز الأهداف الرئيسية لهذه الدراسة على تطور الخواص التركيبية والكهربائية في منطقة حدود المرحلةMPB، وتأثير استبدال الباريوم ودرجة الحرارة والتردد على الخصائص الكهربائية. تم استخدام تقنيات مختلفة لتوصيف العينات التي تم الحصول عليها مثل حيود الأشعة السينية XRD والتي تؤكد نتائجها على النقاء العالي للعينات المحضرة، دون الطور الثانوي، وتشير أيضًا إلى التواجد بين الطور الرباعي والمعيني. يتم عرض جميع نطاقات الامتصاص المقابلة لهيكل البيروفسكايت بواسطة مطياف فوريه لتحويل الأشعة تحت الحمراء FTIR. انخفضت درجة حرارة كوري TC مع زيادة محتوى Ba^{2+}. علاوة على ذلك، أظهر تأثير درجة الحرارة والتردد والتركيب على موصلية التيار المتردد وخصائص العزل الكهربائي قيمًا مثيرة للاهتمام

الكلمات المفتاحية PZT :، درجة حرارة كوري ، الهيكلية ، حدود الطور المورفوتروبي ، الخواص العازلة ، موصلية التيار المتردد

Contents

Dedication 5

Acknowledgements 6

List of figures 16

List of tables 19

List of abbreviations 20

General Introduction 22

Chapter I Bibliographic research 25

I.1 Introduction 26

I.2 Ceramics 26

I.3 Piezoelectric materials 27

I.3.1 Applications of piezoelectric materials 27

I.4 Dielectric materials 28

I.4.1 Ideal dielectrics 30

I.4.2 Real Dielectric 30

I.4.2.1 Dielectric constant 30

I.4.2.2 Dielectric loss 31

I.4.3 Variables that influence the dielectric constant 32

I.4.3.1 Influence of the amplitude of the applied electric field 32

I.4.3.2 Influence of the frequency 32

I.4.3.3 Influence of temperature 32

I.4.3.4 Influence of microstructure 33

I.5 Paraelectric materials 34

I.6 Pyroelectric materials 34

I.7 Ferroelectric materials 34
I.7.1 Classical ferroelectric 35
I.7.2 Relaxer ferroelectric 35
I.8 Physical properties of ceramics materials 35
I.8.1 Piezoelectricity 36
I.8.2 Pyroelectricity 36
I.8.3 Ferroelectricity 37
I.8.4 Hysteresis cycle 37
I.8.5 Dielectricity 38
I.8.6 Curie temperature 38
I.8.7 Impedance spectroscopy 38
I.8.7.1 Nyquist plot 40
I.8.7.2 Bode plot 41
I.9 Different types of polarization 41
I.9.1 Space charge polarization (Pc) 42
I.9.2 Dipole polarization (Pd) 42
I.9.3 Atomic or ionic polarization (Pa) 43
I.9.4 Electronic polarization (Pe) 43
I.10 Perovskite structure 44
I.10.1 Classification of the perovskite structure 44
I.10.1.1 Simple perovskite 44
I.10.1.2 Complex perovskite 45
I.10.2 Stability of the perovskite structure 45
I.10.2.1 Electro-neutrality condition 45
I.10.2.2 Ionicity of the bonds 45
I.10.2.3 Tolerance factor 46
I.11 Applications of perovskite materials 46

I.11.1 Electricals applications 46
I.11.2 Catalytic Applications 47
I.11.3 Conductor 47
I.12 Lead Zirconate Titanate (PZT) 47
I.12.1 Overview of the selected material 47
I.13 Morphotropic phase boundary 48
I.14 Effect of doping on the properties of PZT materials 49
I.14.1 Isovalent dopants 49
I.14.2 Donor dopants 49
I.14.3 Acceptor dopants 50
Chapter II Experimental part 52
II.1 Introduction 53
II.2 Solid-state reaction method 53
II.3 Sample preparation 54
II.3.1 Precursor 54
II.3.1.1 Lead monoxide PbO: 54
II.3.1.2 Zirconium dioxide ZrO_2 55
II.3.1.3 Titanium dioxide TiO_2: 55
II.3.2 Dopants 56
II.3.2.1 Al_2O_3: 56
II.3.2.2 Sb_2O_3: 57
II.3.2.3 $BaCO_3$: 57
II.4 Elaboration process 57
II.4.1 Weighing and mixing 59
II.4.2 Grinding 59
II.4.3 Calcination: 59

II.4.4 The shaping of a pellets 60
II.4.5 The sintering 61
II.5 Characterization technique: 62
II.5.1 XRD Analyses 62
II.5.2 Scanning electron microscopy SEM 64
II.5.3 Fourier Transform Infrared Spectroscopy FTIR 64
II.5.4 Density 65
II.5.5 Impedance spectroscopy measurement 66
Chapter III Structural and Microstructural properties of PZT-based ceramics 68
III.1 Introduction 69
III.2 Structural properties 70
III.3 Morphotropic phase boundary 73
III.4 Lattice parameter 77
III.5 Tolerance factor 79
III.6 Fourier Transform Infrared spectroscopy (FTIR) 81
III.7 Density 82
III.7.1 Effect of temperature on density 82
III.7.2 Effect of barium substitution on density 83
III.8 Microstructural analysis 84
III.8.1 Effect of Barium substitution on average grain size 86
III.9 Energy dispersive spectrometric analysis (EDS) 86
III.10 Conclusion 89
Chapter IV Effect of Barium substitution and various parameters on impedance spectroscopy and electrical properties of PZT based ceramics 90
IV.1 Introduction 91
IV.2 Dielectric studies 92
IV.2.1 Dielectric constant and dielectric loss 92

IV.2.1.1 The effect of temperature 92
IV.2.1.2 The effect of Frequency 93
IV.2.1.3 The effect of Barium substitution 95
IV.3 Curie temperature 96
IV.4 Impedance spectroscopy 96
IV.4.1 Nyquist plot 96
IV.4.1.1 The effect of temperature and frequency on electrical properties 97
IV.4.2 Bode plots 100
IV.4.2.1 The Real Part 100
IV.4.2.2 The Imaginary Part 102
IV.5 AC conductivity 104
IV.5.1 The evolution of AC conductivity as function of temperature 104
IV.5.2 The evolution of AC conductivity as function frequency 106
IV.5.3 The Barium effect on AC conductivity 108
IV.6 Conclusion 109
General conclusion 110
References 114
Annexes 127

List of figures

Chapter I

Figure I. 1: Organigram of the 32 Crystal Classes 27

Figure I. 2: Charges on a parallel plate capacitor with a) a vacuum between the plates and b) polarized dipoles in the dielectric between the plates. 29

Figure I. 3: Schematic of a plane capacitor filled with a dielectric under the action of external excitation. 31

Figure I. 4: Deformation between the cubic and quadratic structure of BaTiO3. 33

Figure I. 5: Dielectric constant versus average grain size for $BaTiO_3$ ceramics at 25°C. 34

Figure I. 6: the direct (a) and inverse (b) piezoelectric effect. 36

Figure I. 7: Hysteresis cycle characteristic of a ferroelectric: polarization P versus applied electric field E. 38

Figure I. 8: Electrical model of equivalent circuit and its Cole–Cole plot 40

Figure I. 9: Displacement of free carriers that concentrate at defects, grain boundaries, surfaces, etc. creates polarization at the interfaces. 42

Figure I. 10: Displacement of permanent dipoles (e.g. molecules) which are oriented to be parallel to the field. 42

Figure I. 11: Relative displacement of oppositely charged ions with respect to each other. ... 43

Figure I. 12: Displacement of the center of inertia of the electronic cloud with respect to the center of inertia of the nucleus of the atoms 43

Figure I. 13: Illustration of perovskite crystal structure. 44

Figure I. 14: Phase diagram of PZT 48

Figure I. 15: Defects created in the PZT lattice after substitution by donor (a) or acceptor (b) ions 51

Chapter II

Figure II. 1: The different steps to prepare the samples 58

Figure II. 2: The calcination cycle diagram and the heating oven. 60

Figure II. 3: hydraulic uniaxial press 61

Figure II. 4: The position of the pellets during sintering..... 62

Figure II. 5: XRD instrument (Rigaku Miniflex 600). 63

Figure II. 6: Schematic diagram of a diffractometer system.. 64

Figure II. 7: Schematic diagram of a Fourier transform infrared instrument. 65

Figure II. 8: Electronic Palmer. 66

Chapter III

Figure III. 1: XRD patterns of $Pb_{1-x}Ba_x(Zr_{0.52}Ti_{0.43}(Al_{0.5}Sb_{0.5})_{0.05})O_3$ where (a) x=0.00, (b) x=0.02, (c) x=0.04, (d) x=0.06, (e) x=0.08, and (f) x=0.10. 71

Figure III. 2: The deconvoluted peaks simulated in 2θ range of 42° to 47° and the volume fraction of the Tetragonal (T) and Rhombohedral (R) phases of $Pb_{1-x}Ba_x(Zr_{0.52}\ Ti_{0.43}(Al_{0.5}\ Sb_{0.5})_{0.05})O_3$. 75

Figure III. 3: Variation of the lattice parameters as a function of Barium content. 78

Figure III. 4: Variation of c/a ratio as a function of Barium content. 78

Figure III. 5: The tolerance factor T of $Pb_{1-x}Ba_x(Zr_{0.52}Ti_{0.43}(Al_{0.5}Sb_{0.5})_{0.05})O_3$. 80

Figure III. 6: FTIR patterns of Pb1-xBax(Zr0,52Ti0,43(Al0,5Sb0,5)0,05)O3. 82

Figure III. 7: Influence of the temperature on the density of $Pb_{1-x}Ba_x(Zr_{0.52}Ti_{0.43}(Al_{0.5}Sb_{0.5})_{0.05})O_3$. 83

Figure III. 8: Influence of barium substitution on density of $Pb_{1-x}Ba_x(Zr_{0.52}Ti_{0.43}(Al_{0.5}Sb_{0.5})_{0.05})O_3$. 84

Figure III. 9: SEM images of fracture surface and the average grain size of Pb1-XBaX(Zr0.52Ti0.43(Al0.5Sb0.5)0.05)O3. 85

Figure III. 10: The average grain size as a function of Barium substitution 86

Figure III. 11: X-EDS spectrum for the sample of $Pb_{1-x}Ba_x(Zr_{0.52}Ti_{0.43}(Al_{0.5}Sb_{0.5})_{0.05})O_3$. 87

Chapter IV

Figure IV. 1: Temperature dependence of Dielectric constant εr and Dielectric loss (tgδ) at different frequencies of Pb1-XBaX(Zr0.52Ti0.43(Al0.5Sb0.5)0.05)O3 94

Figure IV. 2: Temperature dependence of Dielectric constant (εr) at 1 kHz of Pb1-XBaX(Zr0.52Ti0.43(Al0.5Sb0.5)0.05)O3. 95

Figure IV. 3: Curie temperature dependent on barium substitution of Pb1-XBaX(Zr0.52Ti0.43(Al0.5Sb0.5)0.05)O3. 96

Figure IV. 4: Z'' depending on Z' at different temperatures of Pb1-xBax(Zr0.52Ti0.43(Al0.5Sb0.5)0.05)O3. 99

Figure IV. 5: Variation of Z′ with frequency at different temperatures of of Pb1-xBax(Zr0.52Ti0.43(Al0.5Sb0.5)0.05)O3. 101

Figure IV. 6: Frequency–temperature dependence of Z" of Pb1-xBax(Zr0.52Ti0.43(Al0.5Sb0.5)0.05)O3. 103

Figure IV. 7: Temperature–frequency dependence of ac conductivity of Pb1-xBax(Zr0.52Ti0.43(Al0.5Sb0.5)0.05)O3. 105

Figure IV. 8: The AC conductivities of Pb1-xBax(Zr0.52Ti0.43(Al0.5Sb0.5)0.05)O3. 107

Figure IV. 9: Barium amount dependence of AC conductivity of Pb1-xBax(Zr0.52Ti0.43(Al0.5Sb0.5)0.05)O3. 108

List of tables

Chapter I

Table I. 1: application of materials according to the effect used 28

Chapter II

Table II. 1: lead oxide datasheet..... 54

Table II. 2: Zirconium dioxide datasheet 55

Table II. 3: Titanium dioxide datasheet..... 55

Table II. 4: Aluminum oxide datasheet 56

Table II. 5: Antimony pentoxide datasheet 57

Table II. 6: Barium carbonate datasheet..... 57

Chapter III

Table III. 1: The angular regions that present the coexistence of the two phases T and R..... 73

Table III. 2: The lattice parameters, c/a ratio, and the crystallite size of Pb1XBaX(Zr0.52Ti0.43(Al0.5Sb0.5)0.05)O3..... 79

Table III. 3: The tolerance factor T of Pb1-XBaX(Zr0.52Ti0.43(Al0.5Sb0.5)0.05)O3. 80

Chapter IV

Table IV. 1: Variation of TC, εr RT, ε max, Tgδ RT and Tgδ Tc of Pb1-XBaX(Zr0.52Ti0.43(Al0.5Sb0.5)0.05)O3 at 1 kHz. 95

List of abbreviations

PZT: Lead zirconate titanate

PBZTAS: $Pb_{1-x}Ba_x(Zr_{0.52}Ti_{0.43}(Al_{0.5}Sb_{0.5})_{0.05})O_3$

XRD: X-ray diffraction

FTIR: Fourier Transform Infrared Spectroscopy

SEM: Scanning electron microscopy

EDS: Energy dispersive spectrometric analysis

TC: Curie Temperature

AC: Alternating current

DC: Direct current

ε_r: the relative dielectric permittivity

ω: the angular frequency

C_0: the free charge capacitance

Z': The real part

Z": the imaginary part

Cp: the parallel capacitance

d: the thickness of the pellet

A: ceramic disc area

ε_0: is the free space permittivity

tgδ RT: dielectric loss at room temperature

tgδ Tc: dielectric loss at curie temperature

ε_{RT}: dielectric constant at room temperature

ε_{max}: dielectric constant at curie temperature

σ_{AC}: AC Conductivity

σ_{DC}: DC conductivity

General Introduction

General Introduction

Lead zirconate titanate PZT materials were exploited in many fields of technology for commercial electronic applications such as sensors, actuators, and memories [1, 2], due to their high dielectric and piezoelectric capabilities [3-5]. These ferroelectric ceramics with the general formula $Pb(Zr_xTi_{1-x})O_3$, commonly referred to as PZT (lead zirconate titanate), are materials that exhibit ferroelectric properties. These ceramics are composed of a solid solution of lead zirconate $PbZrO_3$ and lead titanate $PbTiO_3$, where the ratio of zirconium to titanium (x) can vary. The specific composition of PZT ceramics can be tailored by adjusting the ratio of zirconium to titanium, which allows for tuning their electrical and mechanical properties. This flexibility in composition and resulting properties makes PZT ceramics highly desirable for various technological applications.

The adaptable PZT properties have not yet been adequately replaced; because of those responses occur close to the Morphotropic Phase Boundary (MPB) [6-8]. Perovskite type-oxide ABO_3 involving $Pb(Zr_xTi_{1-x})O_3$ where Pb ion occupied the A-site while Zr^{4+} and Ti^{4+} ions were accommodated at the B-site [7, 9]. Several studies [10, 11] have reported that the substitution effect regardless of the A and/or B site is an effective method to enhance the dielectric properties. The dopants can be classified into three categories [7, 12], the isovalent dopants such as (Ba^{2+}) [13] and (Sr^{2+}) [14], donor dopants (Sb^{5+}) [15], and acceptor dopants (Al^{3+}) [16], These dopants are introduced into the PZT ceramic during the elaboration process by direct incorporation into the precursor materials. The specific dopant selection and concentration depend on the desired electrical, structural, and functional properties required for the intended application of the PZT ceramics.

The category that attracts us is the isovalent dopants (Ba^{2+}) because of their effect on dielectric properties, where they can reduce the curie points and increase the dielectric constant [7], as well as avoid the pyrochlore composition in perovskite structure [17]. This is what prompted some studies to investigate the barium impact substitution into PZT ceramics' dielectric properties [13, 18, 19]. Xiucai Wang et al. [20] found that the Ba^{2+} ion doping into PZT ceramics shows a very interesting effect on the dielectric properties and decreases the curie temperature from 85 to 48°C. The same tendency has been found by Dipti et al. [21] and Neha et al. [10] when Ba^{2+} ions were incorporated into the PZT system.

Therefore, in the present doctoral thesis we are trying to find stable and reproducible characteristics of PZT ceramics in the region of the morphotropic phase boundary, using the solid-state reaction method known as ceramic, a sequence of compositions $Pb_{1-x}Ba_x(Zr_{0.52}Ti_{0.43}(Al_{0.5}Sb_{0.5})_{0.05})O_3$ PBZTAS were x=0.00, 0.02, 0.04, 0.06, 0.08, and 0.10 were created. We aimed also to investigate the fundamental characteristics of PZT-type ceramics, focusing on structural, microstructural, AC conductivity, and dielectric properties.

The research was conducted through a comprehensive literature review and practical experimentation, encompassing an explication of the synthesis method and various characterization techniques.

This thesis is composed of 4 chapters.

In the first chapter, an extensive bibliographic study was carried out to establish a solid foundation for understanding the essential features of PZT ceramics. Key concepts such as piezoelectricity, dielectricity, ferroelectricity, and impedance spectroscopy were defined and explored within the context of the research.

Chapter 2 delved into the practical aspect of the study, presenting the ceramic elaboration method employed and detailing the specific synthesis conditions (grinding time, fabrication of pellets, temperature, and time of calcination and sintering). Furthermore, the various characterization instruments utilized, including X-ray diffraction XRD, Fourier-transform infrared spectroscopy FTIR, scanning electron microscopy SEM, and impedance spectroscopy instruments, were introduced.

In Chapter 3, the structural and microstructural characteristics of the synthesized ceramics were interpreted, including XRD results, FTIR, SEM images, EDS. Additionally, this chapter presented the tolerance factor, lattice parameters, and density of the ceramic samples.

The final chapter focused on impedance spectroscopy, specifically examining the imaginary and real parts of the impedance that presenting by Bode and Nyquist diagrams. The influence of temperature, frequency, and barium substitution on various electrical properties, such as dielectricity and AC conductivity, was thoroughly investigated and discussed.

Finally, we finish this thesis with a general conclusion that sums up all the essential results of our research work that we carried out.

Chapter I Bibliographic research

Chapter I: Bibliographic research

I.1 Introduction

This section aims to provide an overview of the fundamental definitions, characteristics, and properties of PZT-type ceramics. Additionally, it will explore the synthesis method employed for the elaboration of these types of ceramics and discuss their advantages in different application domains. Understanding these fundamental aspects is essential for advancing research and development in the field of PZT ceramics. To comprehend the nature of PZT ceramics, it is necessary to establish a foundation by defining key terms. For instance, Piezoelectricity refers to the ability of certain materials to generate an electrical charge in response to applied mechanical pressure, while dielectricity involves the capacity of a material to store and release electrical energy. Ferroelectricity, on the other hand, describes the reversible spontaneous polarization exhibited by certain materials under an external electric field. By comprehensively exploring the fundamental definitions, characteristics, and advantages of PZT-type ceramics, this bibliographic section aims to provide a solid foundation for the subsequent chapters of this thesis. The knowledge gathered from this review will serve as a basis for the practical investigations and analyses conducted, ultimately contributing to the overall understanding and advancement of PZT ceramics in various fields of application.

I.2 Ceramics

It is not easy to define what ceramic is, because there is no single definition that everyone agrees on. Actuality there are different definitions depending on the point of view adopted, we can consider the points of view of the historian, the engineer, or the industrialist. The ceramics definition, which was known by scientists (physicists, chemists, etc.), is generally defined as "inorganic materials formed at high temperature". The field of use of ceramic materials is very broad, such as electrical and optical components for several sectors (industrial and military). A fundamental understanding of ceramic materials at the atomic level is not only interesting in itself but extremely important to improve material performance and to research or design new materials for novel applications [22-24].

I.3 Piezoelectric materials

In crystalline solids, piezoelectricity is directly related to the symmetry of the crystals and manifests itself as lattice polarization. For a material, to be piezoelectric, its crystalline structure must be non-centrosymmetric (no center of symmetry) [25]. The piezoelectric effect in crystals results essentially from the existence of internal electric dipoles. This dipole moment is created by the separation of the positive and negative charge at the level of each crystal lattice structure under the action of external constraint. This effect can only be observed for crystals whose pattern does not have a center of symmetry. Among the 32 Crystal Classes, 21 are not centro-symmetrical and 20 are piezoelectric

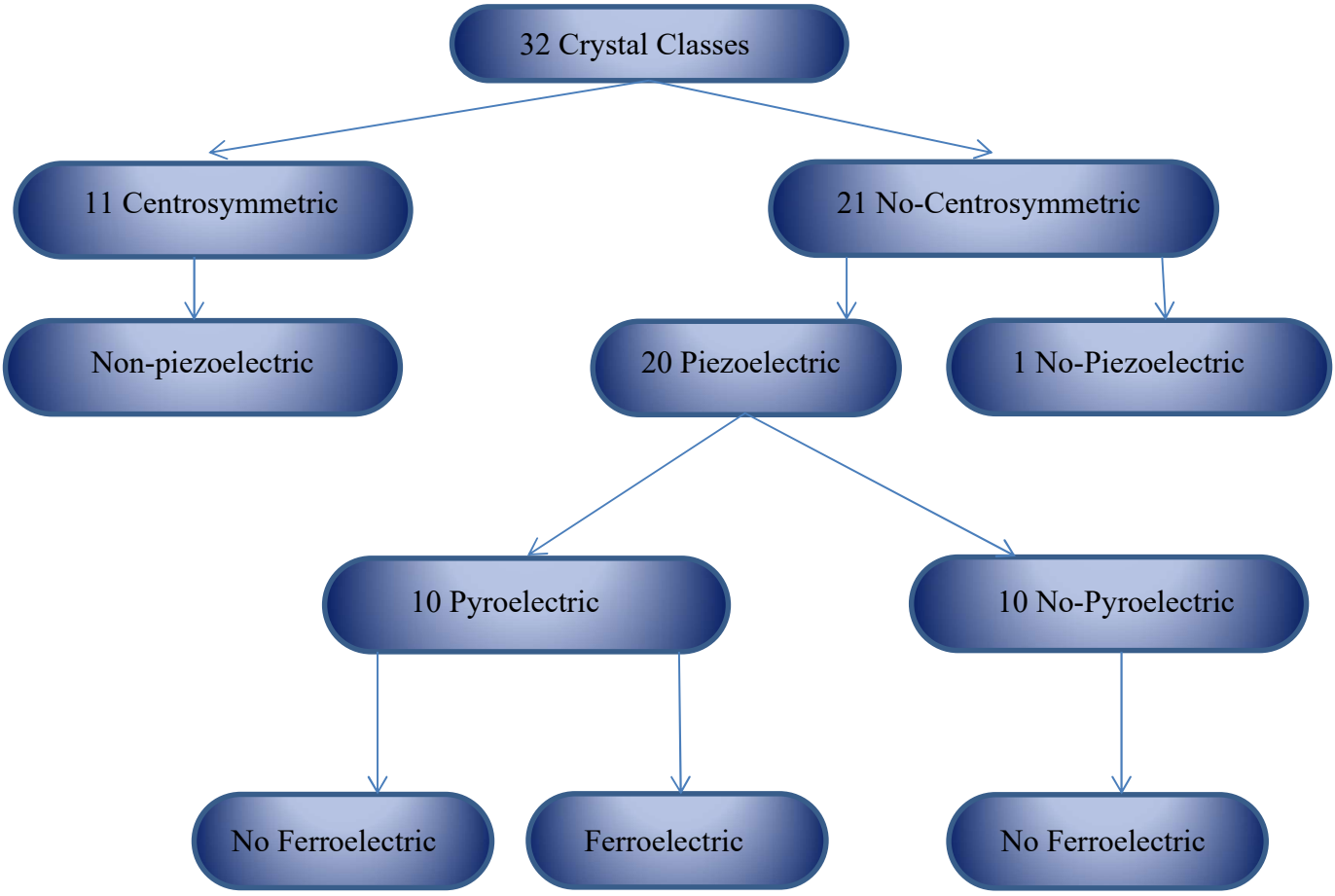

Figure I. 1: Organigram of the 32 Crystal Classes

I.3.1 Applications of piezoelectric materials

Due to the attractive properties of piezoelectric materials, many applications have been found that can be exploited with these materials, concerning either the direct effect, the reverse

effect, or both alternatively. Table I.1 shows some applications of piezoelectric materials according to the effect used [26].

Table I. 1: Application of materials according to the effect used

Application based on the direct effect	Application based on the reverse effect	Application based on both effects
Microphone	Speaker	Ultrasound transducer for medical diagnosis (ultrasound)
Hydrophone	Buzzer	Ultrasonic ndt proximity or presence detector
Shock sensor	Sonar transducer	Distance or flow measurement
Accelerometers	Nebulizer	Gyroscope
Push button	Ultrasonic cleaning	Frequency filters
Lighting	Ultrasonic motor	Delay lines
Pressure or stress sensor	Relay	Piezoelectric transformer
	Micropositioning	
	Laser adjustment	
	Piezoelectric pump	
	Piezoelectric scalpel	

I.4 Dielectric materials

These materials "dielectric materials" were first named in 1839 by Faraday, the word dielectric is derived from the Greek word prex dia, which means "through", contrary to metal, the dielectric materials are substances that have low free charges and are therefore low conductors. However, these materials are electrically insulating materials but actually are not neutral because the application of an electric field can induce polarization; this definition allows us to consider the two words dielectric and insulator as synonyms. This dielectric study is used to see the response of atoms or molecules inside a material after applied an electric field, for example, when a metallic material is submitted to an electric field, the free electrons of this material move in the opposite direction to the field [27].

The dielectric phenomenon is easy to comprehend if one assumes a parallel plate capacitor as shown in Figure I.2.

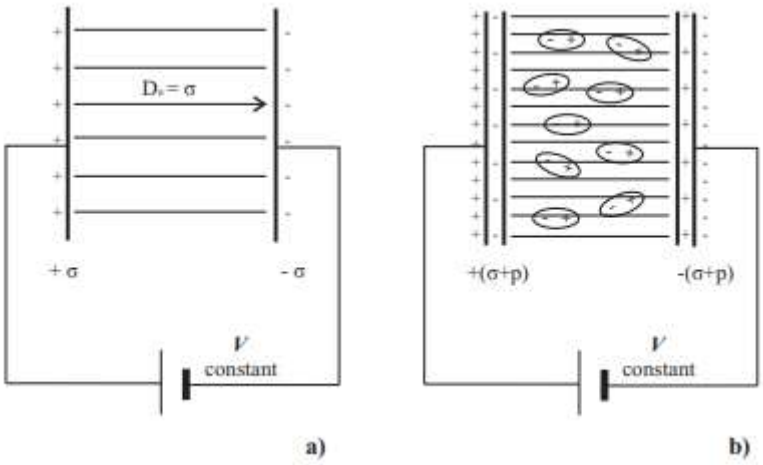

Figure I. 2: Charges on a parallel plate capacitor with a) a vacuum between the plates and b) polarized dipoles in the dielectric between the plates.

The capacitor is made of two parallel metal electrodes with area (A) separated by a distance (d) in a vacuum (Fig. I.2(a)). When the plates are subjected to an electric field the plates of the capacitor are accumulated by the +Aσ and -Aσ charges, The charge density +σ is the source of a uniform electric flux density D_0, which terminates at the charge density - σ and is directly proportional to the electric field, E=V/d, and can be given as follows:

$$D_0 = \varepsilon_0 E \qquad (I.1)$$

Where the constant of proportionality ε_0 is called permittivity of free space and has the value of ($\varepsilon_0 = 1/(36*\pi*10^9) = 8{,}85$ pF/m). The ratio of the charge on the plate to the difference in potential is the capacitance:

$$C_0 = \frac{A\sigma}{V} = \frac{\varepsilon_0 A}{A} \qquad (I.2)$$

If a homogeneous dielectric is introduced between the plates keeping the potential constant (Fig. I.2(b)), the charge density on the plates increases from σ to σ + p, leading to an increase of the capacitance.

$$C = \frac{A(\sigma + p)}{V} \qquad (I.3)$$

The dielectric material reacts to the electric field by changing the distribution of its charges, an effect known as polarization. If the material is not polar, the displacement of the negative charges is in the opposite direction of the applied field and the positive charges in the direction of the field polarizes the material. The bound charge densities ±p, that appear on the surfaces of the dielectric are the external effect of the polarization of the individual elements

of the dielectric. The increase in the charge density to σ + p leads to an increase in the flux density, which adopts a more general vector notation and can be defined as:

$$\bar{D}_0 = \bar{\varepsilon}_0 \ \bar{E} + \bar{P} \qquad \text{(I.4)}$$

This increase in flux density occurs without an increase in the potential gradient and is a measure of the electrical displacement in the material. The C/C_0 ratio is characteristic of the dielectric material between the plates and is known as the static relative permittivity:

$$\varepsilon_s = \frac{C}{C_0} = \frac{\sigma + P}{\sigma} = \frac{\varepsilon_0 \bar{E} + \bar{P}}{\varepsilon_0 \bar{E}} = 1 + \frac{\bar{P}}{\varepsilon_0 \bar{E}} = 1 + \chi \qquad \text{(I.5)}$$

Where $\chi = \frac{\bar{P}}{\varepsilon_0 \bar{E}}$ is the electric susceptibility of the material. Every material has a specific relative permittivity that depends on its polarization and is fundamentally independent of the applied voltage or field, which we generally call the dielectric constant of the material. However, this is a complex parameter, which depends on the frequency, more appropriately referred to as the relative permittivity (relative to the absolute permittivity of free space); this term will be used in this thesis [28].

There are two types of dielectric: Ideal dielectrics and Real Dielectric.

I.4.1 Ideal dielectrics

The term "ideal dielectric" refers to a theoretical concept used to describe a material that exhibits certain idealized properties; ideal dielectric materials are completely insulating materials so that there is no conductivity because there are not even free charges in their structure, this ideal dielectric has several properties among them: Infinite Dielectric Constant, zero Dielectric Loss.

I.4.2 Real Dielectric

The real dielectric materials contain very few free charges represented by impurities so the material shows slight surface conduction, especially at low frequencies. Dielectric materials are characterized by several main properties among which are [28-30]:

I.4.2.1 Dielectric constant

The dielectric constant ε_r presents the response of a material under an electric field. This physical constant measures the polarizability of a substance. The more the material limits the passage of an electric current, the higher its dielectric constant is [31]. In most of the literature, we find the relative dielectric constant that defines the ratio of the dielectric

constant of the material and that of the vacuum. The value of the dielectric constant is calculated from the following relation (I.6) [32, 33].

$$\varepsilon_r = \frac{C_p * d}{\varepsilon_0 * A} \qquad \text{(I.6)}$$

Where Cp is the parallel capacitance, the thickness of the pellet is denoted by d, A is a ceramic disc area and ε_0 is the free space permittivity.

If we apply an electric field to a plane capacitor filled with a dielectric, charges P appear on the surface of the dielectric and compensate the charges brought by the source on the armatures (Figure I.3).

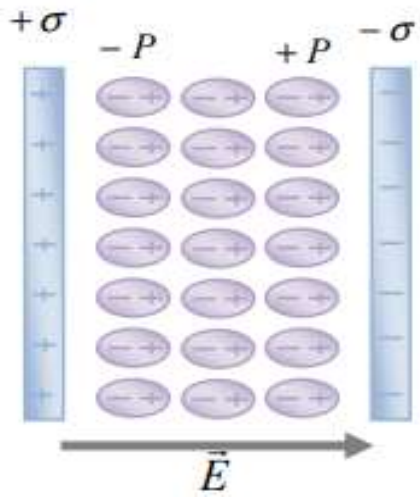

Figure I. 3: Schematic of a plane capacitor filled with a dielectric under the action of external excitation.

I.4.2.2 Dielectric loss

The dielectric loss is electrical energy that transforms into thermal energy from a dielectric material, a part of these losses due to the momentary current is called ohmic; the other part associated with the displacement of charges is called dielectric losses. These losses can be by absorption and/or diffusion, the amount of energy lost compared to that stored in the dielectric expressed by the dissipation factor. If a dielectric material is excited by a sinusoidal electric field, given the time for the polarization to be established, a delay or phase shift δ (depending on the frequency) may appear between the applied electric field and the induced polarization. Necessarily the electric induction will be sinusoidal with the same delay δ with respect to the applied field [34]. The tangent of the loss angle (tan δ) is equal to the dissipation factor, which is generally expressed by the following equation [35, 36] :

$$\tan \delta = \frac{\varepsilon''}{\varepsilon'} \quad \text{(I.7)}$$

I.4.3 Variables that influence the dielectric constant

There are several parameters that can influence the dielectric constant, including the amplitude of the applied electric field, frequency, temperature, microstructure, external pressure, etc.

I.4.3.1 Influence of the amplitude of the applied electric field

The variation of the electric field across a dielectric material affects its permittivity. This is particularly the case for ferroelectrics whose spontaneous polarization can be oriented or even reversed by applying a sufficient electric field. Their polarization is not a linear function of the applied electric field, and spontaneous polarization remains even in the absence of a field [37].

I.4.3.2 Influence of the frequency

The lowest frequencies increase the value of the relative permittivity. As the frequency increases, the contributions made by each type of polarization disappear one after the other, therefore, the permittivity decreases with frequency. The polarization takes a delay with the electric field with a dissipation of energy [38].

I.4.3.3 Influence of temperature

The effect of temperature on the dielectric constant or capacitance is often described by the temperature coefficient of capacitance TCC, which is expressed in ppm/C and can be defined by the following equation [38]:

$$\text{TCC} = \frac{dC}{CdT} = \frac{\Delta C}{C\Delta T} \quad \text{(I.8)}$$

Where C is the capacity at temperature T. The temperature has different effects on the various polarizations of the material. The two types of polarization most influenced are orientation and interfacial polarizations. The first one increases the mobility of the dipoles by breaking the interactions (decrease of the viscosity forces) and the other one by the mobility of the charges.

The effect of temperature on materials can be demonstrated by several examples. In the domain of polymers, at the glass transition temperature, there is an increase in permittivity due to the mobility of permanent dipoles. For ceramics, the most studied example in the literature is $BaTiO_3$. The increase in temperature tends to deform its cubic lattice while changing the lattice parameters a, b, and c. The barycenter of the positive charges Ba^{2+} and Ti^{4+} no longer coincides with that of the negative charges O^{2-} ; a spontaneous polarization is established along the elongation direction (polar axis). The quadratic phase of $BaTiO_3$ is thus ferroelectric (Figure I.4) [34].

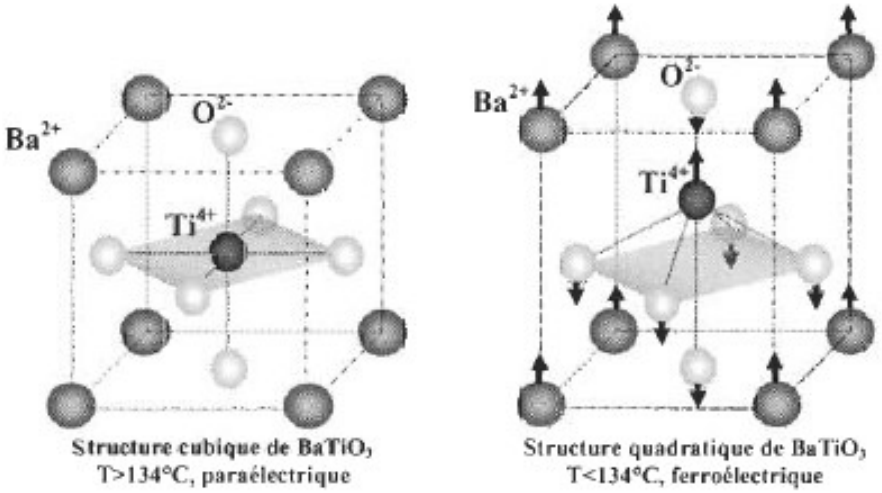

Figure I. 4: Deformation between the cubic and quadratic structure of BaTiO3.

I.4.3.4 Influence of microstructure

The relative permittivity of materials can also depend on their microstructure. Generally, ceramics are governed by their grain size. The grain size has a major effect on the dielectric constant. A close relationship between this parameter and the dielectric susceptibility of different materials has been observed, more precisely in the case of $BaTiO_3$ [39]. The dielectric permittivity of the latter at room temperature shows a particular variation in grain size associated with the evolution of the ferroelectric domain configuration [39-41]. A maximum permittivity at room temperature can be obtained with grains of the order of 0.8 to 1 µm as shown in Figure I.5 [42].

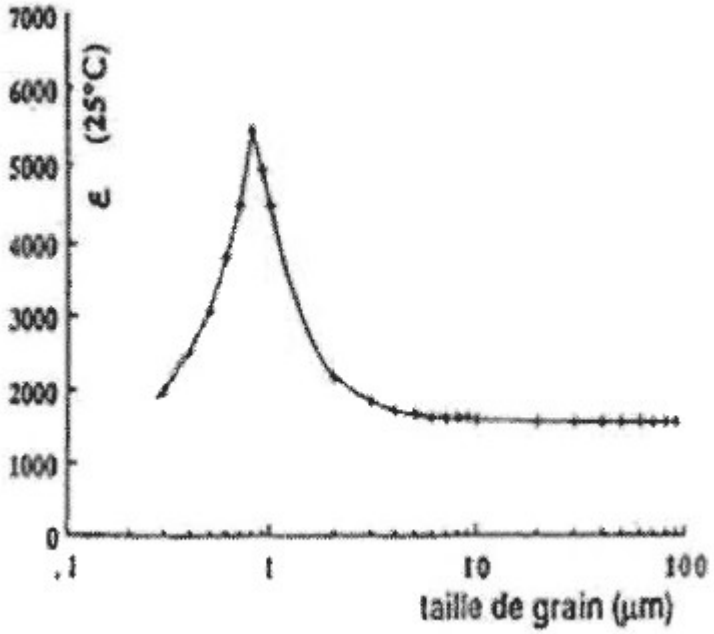

Figure I. 5: Dielectric constant versus average grain size for $BaTiO_3$ ceramics at 25°C.

I.5 Paraelectric materials

Some dielectric materials are considered polarizable: under the action of an electric field, their positive charges move in the direction of the field, while their negative charges in the opposite direction, creating +/- electric dipoles oriented parallel to the field. When the electric field is cancelled, the charges return to their equilibrium position and the polarization disappears. These are paraelectric materials.

I.6 Pyroelectric materials

Among the piezoelectric crystals, some crystals can show an electric polarization even in the absence of mechanical constraint or external electric field; they are called pyroelectric, in which the temperature affects on their permanent dipole moment. Among the 20 piezoelectric classes, only the 10 with a polar axis are pyroelectric (the existence of a single polar axis prevents a combination of symmetry elements that can reverse the direction of a dipole) [43, 44].

I.7 Ferroelectric materials

Spontaneous polarization occurs in materials characterized by the presence of regions, called domains, with identically polarized particles. The domains, disordered at the beginning, orient themselves when the field is applied and according to this field spontaneous polarization

appears. Materials characterized by spontaneous polarization are called ferroelectric materials. In polycrystalline ferroelectric materials, the grains are made of ferroelectric domains separated by domain boundaries. Each domain has its own orientation which is related to its crystal structure. Ferroelectric materials have a phase called ferroelectric at a temperature below a characteristic temperature called Curie temperature TC. These ferroelectric materials have good piezoelectric activity and a high dielectric constant. Ferroelectric materials are divided into two families: classical ferroelectrics and relaxers ferroelectrics, characterized by their phase transition behavior [45].

I.7.1 Classical ferroelectric

Classical ferroelectrics present at least one structural phase transition from a cubic paraelectric phase to a polar ferroelectric phase. This transition can be of the first or second order depending on whether the polarization undergoes a discontinuity or not. At the transition temperature, the dielectric permittivity curve shows a narrow maximum. Above, the dielectric permittivity follows a Curie-Weiss law and its maximum is located near the Curie temperature whatever the frequency of measurement.

I.7.2 Relaxer ferroelectric

In some materials, the dielectric relaxation is anticipated by a ferroelectric phase transition. We thus witness a change in relaxer ferroelectric behavior. The relaxer effect appears only in complex perovskites for which the sites or/and are occupied by at least two different cations. It is characterized by the existence in a large temperature range of a strong dielectric permittivity and by a dielectric relaxation (decrease of a maximum of ε' and increase of the temperature of this maximum when the frequency of measurement increases) in a wide frequency range. The compounds presenting the effect relaxant effect are characterized, from a structural point of view, by a disorder of the cations, compared to classical ferroelectrics; relaxer ferroelectrics exhibit no phase transition and are characterized by the absence of a macroscopic polarization

I.8 Physical properties of ceramics materials

Piezoelectricity, Pyroelectricity, and ferroelectricity have been known for many years, the electrical phenomenon resulting from the action of mechanical constraint on certain crystals was observed qualitatively for the first time in 1817 by Abbé René Just HAUY[25].

I.8.1 Piezoelectricity

The word "piezoelectricity" comes from the contraction of the Greek words piezein (pressure) and elektron. Piezoelectricity is the ability of certain materials (crystals, ceramics, polymers or composites) to transform mechanical energy into electrical energy (and vice versa) [46]. In 1880, the Curie brothers observed and exploited the direct effect [47], but it was Lippmann who theoretically determined the inverse effect, a notion later experimentally confirmed by the Curie brothers [48], these piezoelectric effects can only be observed on insulating materials, as illustrated in Figure I.6.

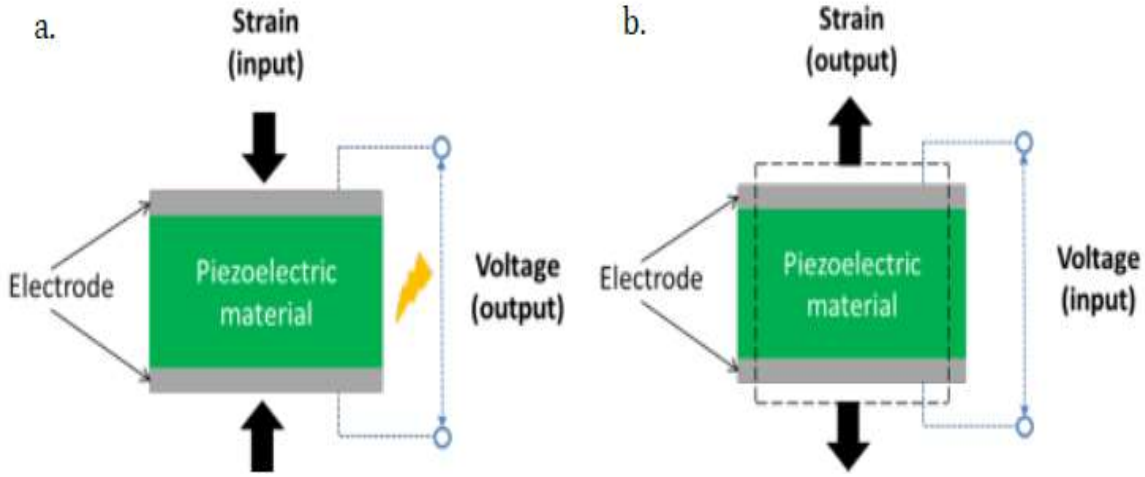

Figure I. 6: the direct (a) and inverse (b) piezoelectric effect [49].

I.8.2 Pyroelectricity

The pyroelectric phynomene is based on the electric charge released by the surfaces of certain non-centrosymmetric and optically active crystals which present a polar axis in their responses to a change of temperature, the pyroelectric materials are polar because they present a spontaneous polarization. The temperature has a major effect on the intensity of this polarization, according to a monotonic law which means that any variation of the temperature of the crystal causes the appearance or the disappearance of electric charges on the faces of the crystal, perpendicular to the polar axis and thus gives rise to a measurable current in an external circuit. In this type of crystal, the temperature has a major effect on the intensity of this polarization, according to a monotonic law which means that any variation in the temperature of the crystal causes the appearance or disappearance of electric charges on the faces of the crystal, perpendicular to the polar axis and thus gives rise to a measurable current in an external circuit, this effect was named by David Brewster [50].

I.8.3 Ferroelectricity

Ferroelectricity remained a scientific curiosity for many years without any real opportunities. However, the discovery of many new materials in the middle of the XXth century, such as $BaTiO_3$, and more particularly the solid solution $Pb(Zr,Ti)O_3$, PZT by Jaffe, Roth and Marzullo [51] will allow both to bring many theoretical answers to the phenomenon of ferroelectricity and to open the way to a wide range of applications. The majority of pyroelectric crystals have a spontaneous polarization Ps in certain temperature, to reverse the direction of the Ps by applying an external electric field. These crystals are called ferroelectric crystals [52]. This definition may have been published for the first time in 1952 by H. Megaw [53] and by A. von Hippel [54].

I.8.4 Hysteresis cycle

Applying an electric field in the opposite direction can reverse the remanent polarization of ferroelectric materials, which is the origin of the hysteresis cycle. The hysteresis cycle is a diagram in the form of a buckle, as shown in Figure I.7, we can present this hysteresis cycle by the variation of the polarization P as a function of the applied electric field E. We can determine from this diagram [55]:

- Determine the coercive field Ec, the minimum field strength necessary for the material to polarize
- determine the remanent polarization Pr, the value of the polarization at zero field (E=0)
- the saturation polarization Ps, often called spontaneous polarization, is the maximum value of the polarization that can be attained

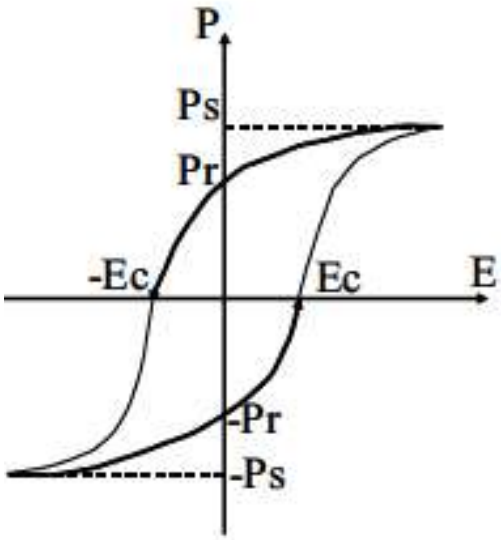

Figure I. 7: Hysteresis cycle characteristic of a ferroelectric: polarization P versus applied electric field E.

I.8.5 Dielectricity

When a dielectric material is installed between two electrodes, it becomes polarized because of the increase in electrical charge between the two poles, so when there is a vacuum between the two electrodes, the phenomenon of dielectricity allows the accumulation of electric charges, the capacitor response changes and its characteristics depend directly on whether the voltage applied between the two armatures is AC or DC [56].

I.8.6 Curie temperature

The increase in temperature decreases the polarization of piezoelectric ceramics until it is cancelled at TC called Curie temperature. Above this temperature, the piezoelectric material is in a non-polar paraelectric state. The polar-nonpolar transition corresponds to a phase transition. The crystal symmetry of the non-polar phase is always higher than that of the polar phase; the relative dielectric permittivity εr has a maximum value at the Curie temperature [57].

I.8.7 Impedance spectroscopy

Impedance spectroscopy is an experimental method for determining the microstructural and electrical properties of some electronic materials; the basis of this technique is the analysis of the AC response of a system and the subsequent calculation of the impedance as a function of

frequency, properties such as conductivity, dielectric constant, dielectric losses, etc. can be analyzed using this technique. Material properties such as complex permittivity (e*), complex impedance Z*, complex admittance Y*, complex electric modulus M* and dielectric loss that are frequency dependent can be described. The real (e', Z', Y', M') and imaginary (e", Z", Y", M") parts of the complex parameters are in turn related to each other as follows:

$$\varepsilon^* = \varepsilon' + \varepsilon''j \tag{I.9}$$

$$Z^* = Z' + Z''j = (1/j\varepsilon^* C_0\omega) \tag{I.10}$$

$$Y^* = Y' + Y''j = j\varepsilon^* C_0\omega \tag{I.11}$$

$$M^* = M' + M''j = (1/\varepsilon^*) = j\omega C_0 Z \tag{I.12}$$

$$Tan\delta = (\varepsilon''/\varepsilon') = (M'/M'') = (Y'/Y'') = (Z'/Z'') \tag{I.13}$$

Where $\omega = 2\pi f$ is the angular frequency C_0 is the free geometrical capacitance, and $j^2 = -1$. At the microstructural level, a ceramic is composed of grains and grain boundaries, with different resistivities q and dielectric permittivities ε [58]. Figure 1 illustrates the electrical model of the equivalent circuit. The real part Z' and the imaginary part Z" of the complex impedance are defined by the following equations[59]:

$$Z' = R_g/(1+(\omega R_g C_g)^2) + R_{gb}/(1+(\omega R_{gb} C_{gb})^2) \tag{I.14}$$

$$Z'' = \omega R_g^2 C_g/(1+(\omega R_g C_g)^2) + \omega R_{gb}^2 C_{gb}/(1+(\omega R_{gb} C_{gb})^2) \tag{I.15}$$

Where R_g,C_g,R_{gb}, C_{gb} are the resistance and capacitance of the grain and grain boundary respectively

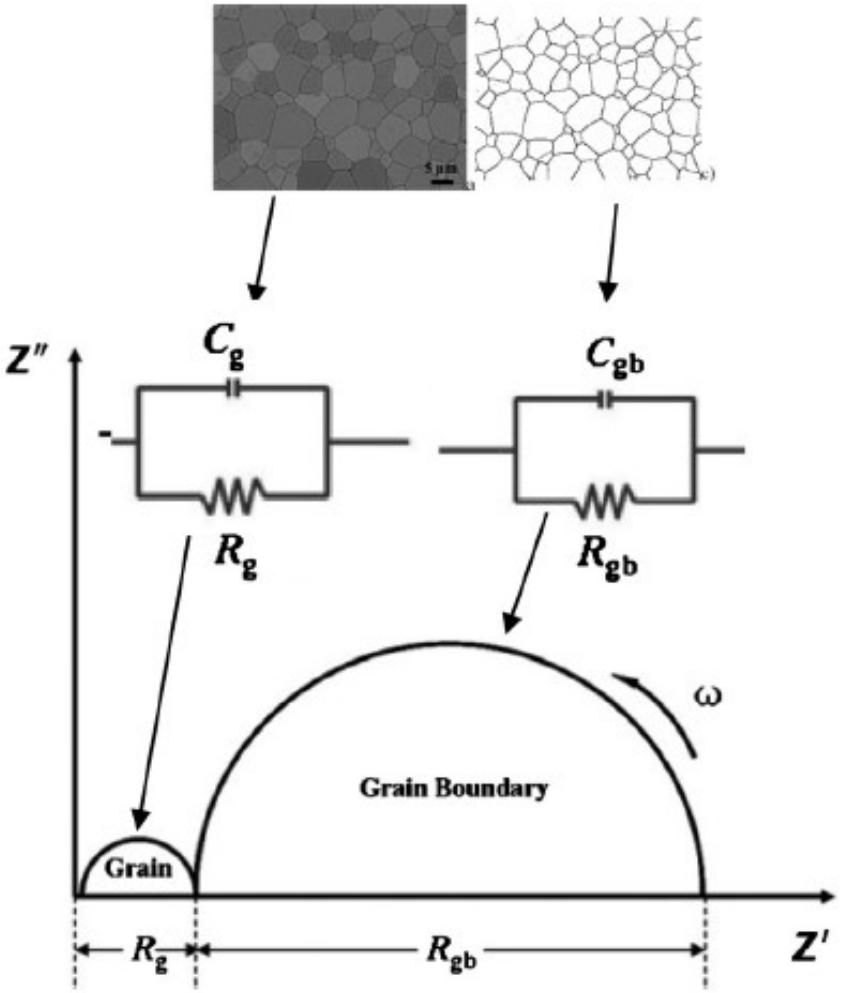

Figure I. 8: Electrical model of equivalent circuit and its Cole–Cole plot [60].

I.8.7.1 Nyquist plot

Nyquist plot (named by Harry Nyquist, a former engineer at Bell Laboratories, USA) is a graphical representation of impedance data obtained from an impedance spectroscopy experiment. It is a plot of the imaginary part of the impedance Z'' against the real part of the impedance Z'. The Nyquist plot is a useful tool for analyzing the electrical properties of materials, such as conductivity, resistance, and capacitance. The shape of the plot can provide information about the microstructure and composition of the material. In a Nyquist plot, the data points typically fall on a semicircle. The center of the semicircle represents the bulk resistance of the material, while the diameter of the semicircle represents the resistance associated with the grain boundaries or interfaces within the material [61].

I.8.7.2 Bode plot

Bode plots are graphical representations commonly used in impedance spectroscopy to analyze the frequency-dependent behavior of materials. These plots provide valuable insights into the electrical properties of the material and its response to different frequencies. When applied to PZT ceramics, the real part of impedance spectroscopy signifies the resistive component of the impedance. It represents the electrical resistance encountered by an alternating current AC signal as it passes through the PZT ceramic sample. The resistive component of impedance in PZT ceramics is influenced by multiple factors, such as the material's conductivity, grain boundaries, defects, and electrode interfaces. By examining the real part of impedance at different frequencies, valuable insights can be obtained regarding the electrical behavior and characteristics of PZT ceramics, including their conductivity, ionic diffusion, and polarization response. Impedance spectroscopy serves as a valuable tool for characterizing and comprehending the electrical properties and performance of PZT ceramics. It aids in understanding the behavior of these materials and provides crucial information for their practical applications.

I.9 Different types of polarization

The appearance of the dipole moment or polarization is the result of the submission of a material to an electric field due to the displacement of positive and negative charges. At sufficiently low frequencies, all moments reorient themselves in the direction of the field and all polarization mechanisms are involved. When the frequency increases, a phase shift can occur between the field tilt and the reorientation of the dipole moments; this phenomenon is the cause of the dissipation of part of the field energy in the material, also called dielectric losses, therefore the dipole moment reacts to the action of the external electric field at different frequencies. Thus, the total polarization of a dielectric material is defined by the following relation [62]:

$$P_T = P_c + P_d + P_a + P_e \qquad \text{(I.16)}$$

where Pc, Pd, Pa, and Pe are the polarization by space, dipole, atomic and electronic charges respectively

I.9.1 Space charge polarization (Pc)

In crystalline materials such as ceramics, the grain boundaries are areas that can accumulate free charges (ions in interstitial positions, gaps, and electrons due to doping...); this type of polarization is present at around 100 Hz.

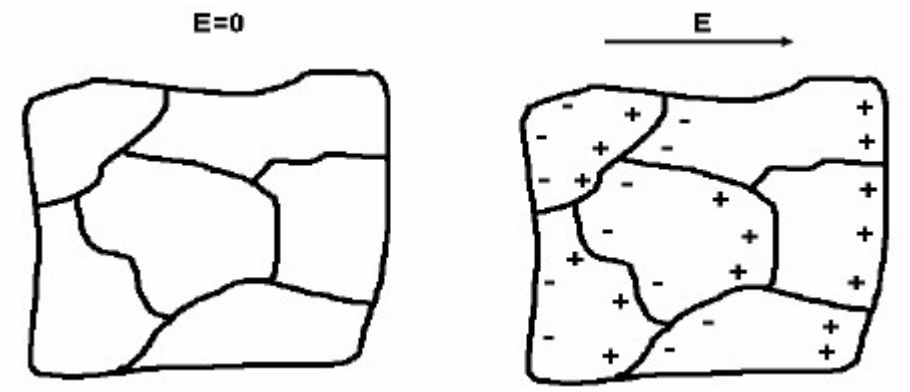

Figure I. 9: Displacement of free carriers that concentrate at defects, grain boundaries, surfaces, etc. creates polarization at the interfaces.

I.9.2 Dipole polarization (Pd)

In the equilibrium state, the global dipole moment of the material is zero, because the permanent dipoles of the material are randomly oriented (Figure I.10). Under an external electric field, the dipoles tend to orient themselves parallel to it and the result is a non-zero overall dipole moment. Dipole moments can be oriented under the action of an electric field at frequencies around 10^5 Hz (100 kHz).

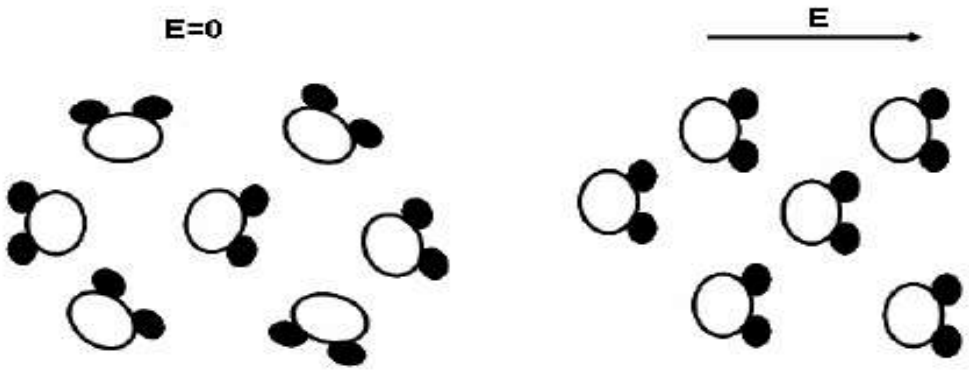

Figure I. 10: Displacement of permanent dipoles (e.g. molecules) which are oriented to be parallel to the field.

I.9.3 Atomic or ionic polarization (Pa)

The appearance of ionic polarization was realized by subjecting the ionic material to an external electric field. The ions leave their mean equilibrium positions and move or not in the direction of the electric field (Figure I.11). This polarization occurs at frequencies on the order of (10 GHz-1 THz).

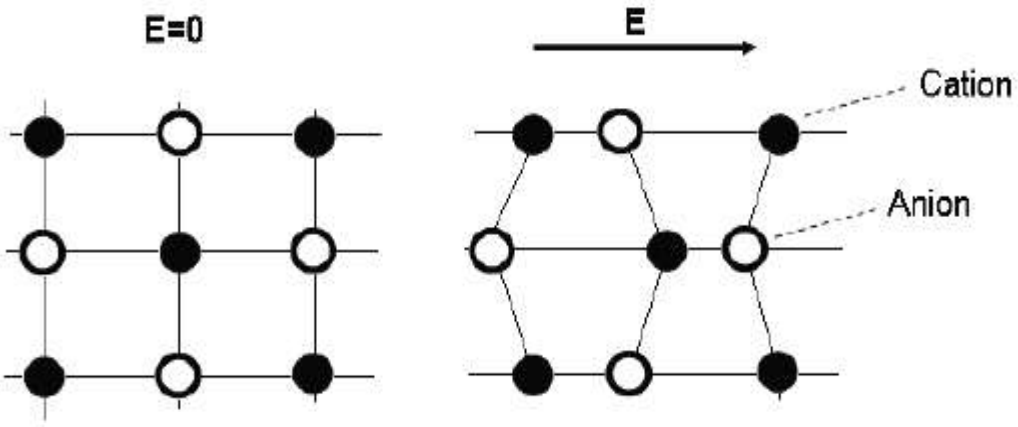

Figure I. 11: Relative displacement of oppositely charged ions with respect to each other.

I.9.4 Electronic polarization (Pe)

An electron orbital has a strong inclination to deform under an electric field with a frequency of 10^{18} Hz. This results in a displacement of the electrons relative to the nucleus, which leads to the formation of an induced electric dipole moment (Figure I.12).

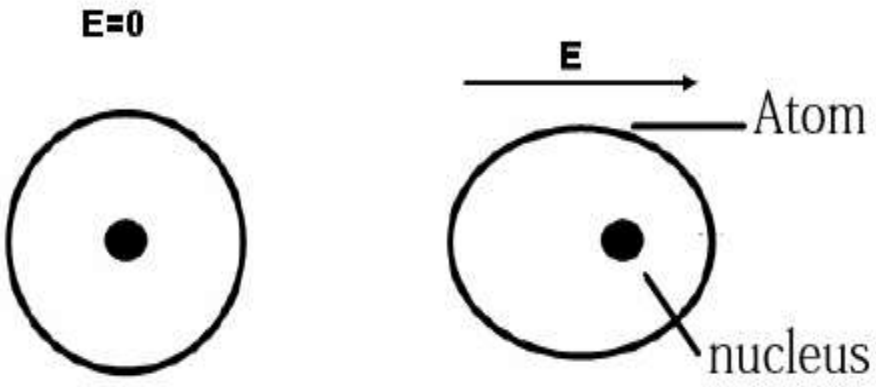

Figure I. 12: Displacement of the center of inertia of the electronic cloud with respect to the center of inertia of the nucleus of the atoms

I.10 Perovskite structure

The origin of the term Perovskite can be traced back to the Russian mineralogist Lev Perovski, who is attributed with his discovery of the mineral $CaTiO_3$ [63], Since then, this term has been used for all classes that have the same general structure ABX_3 [64]. The materials of the perovskite structure have a general formula ABX_3, where the cations occupy the A and B sites, for the B cation is coordinated six times to the X anion, forming a BX_6-cornered octahedron framework, the A cation filling the cavities of the framework [65]. The highest symmetry of the perovskite structure belongs to a cubic space group Pm3m, where the cation A is in the center of the cube-shaped cavity [66], the displacement of cations can decrease the symmetry of the perovskite structure, this deformation makes the perovskite structure generally an orthorhombic or tetragonal phase [67]. The perovskite structure is illustrated in Figure I.13. The excellent piezoelectric properties of the PZT family of ceramics (which have a perovskite structure) prompted and encouraged Jaffe, Roth, and Marzullo to continue their research in this area [51].

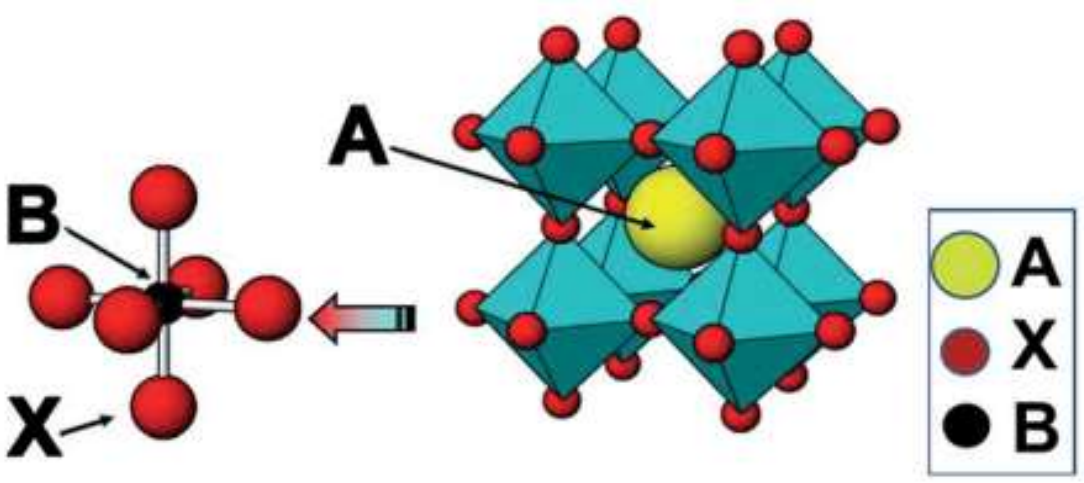

Figure I. 13: Illustration of perovskite crystal structure [68].

I.10.1 Classification of the perovskite structure

In general we can classify perovskites in two types according to their occupation in sites A and B [69].

I.10.1.1 Simple perovskite

Simple perovskites are perovskites that have only one type of ion or one chemical element in the A and B sites like $CaTiO_3$, $BaTiO_3$, and $SrTiO_3$...

I.10.1.2 Complex perovskite

Contrary to simple perovskites, complex perovskites are characterized by the multi-element in the A and B sites i.e. there are two or more chemical elements in both sites, one can also find complex perovskites in which the A and B sites are occupied by two or more chemical elements at the simultaneously as $(Pb_{1-x}La_x)(Zr_yTi_{1-y})O_3$.

I.10.2 Stability of the perovskite structure

To say that a perovskite structure of general formula ABO_3 is stable, it is necessary to check the three following essential conditions: Electroneutrality condition, Stoichiometric condition, tolerance factor.

I.10.2.1 Electro-neutrality condition

Among the conditions of the stability of the perovskite structure of general formula ABO_3 is the electro-neutrality, that is to say, that the sum of the charges of the sites A and B and O is zero because Oxygene is an anion of negative charge O^{-2} (the sum of the anionic charge is equal to -6) and the sum of the cation is the inverse of the anions ((+6) A^{+2} and B^{+4}).

$$\sum_{i=1}^{n} X_{Ai}Z_{Ai} + \sum_{j=1}^{n} X_{Bi}Z_{Bi} = 6 \qquad \text{(I.17)}$$

With:

X_{Ai} : The fraction of moles of cation Ai .

X_{Bj} : The fraction of moles of the cation Bj.

Z_{Ai} : Valence number of cation Ai.

Z_{Bj} : Valence number of cation Bj.

I.10.2.2 Ionicity of the bonds

To evaluate the stability of the perovskite structure ABO_3 it is necessary to determine the difference in electronegativity between the ions [70]. Perovskite structures will be more thermally stable the more pronounced the ionic character of the cation-anion bonds. The ionicity of the bonds can be determined by the following formula:

$$\Delta E = \frac{\bar{\chi}_{A-O} + \bar{\chi}_{B-O}}{2} \quad \text{(I.18)}$$

Where $\bar{\chi}_{A-O}$ and $\bar{\chi}_{B-O}$ are the differences in electronegativity between cations A and B and the associated oxygens, high ΔE values support the thermal stability of the perovskite structure.

I.10.2.3 Tolerance factor

Megaw [71] was the first to propose the tolerance factor "T". This factor is fixed to determine the stability of the perovskite structure for a given set of anions and cations, among the important parameters related to the symmetry of perovskites and which have a considerable influence on the dielectric properties are the tolerance factor and the lattice parameter. In the structure of perovskite, the A cations, slightly larger than the B cation, are coordinated with 12 oxygen ions, while the B cations with 6 oxygen ions. Meanwhile the oxygen anions are coordinated with two B-site cations and four A cations. The definition of the tolerance factor was made by Goldschmidt [72] we used the following equation to calculate the tolerance factor [73]

$$T = \frac{R_A + R_O}{\sqrt{2}(R_B + R_O)} \quad \text{(I.19)}$$

In which R_A, R_B, and R_O are the ionic radii of the A-site, B-site, and oxygen atoms, respectively. The most stable perovskite structure is the structure that has the tolerance factor closest to 1, moreover when t >1 the ferroelectric phase will be stable on the other hand if t <1 the anti-ferroelectric phase becomes the most stable [74].

I.11 Applications of perovskite materials

Over time, perovskite-type materials have become increasingly used as they have great potential to contribute to solid fuel cells, solid electrolytes, fixed resistors, actuators, electromechanical devices, transducers, etc., due to the particular crystalline structure, magnetism, electrical conductivity, piezoelectric and electro-optical properties, catalytic activity and gas sensitivity,...etc [75, 76].

I.11.1 Electricals applications

The role played by perovskite in modern electronics is certainly very important. They have a wide range of applications such as memories, capacitors, microwave devices, pressure gauges, and ultrafast electronics. They are superconduct at relatively high temperatures, convert mechanical pressure or heat into electricity (piezoelectricity), accelerate chemical reactions

(catalysts), and suddenly change their electrical resistance when placed in a magnetic field (magnetoresistance). Several electrochemical studies on electrodes based on perovskite-type materials have been carried out in aqueous medium [77]. They revealed an important electro-catalytic role in the oxygen electrode reaction at room temperature.

I.11.2 Catalytic Applications

The catalyst layer is typically a metal grid, or other ceramic matrix structure designed to provide maximum surface area support for the catalyst. The active material is deposited on this support in a way that maintains a large active surface area. In the catalytic oxidation phenomenon, oxygen is fixed in the crystal lattice and it is involved in the gas phase. The mechanism of this phenomenon includes an oxidation cycle (which takes place on the surface of the oxide) between the anionic oxygen present on the surface and a reactant in the gas phase.

I.11.3 Conductor

The electronic or essentially electronic conductive materials used as fuel cell [78] cathodes are ABO_3 formulated perovskites where A is generally rare earth and B a transition metal. The perovskites also have become a burning topic in solar cell research in recent years due to the rapid increase in energy conversion efficiency exceeding 20% and the ease of precursor processing from solution. Emerging from the dye-sensitized solar cell [79], the device concept of perovskite solar cells has developed into a typical thin-film design with a compact nanocrystalline perovskite layer of about half a micron thickness sandwiched between charge transport layers (solid-state) and planar electrodes [80].

I.12 Lead Zirconate Titanate (PZT)

I.12.1 Overview of the selected material

Since the 1950's, PZT materials have been a challenge for Shirane and his team [81, 82], since then, studies have commenced on these materials. Lead zircano-titanate (abbreviated to PZT) is a polycrystalline solid solution with a perovskite ABO_3 structure consisting of two components lead titanate ($PbTiO_3$) and lead zirconate ($PbZrO_3$), which are ferroelectric and anti-ferroelectric materials respectively [7], whose piezoelectric and dielectric characteristics are significantly better than those of the initial compounds [83] the same system of this solid solution can be elaborated with different compositions just by varying the Zr/Ti ratio. If the

composition is rich in Zr the structure obtained is Rhombohedral (Zr/Ti > 54:46) while when the composition is rich in Ti (Zr/Ti < 48:52) our structure is tetragonal.

I.13 Morphotropic phase boundary

Some ferroelectric perovskite-type solid solutions have excellent properties such as high piezoelectric response and dielectric constant, Among the ferroelectric materials that are commonly used for Morphotropic applications (generally complex oxides) are Lead Titano-Zirconate PZT ($Pb[Zr_{1-x}Ti_x]O_3$). Historically, the Zr/Ti ratio of the PZT system has not been precisely defined to say that we are in or near the region where the morphotropic phase boundary [82, 84, 85]. The two phases or the two rhombohedral and tetragonal structures coexist in an intermediate composition, this composition is located in a region called morphotropic phase boundary MPB where the region that associates these two structures at room temperature, this region is located at a Zr:Ti "53:47 point [55]. Studies of the PZT system in recent years have found that below the paraelectric-ferroelectric transition temperature there is a region of coexistence of tetragonal and rhombohedral phases close to the MPB composition, although the extent of this region is still subject to debate. The effect of adding small amounts of dopant can shift the MPB and increase the width of the coexistence region [86]. It is a region where the piezoelectric and dielectric properties are maximal. Jaffe and Cook determined the phase diagram from X-Ray Diffraction (XRD); this diagram is illustrated in figure I.14. In the phase diagram, the MPB is represented as a line, it is generally found that the tetragonal and rhombohedral phases coexist in a limited range of compositions around the MPB [87, 88], more factors can influence this range such as precursors, processing conditions, etc.

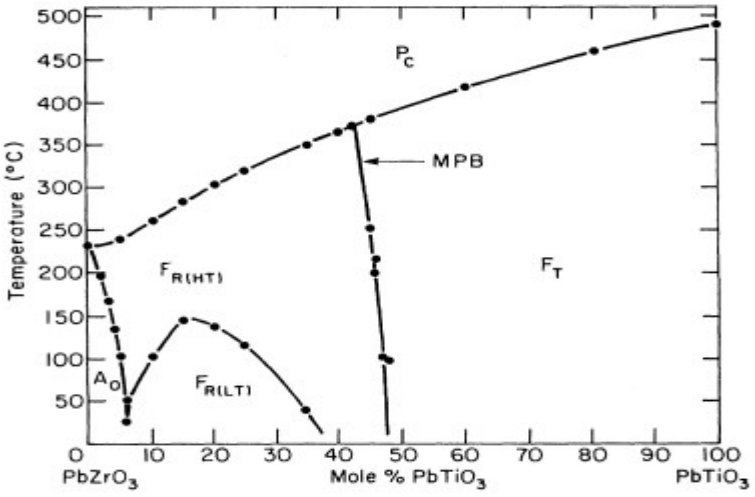

Figure I. 14: Phase diagram of PZT [89]

I.14 Effect of doping on the properties of PZT materials

In solid chemistry, to modify or improve the properties of materials and reach the optimal response, we adjust or add an additive that corresponds to the chemical element of our material; we talk about doping of material. A dopant is a small amount of element introduced into the material by incorporating it into the crystal lattice of the chemical material which can improve initial electrical properties. In the case of PZT of general formula $Pb(Zr_{1-x}Ti_x)O_3$ is generally modified by the addition of one or more cations which replace the Pb^{2+} in the A site or the couple (Zr^{4+}/Ti^{4+}) in the B site.

Basically, there are 3 types of dopants that have been generally used in the modification of the composition of PZT: isovalent dopants, acceptor dopants, and donor dopants [7, 90, 91].

I.14.1 Isovalent dopants

They are dopants of valence equal to that of the substituted ion such as Ba^{+2}, Sr^{+2}, Ca^{+2} which can substitute them in the A-site and Ce^{+4} and Sn^{+4} in B-site, the effect of this type of dopants can increase the dielectric permittivity of the PZT and decrease the Curie temperature, Similarly, we can substitute the oxygen ion by the fluorine ion (which is the case in our study), associating a cationic substitution by an ion of lower valence, which allows to obtain materials with a high mechanical quality factor (Q) presenting a great stability of d_{33} under uniaxial constraint, we could also have multiple substitutions by several unstable multiple valence ions or several stable valence ions. The overall influence on the properties depends on the concentration and valence of each ion.

These dopants can increase:

- The ionic character of the mesh
- The stability of the structure
- The permittivity (ε)

and can also reduce the curie temperature Tc .

I.14.2 Donor dopants

Donor dopants, which are higher valence cations than the substituted ion, we mention La^{3+}, Nd^{3+}, Bi^{3+}, Sb^{3+} in the A-site and Nb^{+5}, Sb^{5+}, Ta^{5+}, and W^{6+} in the B-site. The resulting PZT materials are called soft because they are easily polarizable. Cationic vacancies such as Pb^{2+} vacancies in the A site compensate the excess of positive charge provided by the donor dopants, where a change of valence from Ti^{4+} to Ti^{3+}, These ceramics can be used in low

power actuators and transducers (non-destructive testing, medical ultrasound, positioning devices...).

The properties that are increased by the donor dopants are:

- The dielectric permittivity
- Dielectric losses
- Coupling coefficients

There is a decrease of:

- Mechanical quality factor
- Coercive field
- Conductivity and Curie point

I.14.3 Acceptor dopants

Acceptor dopants with a lower valence than the substituted ion, the acceptor dopants make the PZT materials hard because they depolarize with difficulty under the action of a constraint, the acceptor dopants also make the PZT materials hard because they depolarize with difficulty under the action of a stress, they induce the formation of oxygen vacancies (Figure I.15) resulting in a contraction of the lattice, it has been observed that the field application reduces the movement of the domain walls, but their characteristics remain stable under a high field.

This type of dopant increases:

- Mechanical quality factor
- Coercive field
- Conductivity

and a decrease in:

- Permittivity
- Dielectric losses
- Coupling coefficients

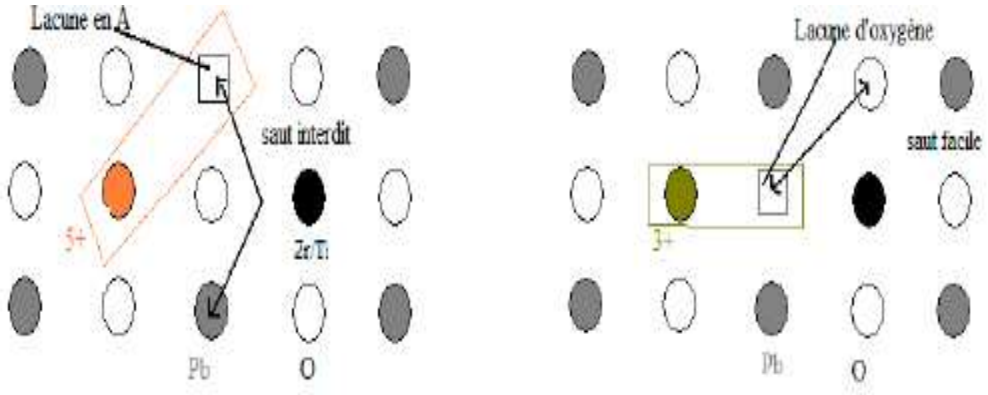

a) Donor doping (soft materials) b) Acceptor doping (hard materials)

Figure I. 15: Defects created in the PZT lattice after substitution by donor (a) or acceptor (b) ions [55]

Chapter II Experimental part

Chapter II: Experimental part

II.1 Introduction

The experimental chapter of this thesis aims to present the different steps of the experimental protocols. In this chapter, we will describe in detail the different steps and techniques used for the synthesis of our materials, their characterization, and their evaluation. We will also explain the reaction conditions, the experimental parameters, and the equipment used to carry out these experiments.

First, we will explain the synthesis method that we have chosen in the experimental part of the studied compounds, as well as the characterization techniques used to confirm their structure and purity.

In a second time, we detailed and discussed the starting materials or precursors and dopants (oxides). Finally, we will detail the experimental protocols implemented to evaluate the performance of the studied compounds. We will present the different analytical techniques used to evaluate the physicochemical properties of the compounds, such as X-ray diffraction, FTIR, and SEM.

Among the most important factors that can influence the properties of our materials are the method of synthesis and the precursors, so it is necessary to choose the method of synthesis, generally, there are two main methods of synthesis or elaboration: solid method such as the solid state reaction method (ceramic method) [92] and liquid method such as the sol-gel and [93] the hydrothermal synthesis [94].

So the method we are interested in is the solid-state method, it's the method of synthesis by solid way.

II.2 Solid-state reaction method

The solid-state reaction method, also known as solid-state synthesis, is a widely used process in materials science and chemistry for synthesizing new compounds from solid precursors. It involves the mixing of reactants in a solid state, followed by heating to initiate a chemical reaction that results in the formation of a new solid product.

Solid-state reactions can occur through various mechanisms, such as diffusion of atoms through the solid, melting and recrystallization, and formation of intermediate phases. The reaction can take place in a variety of environments, such as a vacuum or an inert gas atmosphere, and the reaction temperature can range from room temperature to several hundred degrees Celsius.

This method has been utilized in the synthesis of a diverse range of materials, including ceramics, intermetallic, and organic compounds, and has important applications in fields such as energy storage, catalysis, and electronic materials [95, 96].

II.3 Sample preparation

In our study, we will prepare a series of the composition of PZT type ceramics $Pb_{1-x}Ba_x(Zr_{0.52}Ti_{0.43}(Al_{0.5}Sb_{0.5})_{0.05})O_3$ where x =0.00, 0.02, 0.04, 0.06, 0.08, and 0.10. The exception of this study is the diversity of dopants, so there are several dopants that we added in our basic matrix, but the most important study that we will base on is the effect of barium substitution in our basic matrix on structural, morphological, and dielectric properties.

II.3.1 Precursor

The basic components of these types of materials are oxides such as PbO, ZnO_2, and TiO_2.

II.3.1.1 Lead monoxide PbO:

Lead monoxide, also known as lead (II) oxide, is a chemical compound composed of lead and oxygen, with the molecular formula PbO. It is a yellow or reddish-brown powder and is commonly employed as a precursor in the preparation of PZT-type ceramics.

It is produced industrially by heating lead in the presence of air, a process known as roasting. The resulting lead oxide is then reduced to lead metal using carbon or another reducing agent.

The following table details the datasheet for lead oxide

Table II. 1: lead oxide datasheet

Chemical formula	PbO
Molecular weight	223.20 g/mol
CAS number	1317-36-8
Appearance	Yellow
Melting point	888°C
Boiling point	1470°C
Solubility	Insoluble in water, soluble in acids
Density	9.53 g/cm^3

II.3.1.2 Zirconium dioxide ZrO_2

Zirconium dioxide, also known as zerconia, is a white crystalline oxide of zirconium; it is mostly produced synthetically for various industrial applications such as ceramics, refractor materials, and high-performance coatings [97].

Table II. 2: Zirconium dioxide datasheet

Chemical formula	ZrO_2
Molecular weight	123,22 g/mol
CAS number	13463-67-7
Appearance	White powder
Purity	99%
Boiling point	4000 °C
Melting point	2715 °C
Solubility	insoluble in water and organic solvents
Density	5.68 g/cm^3

II.3.1.3 Titanium dioxide TiO_2:

Titanium dioxide, also known as TiO_2, is a naturally occurring mineral with the chemical formula TiO2. It is widely used in various industries, including cosmetics, food, and electronics, due to its unique properties such as excellent UV absorption capacity and photocatalytic activity. Regarding its chemical structure, titanium dioxide comprises titanium and oxygen atoms arranged in a crystalline lattice structure [98].

Table II. 3: Titanium dioxide datasheet

Chemical formula	TiO_2
Molecular weight	79.9 g/mol
CAS number	13463-67-7
Appearance	White powder
Purity	99%
Melting point	1843°C
Solubility	insoluble in water and organic solvents
Density	3.9 g/cm^3

II.3.2 Dopants

Several studies [10, 11] have reported that the substitution effect regardless of the A and/or B site is an effective method to enhance the dielectric properties. The dopants can be classified into three categories [7, 12], the isovalent dopants such as (Ba^{2+}) [13] and (Sr^{+2}) [14], donor dopants (Sb^{+5}) [15], and acceptor dopants (Al^{+3}) [16], the category that attracts us is the isovalent dopants (Ba^{2+}) because of their effect on dielectric properties, where they can reduce the curie points, increase the dielectric constant [7], as well as avoiding the pyrochlore composition in perovskite structure [17]. This is what prompted some studies to investigate the barium impact substitution into PZT ceramics' dielectric properties [13, 18, 19]. Xiucai Wang et al. [20] found that the Ba^{2+} ion doping into PZT ceramics shows a very interesting effect on the dielectric properties and decreases the curie temperature from 85 to 48°C. The same tendency has been found by Dipti et al. [21] and Neha et al. [10] when Ba^{2+} ions were incorporated into the PZT system.

Among the dopants we used in this experimental part are:

II.3.2.1 Al_2O_3:

Al_2O_3, also known as aluminum oxide or alumina, is a chemical compound with the formula Al_2O_3. It is one of the most commonly used materials in ceramics and other high-temperature applications due to its high melting point [99].

Table II. 4: Aluminum oxide datasheet

Chemical formula	Al_2O_3
Molecular weight	101.96 g/mol
CAS number	1344-28-1
Appearance	White powder
Purity	98%
Melting point	2,072°C (3,762°F)
Solubility	low solubility in water
Density	from 3.95 to 4.1 g/cm^3

II.3.2.2 Sb_2O_5:

Antimony pentoxide (Sb_2O_5) is an oxide of antimony; it is commonly used materials in ceramics, Sb_2O_5 has a molecular weight of 323.52 g/mol and a melting point of 380 °C. Sb_2O_5 is used in the production of glass and ceramics as a fining agent to improve clarity [100].

Table II. 5: Antimony pentoxide datasheet

Chemical formula	Sb_2O_5
Molecular weight	323.52 g/mol
CAS number	1314-60-9
Appearance	White powder
Purity	99.99 %
Melting point	380°C (716°F)
Solubility	low solubility in water
Density	3.78 g/cm^3

II.3.2.3 $BaCO_3$:

Barium carbonate ($BaCO_3$) is a white crystalline powder composed of barium and carbonate ions. It is commonly used in the production of glass and ceramics, as well as in the manufacturing of other barium compounds [101].

Table II. 6: Barium carbonate datasheet

Chemical formula	$BaCO_3$
Molecular weight	197.34 g/mol
CAS number	513-77-9
Appearance	White powder
Purity	99%
Melting point	811°C (1,492°F)
Solubility	low solubility in water
Density	4.29 g/cm^3

II.4 Elaboration process

The sample preparation is a crucial step in the characterization of materials, especially in research materials such as ceramics. The quality of the characterization results depends to a

large extent on the quality of the prepared samples, sample synthesis must be carefully carried out to produce homogeneous and reproducible samples, the following figure illustrates in detail the steps of the synthesis method we have chosen (ceramic method).

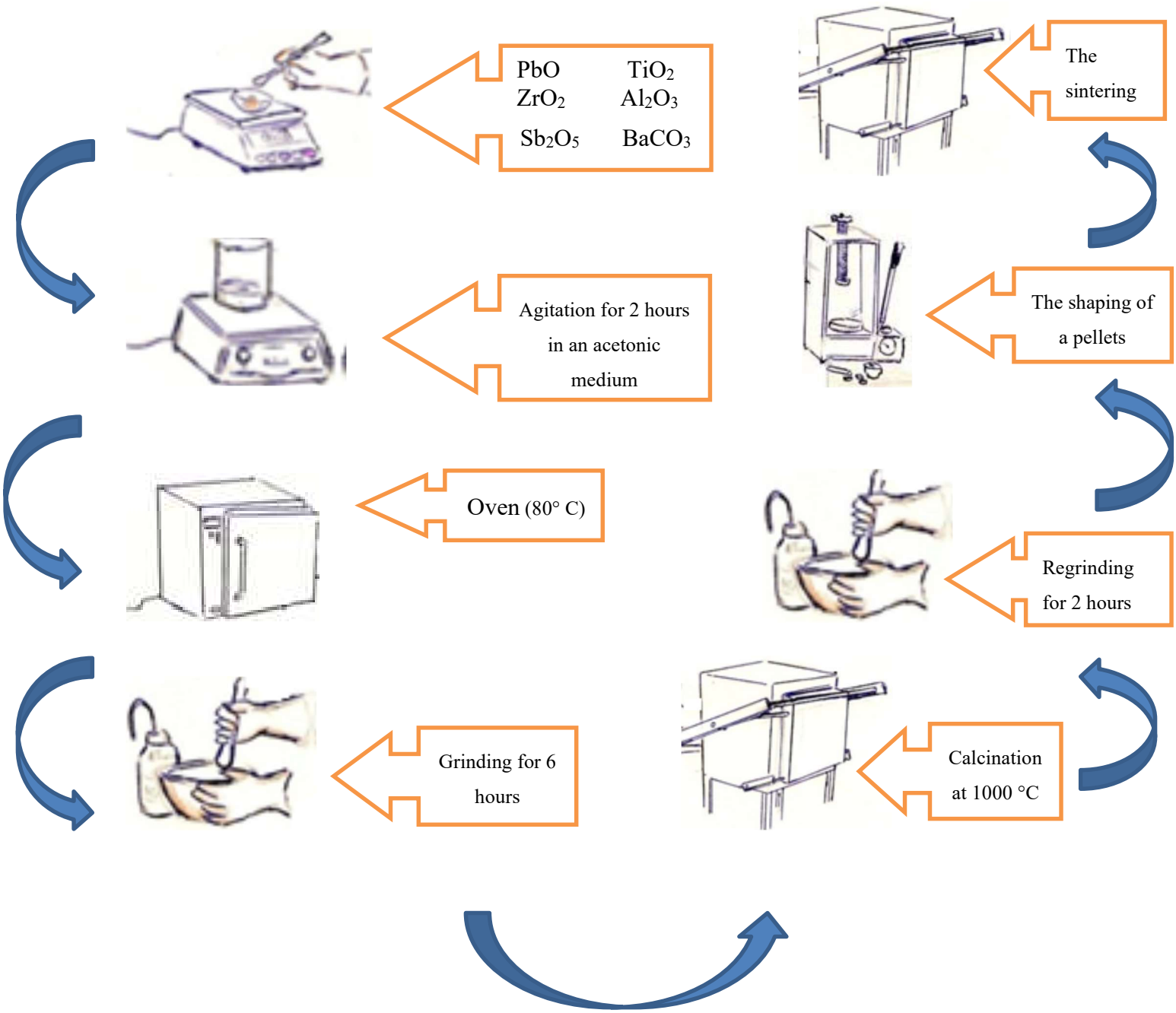

Figure II. 1: The different steps to prepare the samples [102].

II.4.1 Weighing and mixing

The first step in the preparation of ceramic material is to weigh and mix the necessary powders. This step is of paramount importance as it ensures the composition and purity of the final ceramic. To obtain a homogeneous composition, it is essential to accurately weigh the different powders and mix them efficiently. We followed an equation to calculate the initial masses of the starting materials (the basic matrix materials and the dopants) before weighing and mixing them. Errors in weighing or mixing can cause significant variations in the composition we are trying to obtain, which can affect its properties and performance. We put this mixture in a beaker under agitation for 2 hours in an acetonic medium (because the acetone evaporation temperature is low) to facilitate the distribution of the grains and to obtain a very homogeneous mixture, and then we dry it in an oven for another 2 hours at 80° C.

II.4.2 Grinding

Grinding is an essential step in the preparation of PZT ceramics. It allows to reduce the size of the powders used and to obtain very fine particles as well as to homogenize the composition of the ceramic.

It allows the reduction of the size of the powders used, obtains wonderful particles, and homogenizes the composition of the ceramic

In our case, after taking our sample out of the oven, we have to grind it for 6h, which makes the grains closer to each other to help the formation of the perovskite structure during the heat treatment step.

II.4.3 Calcination:

The calcination step is a crucial part of the synthesis of PZT ceramics. It involves heating the mixture of PZT precursors to high temperatures to convert them to the desired perovskite phase. During this process, the organic components of the precursors are decomposed and removed, and the remaining inorganic components react to form the perovskite structure. The calcination temperature we want to achieve to form the perovskite structure is 1000 °C for 2h with a heating rate of 2°C/min in a programmable heater [103]. The calcination temperature and duration are carefully controlled to ensure the formation of the perovskite phase, while minimizing the formation of undesirable secondary phases, the calcination cycle scheme is shown in Figure II.2.

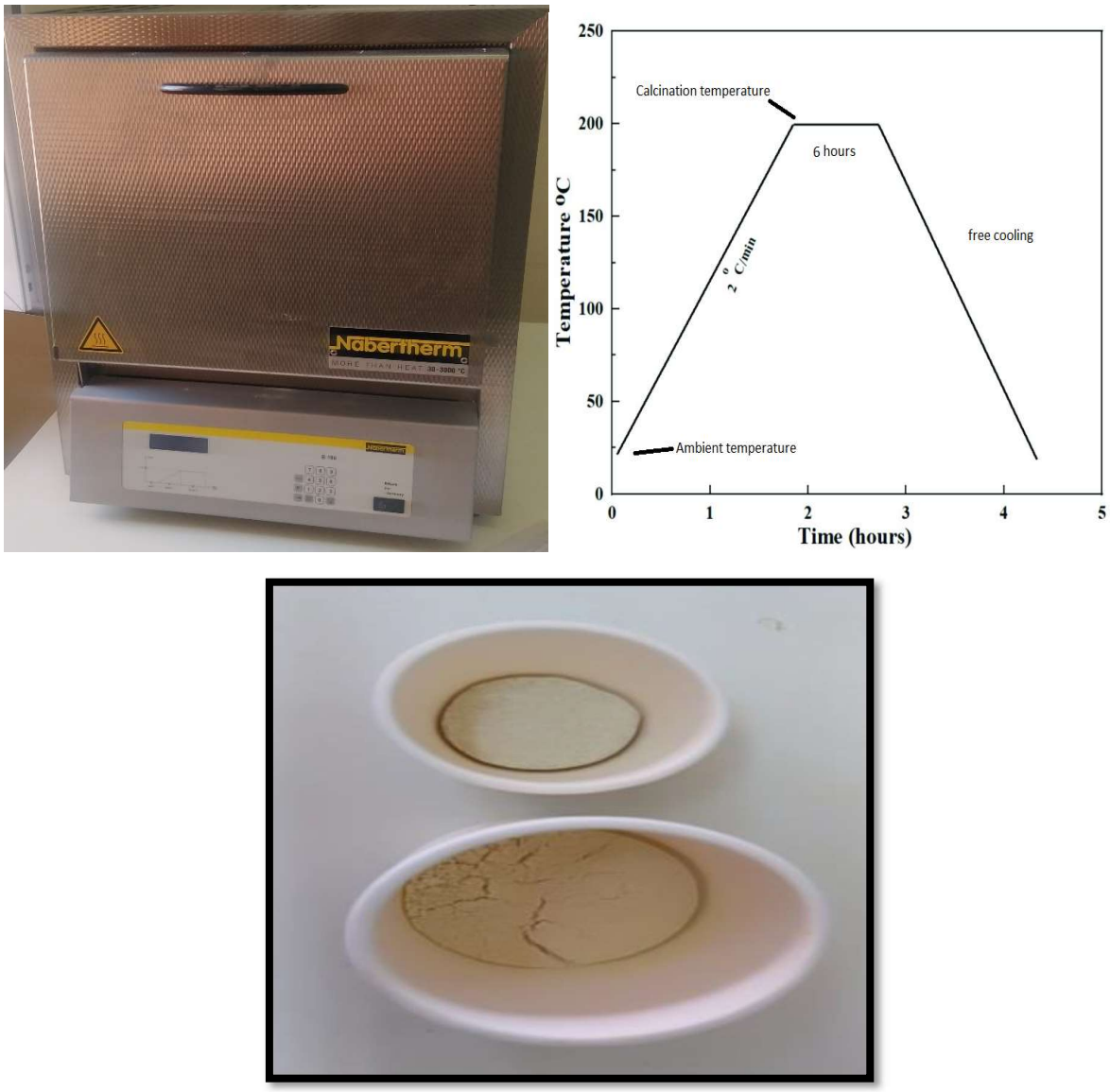

Figure II. 2: The calcination cycle diagram and the heating oven.

II.4.4 The shaping of a pellets

We take the mixture out of the heating oven and grind it again for 2 hours. The grinding of calcined powder aims to reduce the grain size and homogenize the powder; this allows for improving the properties of our sample, such as density and conductivity. The obtained powders were mixed with 5% by weight of polyvinyl alcohol as a binder before being compacted into disk-shaped specimens and pressed into cylindrical pellets of 10 mm diameter and about 3 mm height by pressing at 1 ton/cm^2 for 5 min by a hydraulic uniaxial press.

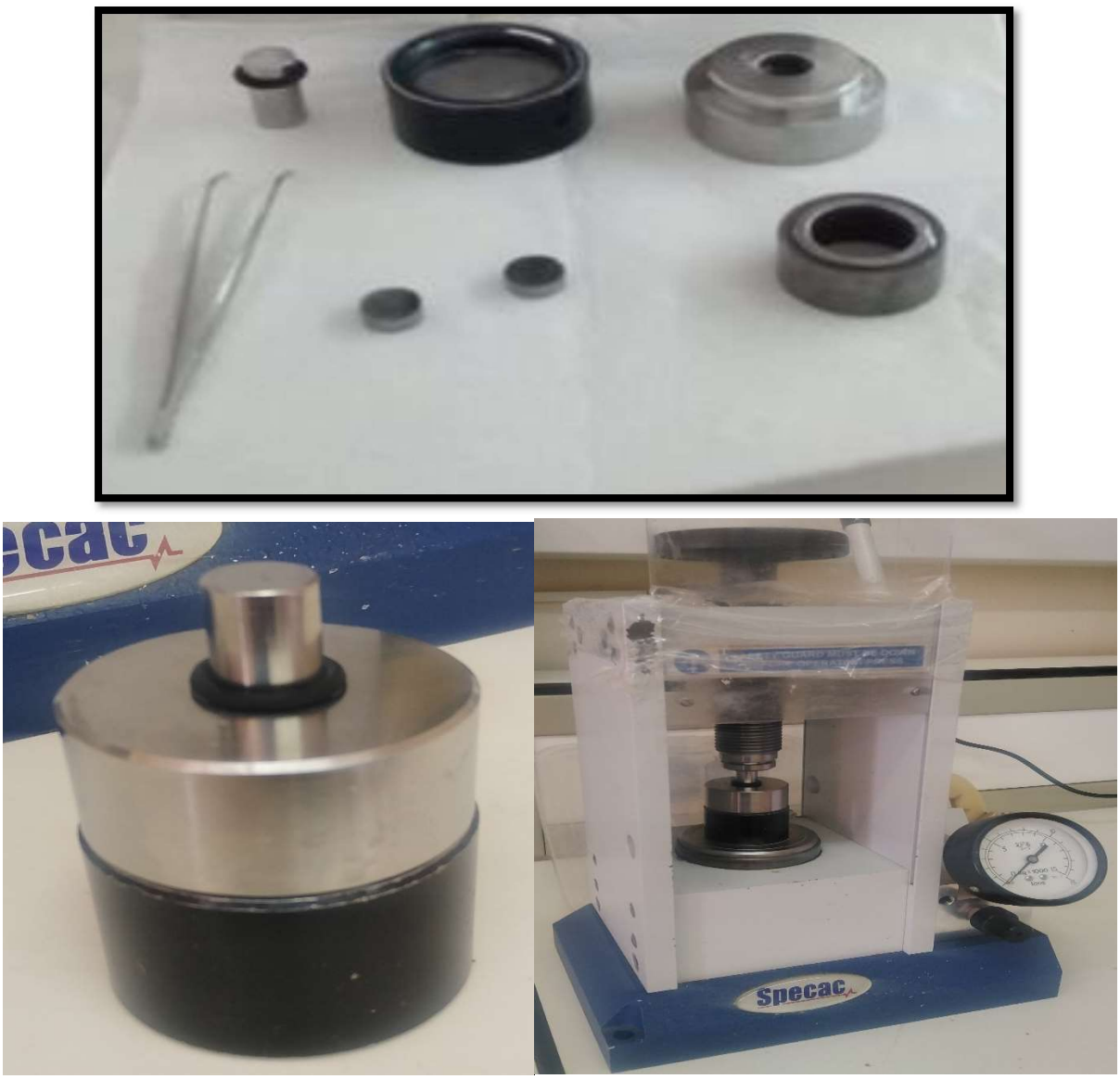

Figure II. 3: hydraulic uniaxial press

II.4.5 The sintering

This heat treatment process, called sintering, is an essential step in the preparation of samples to achieve the desired properties. Typically, after the synthesis and shaping of the specimens, the green compact is subjected to heat treatment at elevated temperatures. This removes any residual organic material from the sample and facilitates the densification of our material. The temperature and the duration of sintering are critical factors that affect the final microstructure and properties of the PZT ceramic [104]. Thereafter, to compact the pellet and reduce the porosity, the pellets were sintered at several temperatures (1190, 1210, 1230, 1250, and 1270

°C) for 2 hrs, with the same heating rate. To avoid lead loss during the sintering process and improve the density, lead zirconate (PZ) should be added [9, 105].

Figure II. 4: The position of the pellets during sintering.

II.5 Characterization technique:

II.5.1 XRD Analyses

X-ray diffraction (XRD) analysis is a technique used to study the atomic and molecular structure of crystalline materials. It involves irradiating a sample with X-rays and measuring the diffraction pattern of the diffracted X-rays. This pattern provides information about the arrangement of atoms in the sample, such as crystal lattice parameters, unit cell dimensions, and the presence of crystallographic defects or impurities. XRD is based on the principle of constructive interference of X-rays diffused by the planes of the crystal lattice. By measuring the angles and intensities of the diffracted X-rays, researchers can determine the spacing between the lattice planes and calculate the crystal structure of the material under study. This information is crucial for understanding the physical and chemical properties of materials, as well as for identifying unknown substances [106].

The Bragg's law, named after Sir William Lawrence Bragg and his father Sir William Henry Bragg, is a fundamental principle in the field of X-ray crystallography. It describes the relationship between the angles of incidence and the resulting constructive interference of X-rays when they interact with crystalline material. The Bragg's law, named after Sir William Lawrence Bragg and his father Sir William Henry Bragg, is a fundamental principle in the field of X-ray crystallography. It describes the relationship between the angles of incidence

and the resulting constructive interference of X-rays when they interact with crystalline material. According to Bragg's law, the X-rays incident on a crystal lattice will undergo constructive interference and produce a diffracted beam if the following condition is met:

$n\lambda = 2d \sin(\theta)$

where:

- n is an integer representing the order of the diffracted beam.

- λ is the wavelength of the incident X-rays.

- d is the spacing between the crystal lattice planes.

- θ is the angle of incidence between the incident X-rays and the crystal lattice planes.

Bragg's law has been instrumental in the advancement of X-ray crystallography and has contributed to numerous scientific discoveries and applications, including the determination of crystal structures, the study of molecular and atomic arrangements, and the analysis of crystal defects [107]. The instrument used for this analysis is Rigaku Miniflex 600 used the radiation of Cu Ka of Copper y= 1.5406 Å. The phase ratios (tetragonal and rhombohedral) were determined by peak deconvolution using Origin, the Bragg's angle (2θ) has been scanned from 10° to 90° with a scanning rate of 0.04°/sec at room temperature.

Figure II. 5: XRD instrument (Rigaku Miniflex 600).

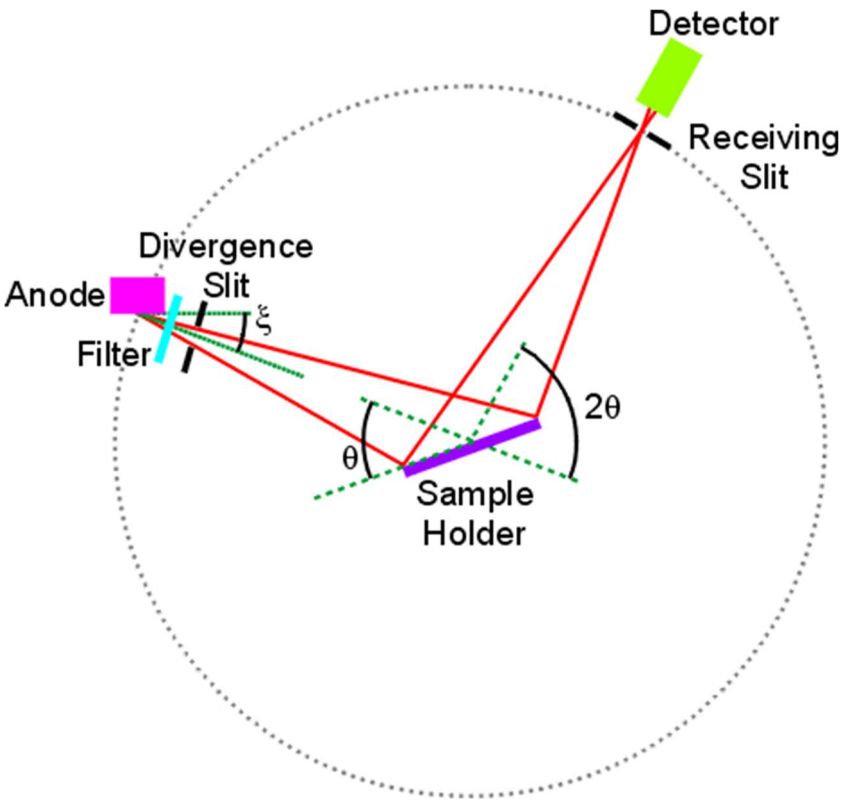

Figure II. 6: Schematic diagram of a diffractometer system. [108].

II.5.2 Scanning electron microscopy SEM

Scanning electron microscopy SEM is a very useful imaging technique that is widely used in a variety of scientific fields. It enables the surface composition of a sample to be viewed at high resolution. In this technique, a focused electron stream is scanned through the sample, and the resulting signals are collected to generate an image [109, 110]. Advanced SEM systems can also offer additional features such as energy-dispersive X-ray spectroscopy EDS for elemental analysis. In conclusion, scanning electron microscopy SEM is a versatile technique for obtaining high-resolution images of a sample's surface composition. SEM provides also valuable information on the porosity and density of materials [111]. All the SEM analyses we have presented in this study are carried out in the CRAPCI analysis laboratory.

II.5.3 Fourier Transform Infrared Spectroscopy FTIR

FTIR, which stands for Fourier Transform Infrared Spectroscopy, is a widely used analytical technique that provides valuable information about the chemical composition and molecular structure of a sample by analyzing its interaction with infrared radiation. In FTIR spectroscopy, a beam of infrared light is passed through a sample, and the absorption and

scattering of the light by the sample are measured. The infrared light consists of a range of wavelengths that correspond to different vibrational modes of the sample's constituent molecules. When the sample absorbs specific frequencies of infrared light, it causes characteristic energy transitions that can be used to identify functional groups and chemical bonds present in the sample.

The key principle behind FTIR spectroscopy lies in the use of an interferometer. The interferometer splits the incoming infrared beam into two paths: one that interacts with the sample and another that serves as a reference. The two beams are recombined, creating an interference pattern known as an interferogram. By applying a mathematical technique called Fourier transform to the interferogram, a spectrum is obtained, which represents the absorption intensity as a function of wavelength or wavenumber. FTIR spectroscopy has a wide range of applications in various fields, including chemistry, pharmaceuticals, polymers, materials science, and environmental analysis. It enables the identification of unknown substances, characterization of functional groups, analysis of chemical reactions, determination of molecular structures, and investigation of material properties [112, 113]. The Fourier Transform Infrared spectroscopy FTIR of the samples was carried out on a PerkinElmer FT-IR Spectrum Two Spectrophotometer in the wavelength range of 400–1500 cm^{-1} in the photonic physics and multi-functional nanomaterials research laboratory LPPNM at the University of Biskra, which is controlled by a computer using UV Winlab software.

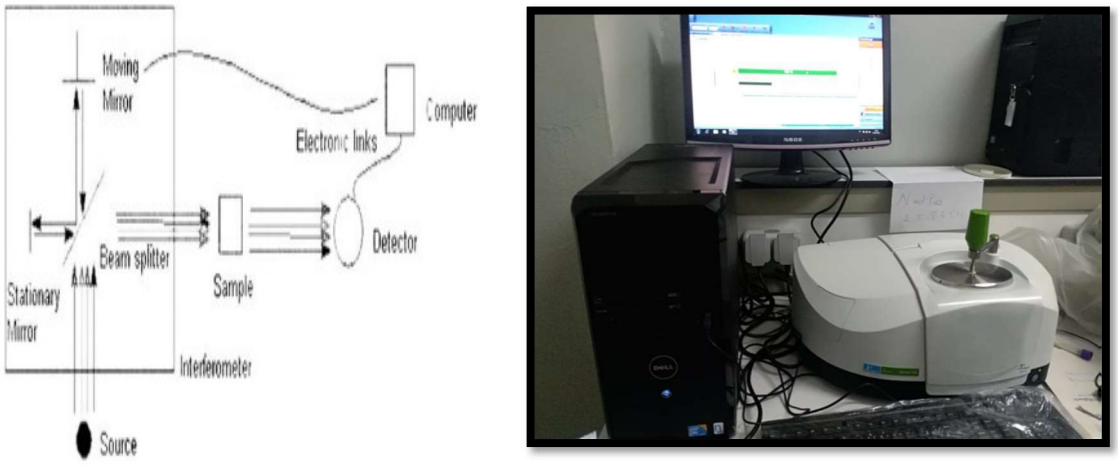

Figure II. 7: Schematic diagram of a Fourier transform infrared instrument. [114].

II.5.4 Density

The density of ceramics is an essential factor in achieving the maximum properties of our materials, defined as mass per unit volume. The higher the density, the better the piezoelectric

and Ferroelectric properties were obtained, this is because a denser material allows for better alignment of the crystal structure, leading to enhanced polarization and more efficient conversion of electrical energy into mechanical motion and vice versa. Moreover, the density of PZT ceramics also influences their dielectric properties, including dielectric constant and dielectric loss. Higher densities generally lead to higher dielectric constants, which is desirable for applications requiring efficient energy storage or voltage generation [115, 116]. After determining the optimal temperature corresponding to the maximum density, we used an electronic palmer to measure the density of pellets. The density (d) is calculated by the following formula:

$$d = \frac{m}{(\frac{r}{2})^2.\pi.e} \quad \text{(II.1)}$$

Were:

m: mass of pellet (g).

r: pellet diameter (cm).

e: pellet thickness (cm).

Figure II. 8: Electronic Palmer.

II.5.5 Impedance spectroscopy measurement

Impedance spectroscopy is a widely used technique for characterizing the electrical properties of materials, particularly their impedance response as a function of frequency. It provides valuable information about the complex impedance, which includes both resistive and reactive components and can be used to extract various dielectric properties of the material. One of the key advantages of impedance spectroscopy is its ability to analyze the behavior of materials over a wide frequency and temperature range By applying an AC signal at different

frequencies and measuring the resulting voltage and current responses, a frequency-dependent impedance spectrum is obtained. This spectrum can be used to extract several important parameters, such as capacitance and resistance. Impedance spectroscopy has found applications in various fields, including materials science and electrochemistry. It is used for studying dielectric materials, electrolytes, batteries, sensors, and many other systems. The technique provides valuable insights into charge transport processes, interfacial phenomena, and material properties, making it a powerful tool for both fundamental research and practical applications [117, 118]. The instrument used in this study is Wayne-Kerr 6425 analyzer, with a frequency range from 1000 Hz to 1 MHz and a temperature range from 300 K to 700 K. To improve the conductivity of the pellets, it is necessary to paint them with a high-purity silver paste and dry them at 423K in an oven for 4 hours, then leave them to cool to room temperature [119].

Chapter III Structural and Microstructural properties of PZT-based ceramics

Chapter III: Structural and microstructural properties of PZT-based ceramics

III.1 Introduction

This chapter presents the results and discussions of the research focused on investigating the structural and microstructural properties of $Pb_{1-X}Ba_X(Zr_{0.52}Ti_{0.43}(Al_{0.5}Sb_{0.5})_{0.05})O_3$ with various amounts of Ba-doped. Understanding the structural and morphological characteristics of our material is essential for optimizing its performance and developing novel applications.

The structural properties play a vital role in determining the functional behavior and overall performance of ceramics. The crystal structure and phase composition of these ceramics significantly influences their electrical and mechanical properties. Therefore, in-depth characterization techniques are necessary to investigate these structural aspects. X-ray diffraction XRD analysis is a powerful tool commonly used to examine the crystal structure and phase composition of materials. By analyzing the diffraction patterns, valuable information about the crystalline phases present in the PZT ceramics can be obtained. Moreover, the identification of any secondary phases or impurities is crucial for understanding the material's properties and optimizing its performance.

Microstructural analysis is equally important in understanding the surface properties using Scanning electron microscopy (SEM), their imagery provides a visual representation of the surface, enabling the assessment of macroscopic features and the analysis of grain characteristics.

The understanding of the structural and microstructural properties of PZT ceramics is important for their effective utilization in various applications. By correlating the structural and microstructural characteristics with the electrical, mechanical, and piezoelectric properties, researchers can gain valuable insights into the fundamental relationships between structure and performance. Such knowledge can guide the optimization of processing techniques and the development of novel materials with improved properties.

In this chapter, the results of the structural and microstructural characterization will be presented and discussed in detail. The findings will be critically analyzed. By examining the interplay between the structural and microstructural.

III.2 Structural properties

X-ray diffraction (XRD) analysis of barium-doped on $Pb(Zr_{0.52}Ti_{0.43}(Al_{0.5}Sb_{0.5})_{0.05})O_3$ provides valuable information about their structural properties and is of significant importance in understanding their composition and crystal structure. XRD is a powerful technique used to determine the crystallographic structure and phase composition of materials.

XRD can be used also to analyze the lattice parameters, which provide information about the crystal symmetry and unit cell dimensions. Moreover, XRD analysis can be used to evaluate the effect of processing conditions on the crystal structure of barium-doped PZT ceramics [13]. It enables researchers to control the crystallographic properties by adjusting parameters such as calcination temperature and dopant concentration during elaboration.

After recovering our compositions from the calcination step, which is done at the temperature of 1000 °C for 2h. Our samples are crushed for 6h and we made a structural characterization in which we determine the purity and the phases that we obtained with the help of a diffractometer Rigaku Miniflex 600 using the radiation Kα of copper (λCu Kα1 = 1, 540593 Å) and at room temperature.

The powder diffractograms are recorded in the angular range $10°<2\theta<90°$ which seems to be sufficient for the identification of the different phases. Figure III.1 presents the XRD patterns of the analyzed samples calcined at 1000 °C for 2hrs as a function of different barium content (Ba^{2+}) as a dopant. XRD peaks corresponding to each sample have been superposed to those of the crystallographic database namely ICDD-PDF2. All the picks that are detected in the diffractograms are corresponding to perovskite structures, so we conclude that the perovskite structure was successfully formed for each composition studied without any detectable secondary phase, indicating that the Ba^{2+} ions are well incorporated in the crystal lattice.

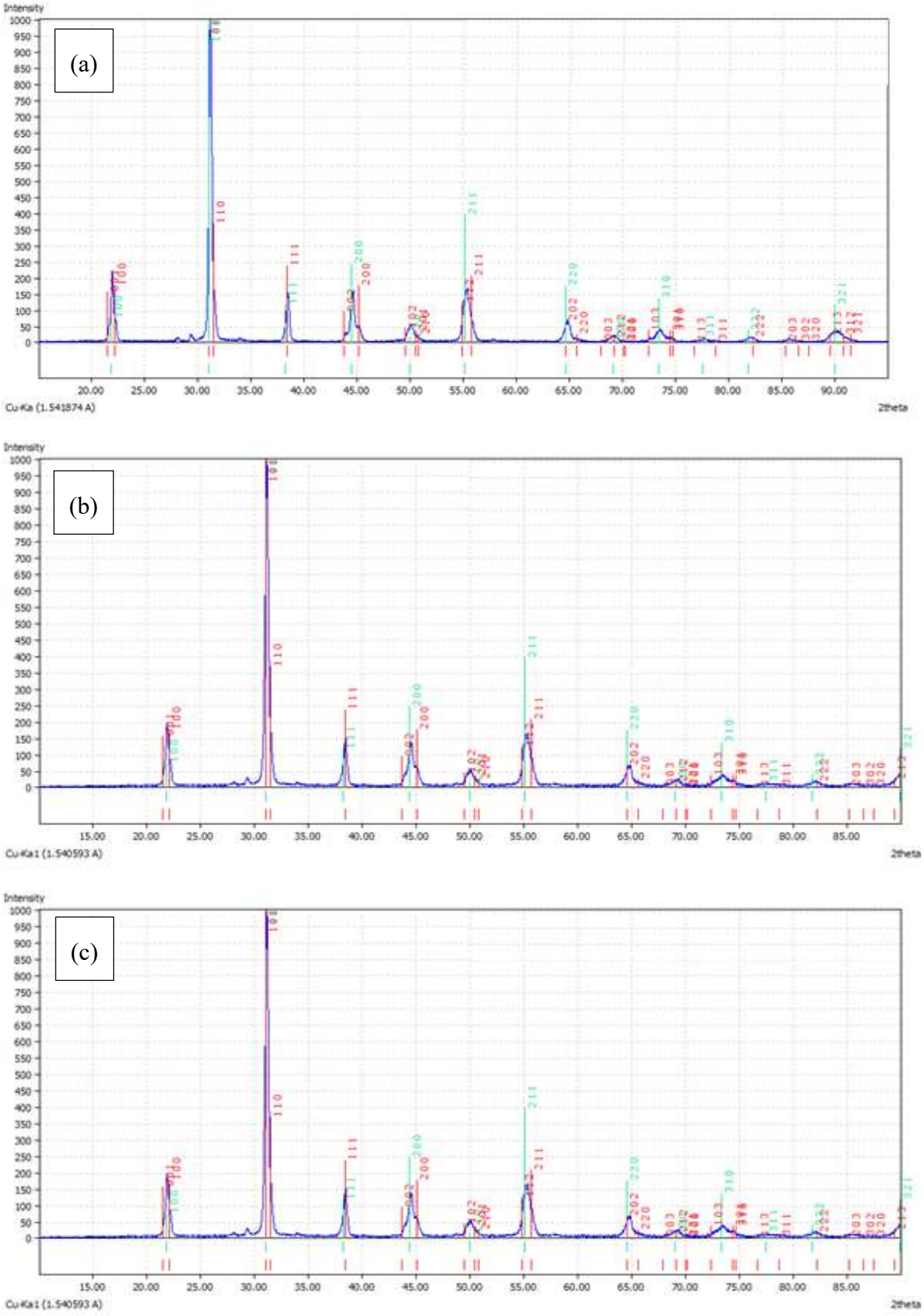

Figure III. 1: XRD patterns of $Pb_{1-X}Ba_X(Zr_{0.52}Ti_{0.43}(Al_{0.5}Sb_{0.5})_{0.05})O_3$ where (a) x=0.00, (b) x=0.02, (c) x=0.04, (d) x=0.06, (e) x=0.08, and (f) x=0.10.

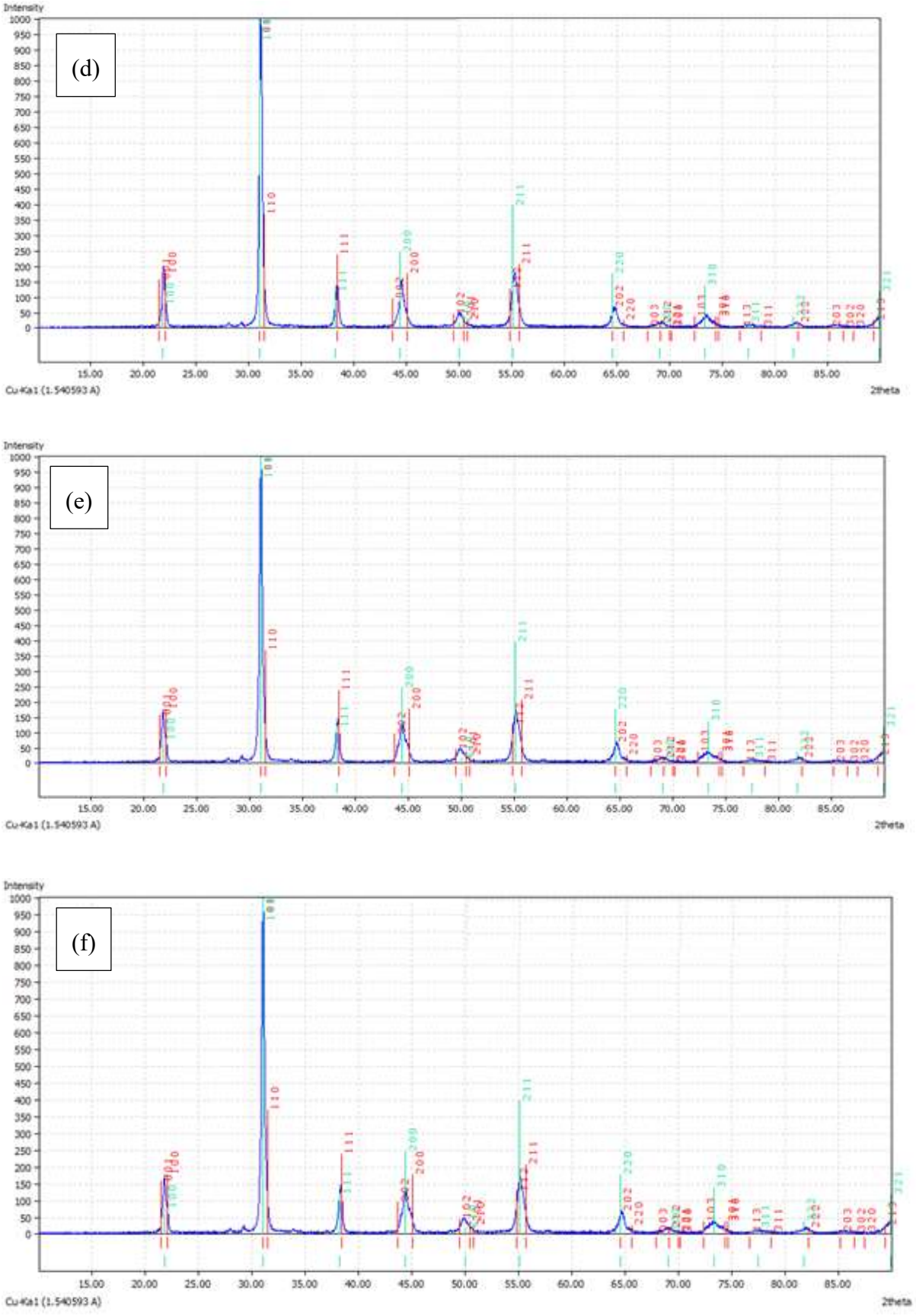

The rest of figure III.1.

III.3 Morphotropic phase boundary

Morphotropic phase boundary MPB is an important concept in the field of piezoelectric materials, particularly in the study of lead zirconate titanate PZT ceramics. The MPB refers to the compositional boundary between two phases with different crystal structures [120], and represents also a delicate balance between the rhombohedral and tetragonal phases in the PZT crystal structure. At the MPB, the material exhibits a maximum in the piezoelectric and dielectric responses [121], which makes it an attractive target for researchers aiming to optimize PZT properties for specific applications. The concept of MPB becomes a well-established area of research in materials science and engineering. The location of the MPB in PZT ceramics can be controlled by adjusting the composition of the material, such as the ratio of zirconium to titanium. The region of the MPB can be modified by adjusting the ratio of Zr and Ti in the PZT composition. Changing the Zr/Ti ratio alters the crystal structure and shifts the position of the MPB. Typically, increasing the Zr content expands the rhombohedral phase region, while increasing the Ti content expands the tetragonal phase region [122].

From the results of the XRD of our samples, there are lines in the diffractogram in which we can say that we have close to the morphotropic phase boundary i.e. the existence of the two phases (tetragonal and rhombohedral). It is known that the lines in which we can say that we have close to the Morphotropic phase boundary are located in the region 2θ (43-47), which corresponds to the peaks 002 and 200 for tetragonal and 200 for Rhombohydric, but there are also other regions in the diffractogram that can detect the existence of this region which are shown in the following table.

Table III. 1: The angular regions that present the coexistence of the two phases T and R[55].

2θ	$(hkl)_T$	$(hkl)_R$
21-23	(001) et (100)	(100)
30-33	(101) et (110)	(110) et (101)
43-47	(002) et (200)	(200)
53-56	(112) et (211)	(211), (211)

Figure III.2 shows the deconvoluted peak situated between 42° and 47° by using the Gaussian function, this function helps us to observe three small peaks corresponding to the (002) and (200) of Tetragonal phase (T) and (200) of the Rhombohedral phase (R), suggesting the

coexistence of two phases T+R at the same time, meaning that we are in the region of the MPB [123]. This is what prompted us to evaluate the fraction of the two tetragonal F_T and rhombohedral F_R phases by estimating the relative intensities of the deconvoluted peaks T(002), T(200), and R(200), using the following equations [124-126] :

$$F_T\,(\%) = \frac{I_{(002)T}+I_{(200)T}}{I_{(002)T}+I_{(200)T}+I_{(200)R}} * 100 \qquad (3.1)$$

$$F_R\,(\%) = 100 - F_T\,(\%) \qquad (3.2)$$

In which $I_{(002)T}$, $I_{(200)T}$, and $I_{(002)R}$ are the integrated area of Tetragonal (002), Tetragonal (200), and Rhombohedral (200) peaks, respectively, the obtained data are illustrated in figure III.2.

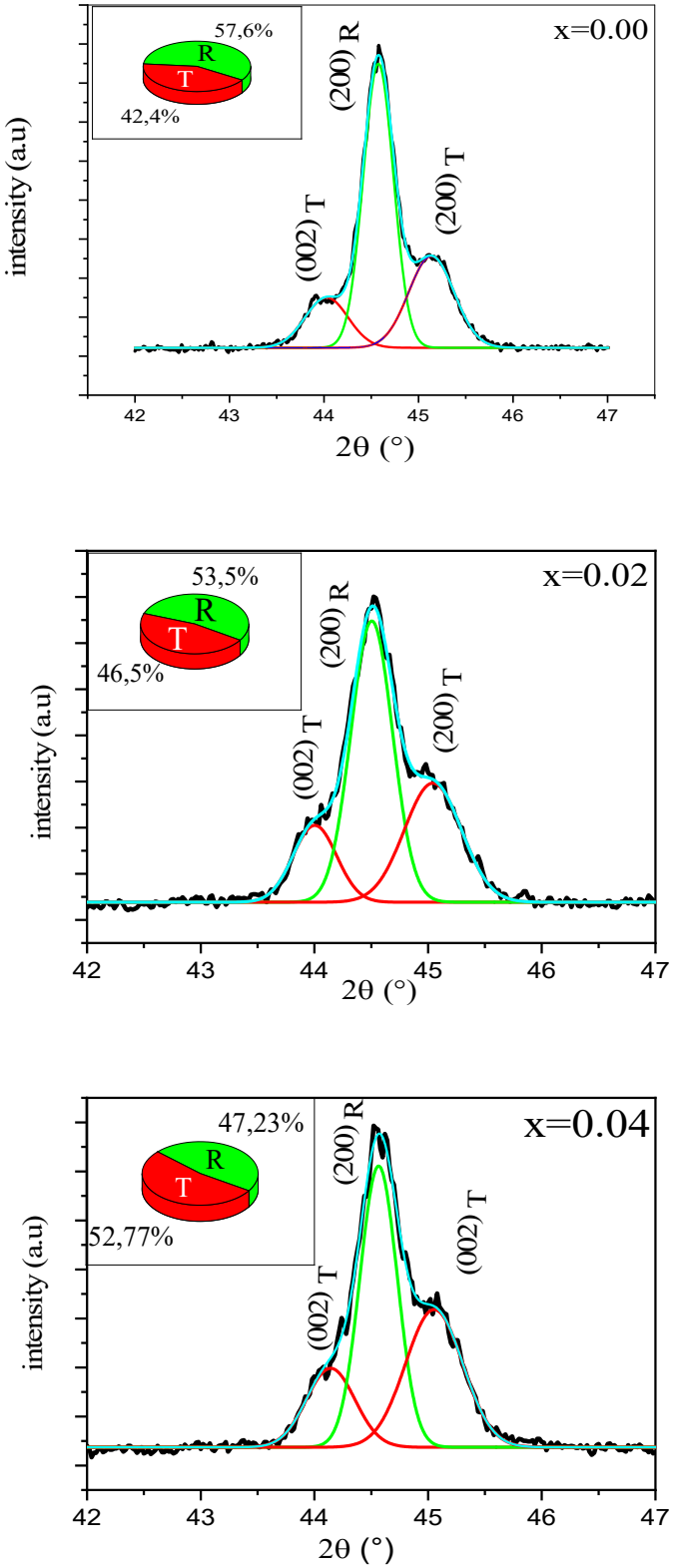

Figure III. 2: The deconvoluted peaks simulated in 2θ range of 42° to 47° and the volume fraction of the Tetragonal (T) and Rhombohedral (R) phases of $Pb_{1-x}Ba_x(Zr_{0.52}\ Ti_{0.43}(Al_{0.5}\ Sb_{0.5})_{0.05})O_3$.

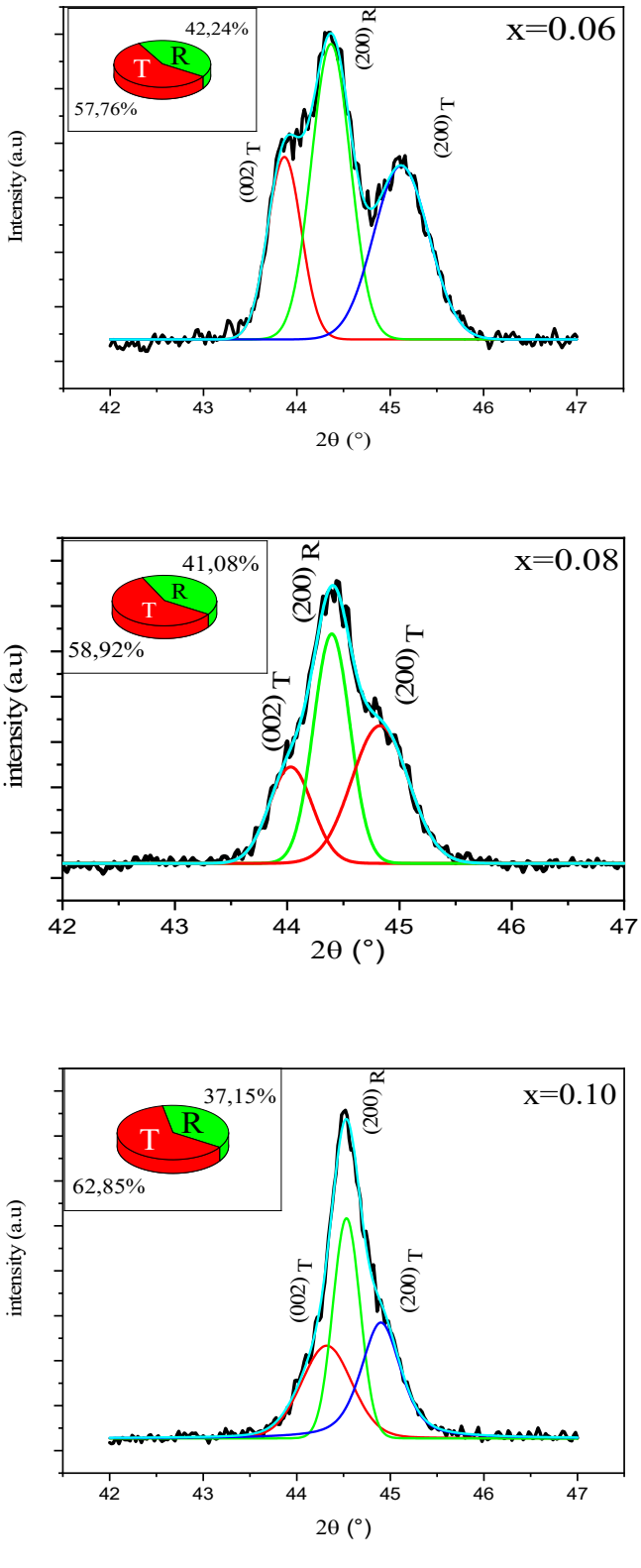

The rest of figure III.2.

III.4 Lattice parameter

The lattice parameter is a fundamental property that characterizes the crystal structure of materials. Understanding the lattice parameter of our material and its variations is crucial for determining the structural stability and functional properties of the material. The lattice parameter of PZT ceramics is determined by the ionic radii of the constituent elements, their crystallographic arrangement, and the degree of cation substitution. Barium substitution can introduce changes in the lattice parameter due to differences in ionic radii between barium and lead. The larger ionic radius of barium compared to lead can cause lattice expansion and affect the crystal symmetry and structural stability. Several studies have investigated the effect of barium substitution on the lattice parameter [127, 128]. X-ray diffraction XRD analysis is commonly employed to determine the lattice parameter by measuring the positions of diffraction peaks. The lattice parameter can be calculated using Bragg's law and compared between the undoped composition and the barium-doped composition.

In this part, an evaluation of the lattice parameter was made for the $Pb_{1-X}Ba_X(Zr_{0.52}\ Ti_{0.43}(Al_{0.5}\ Sb_{0.5})_{0.05})O_3$ composition which varied according to the concentration of Barium; these compositions are calcined at a temperature of 1000 °C. We noticed that the substitution of Barium has a very low effect on the lattice parameter (a and c) of our composition. The c/a ratio represents the tetragonality of the specimens prepared [129], which increases with the increase of Ba^{2+} ion amount, the rise of tetragonality suggesting that the substitution of Ba^{2+} ion could be preferred the formation of the tetragonal phase rather than the rhombohedral phase. The crystallite size was calculated using the Debye-Scherer formula [130, 131]:

$$D = \frac{0.9\lambda}{\beta \cos\theta} \qquad \text{(III.1)}$$

Where D is the size of the crystallites, λ= 1.5406 Å represents the wavelength of CuKa X-ray, θ is the angle of Bragg in degrees, β means the full width at half-maximum FWHM, the results were showing in table III.2. The crystallite size increase with increasing of Ba^{2+} content due to the difference between the ionic sizes of Ba^{2+} (1.61 Å) and Pb^{2+} (1.49 Å) [132].

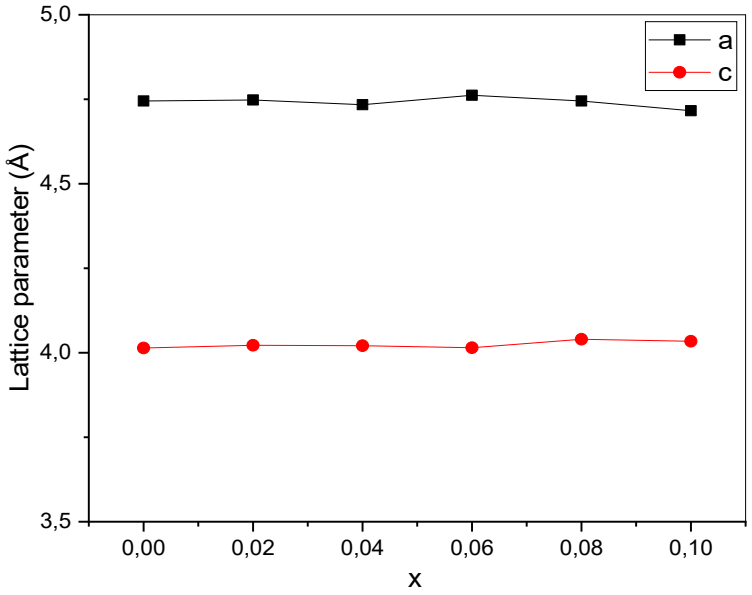

Figure III. 3: Variation of the lattice parameters as a function of Barium content.

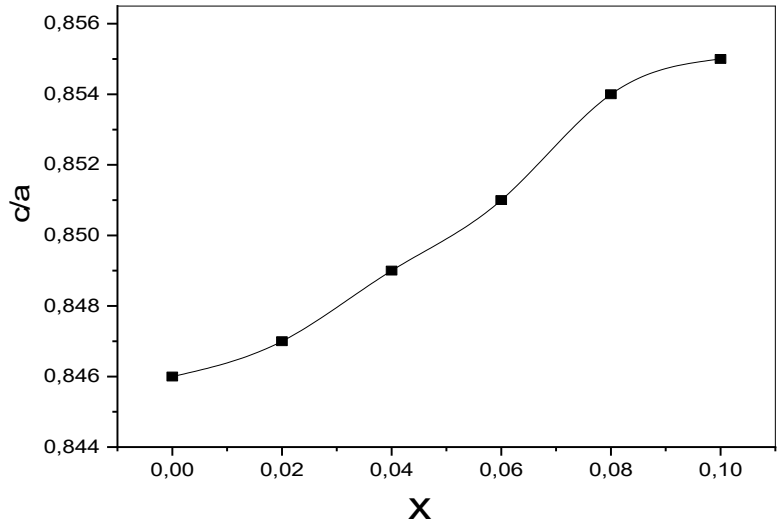

Figure III. 4: Variation of c/a ratio as a function of Barium content.

Table III. 2: The lattice parameters, c/a ratio, and the crystallite size of $Pb_{1-X}Ba_X(Zr_{0.52}Ti_{0.43}(Al_{0.5}Sb_{0.5})_{0.05})O_3$.

Samples	crystallite size (nm)	Lattice parameter		
		a (Å)	c (Å)	c/a
X= 0.00	14,80	4,745	4,014	0.846
X= 0.02	13,78	4.748	4.022	0.847
X= 0.04	15,56	4.734	4.021	0.849
X= 0.06	10,09	4.745	4.040	0.851
X= 0.08	15,80	4.762	4.066	0.854
X= 0.10	16,89	4.716	4.034	0.855

In conclusion, the lattice parameter of $Pb_{1-X}Ba_X(Zr_{0.52}Ti_{0.43}(Al_{0.5}Sb_{0.5})_{0.05})O_3$ plays a significant role in determining their structural stability and functional properties. The investigation of the lattice parameter and its variations through barium doping provides valuable insights into the structure property.

III.5 Tolerance factor

The tolerance factor is a parameter used to describe and evaluate the stability of the perovskite structure. In the case of PZT ceramics, a too-high or too-low tolerance factor can result in the formation of secondary phases, reduced ferroelectricity, and decreased piezoelectric coefficients.

To ensure the desired properties, it is important to understand and control the tolerance factor during the elaboration. By adjusting the composition and processing conditions, it is possible to tailor the tolerance factor to optimize the crystal structure and properties of the ceramic. This involves careful selection of the cationic ratios, such as the ratio of lead, aluminum, antimony, Barium, zirconium and titanium, to achieve the desired tolerance factor range. In summary, the tolerance factor is of great importance in determining the crystal structure and properties of these materials.

It's calculated based on the ionic radii of the constituent cations in the crystal lattice using the following equation [73]:

$$T = \frac{R_A + R_O}{\sqrt{2}(R_B + R_O)} \quad (3.4)$$

In which R_{Am}, R_{Bm}, and R_O are the average ionic radii of the A-site, B-site, and oxygen atoms, respectively. Where the ionic radii of Pb^{2+}, Ba^{2+}, Zr^{4+}, Ti^{4+}, Sb^{5+}, Al^{3+}, and O^{2-} are 1.49, 1.61, 0.72, 0.605, 0.62, 0.54, and 1.35 Å, respectively [20, 133, 134].

The calculated values of T are listed in Table 1 and showing in figure III.5 the results of the tolerance factor are in the range of 0.9968 and 1.0001 which indicates the stability of the perovskite structure [135], in addition, the increase of Ba^{2+} amounts brings the tolerance factor close to 1, which makes the perovskite structure more stable [136].

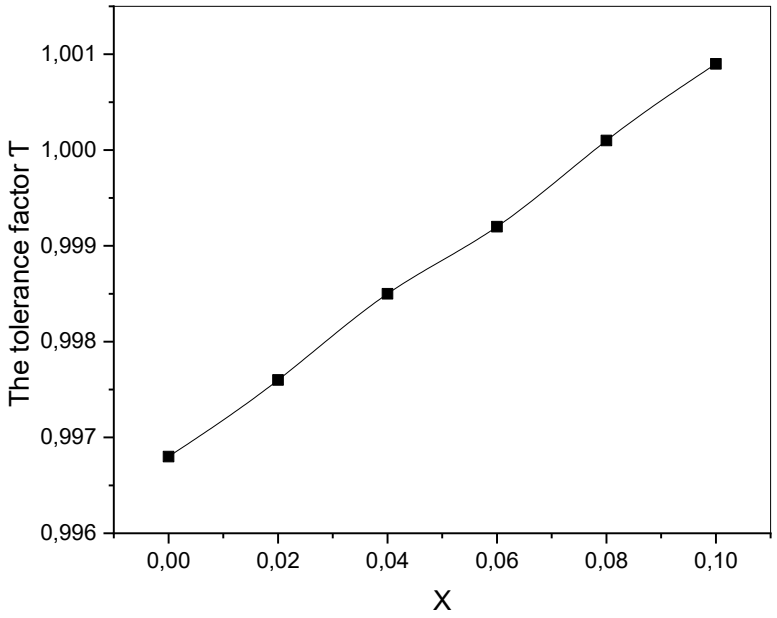

Figure III. 5: The tolerance factor T of $Pb_{1-X}Ba_X(Zr_{0.52}Ti_{0.43}(Al_{0.5}Sb_{0.5})_{0.05})O_3$.

Table III. 3: The tolerance factor T of Pb1-XBaX(Zr0.52Ti0.43(Al0.5Sb0.5)0.05)O3.

Samples	X= 0.00	X= 0.02	X= 0.04	X= 0.06	X= 0.08	X= 0.10
T	0.9968	0,9976	0.9985	0,9992	1.0001	1,0009

III.6 Fourier Transform Infrared spectroscopy (FTIR)

Fourier Transform Infrared spectroscopy FTIR is a widely used analytical technique for the characterization of materials; it is a non-destructive and non-invasive technique that provides information on the chemical structure and composition of a sample. Several infrared absorption studies on perovskite have been carried out to evaluate the frequencies of the normal modes of vibration of these compositions [137, 138]. The Fourier Transform Infrared spectroscopy FTIR of the samples was carried out on a PerkinElmer FT-IR Spectrum Two Spectrophotometer in the wavelength range of 400–1500 cm^{-1} in the photonic physics and multi-functional nanomaterials research laboratory LPPNM at the University of Biskra, which is controlled by a computer using UV Winlab software. FTIR spectroscopy has been used to investigate the chemical composition and structural properties. Several studies have reported the use of FTIR spectroscopy to analyze PZT ceramics. For example, a study by PK Panda et al [139] used FTIR spectroscopy to investigate the effect of Zr^{4+} on piezoelectric, dielectric, and ferroelectric properties. Another study by A Mirzaei et al. used FTIR spectroscopy to the effect of Nb doping on sintering and dielectric properties.

The PZT-based materials have four vibration modes, two vibration modes which are located below 400 cm^{-1}. These two modes correspond to the vibrations in the Pb-TiO_3 or ZrO_3 bond, the third mode has a wavenumber range of 390 - 410 cm^{-1}, where it is caused by the stretching vibrations of O-Zr and Ti-O [140], these three modes can't be observed due to the measurement limitation of our equipment which begins measuring from 400 cm^{-1}, the fourth vibration mode is the most important band which is between 440 cm^{-1} and 640 cm^{-1}, it's characterized by the vibration of M-O (M= Zr, Ti, and Pb) octahedron asymmetrical stretching which is presented in figure III.3 [141-143]. The FTIR results are consistent with the XRD results above and confirmed that the perovskite structure was successfully formed.

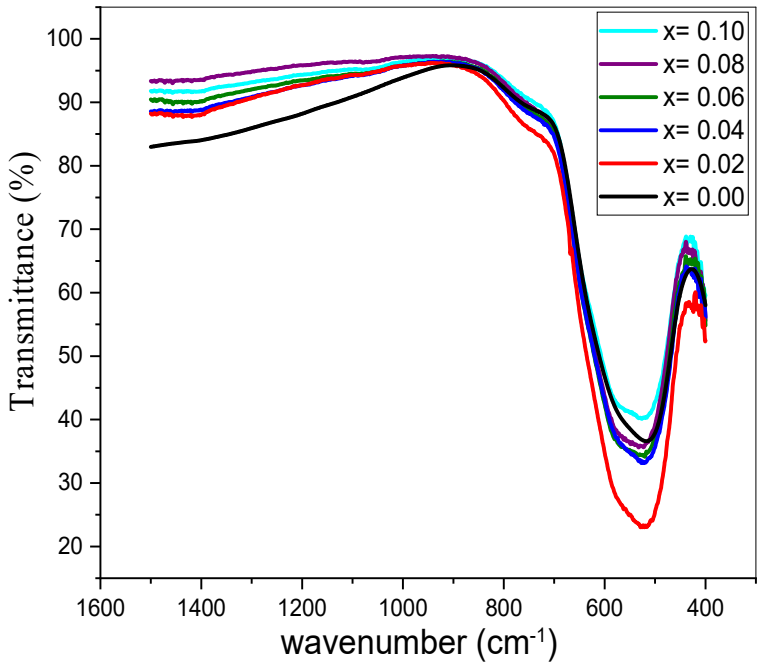

Figure III. 6: FTIR patterns of Pb1-xBax(Zr0,52Ti0,43(Al0,5Sb0,5)0,05)O3.

III.7 Density

The density of ceramics can have a significant impact on their dielectric properties and conductivity. Density refers to the mass of material per unit volume and can be measured in g/cm³. The density of PZT ceramics can influence their dielectric properties in several ways. Firstly, higher density can result in reduced porosity within the ceramic, which generally improves dielectric properties. A denser ceramic also has reduced voids or defects, which can reduce dielectric losses and improve material quality.

Regarding conductivity, density can also play an important role. A denser ceramic typically exhibits better electrical conductivity. This is due to enhanced connectivity between ceramic grains, facilitating the movement of electric charges through the material [144].

III.7.1 Effect of temperature on density

The best morphological properties of our samples are having a minimum of pores, more compact and dense; to obtain this type of samples it is necessary to find the optimal temperature of sintering. To determine this temperature, we sintered our samples with several temperatures between 1170°C to 1270°C with a step of 20°C. Figure III.7 represents the

variation of the density of different compositions doped by Ba^{2+} ion as a function of the sintering temperature, the best temperature of sintering is 1220°C which offers the densest samples with a density value of around 7.2 g/cm^3, this is a very favorable factor for excellent dielectric properties [145].

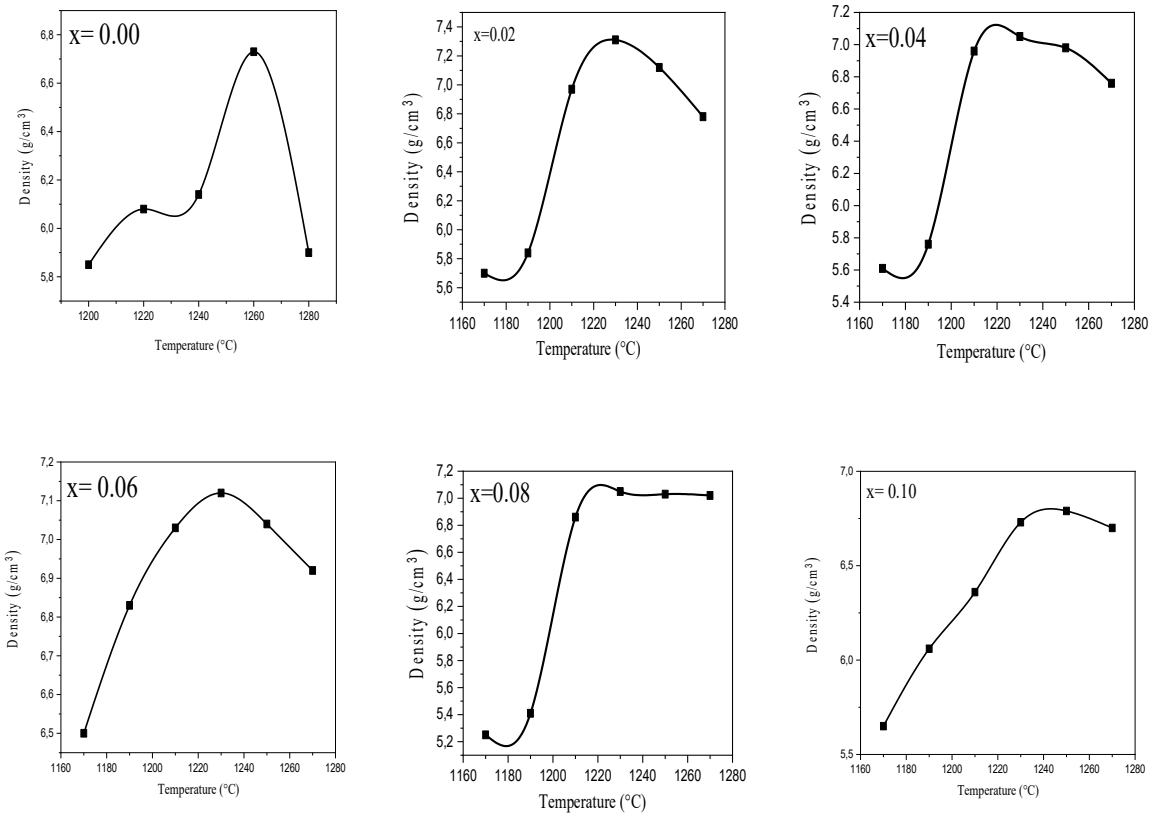

Figure III. 7: Influence of the temperature on the density of $Pb_{1-x}Ba_x(Zr_{0.52}Ti_{0.43}(Al_{0.5}Sb_{0.5})_{0.05})O_3$.

III.7.2 Effect of barium substitution on density

The previous study is based on the search for the optimum sintering temperature for our pellets, but in this section, we have taken this temperature (T= 1220°C) to study the density as a function of the barium substitution rate at this temperature. From Figure III.8 we observe that the effect of Barium substitution on density is significantly clear, in that the density of the pellets increases with increasing Barium content, reaches up to 7.17 g/cm^3.

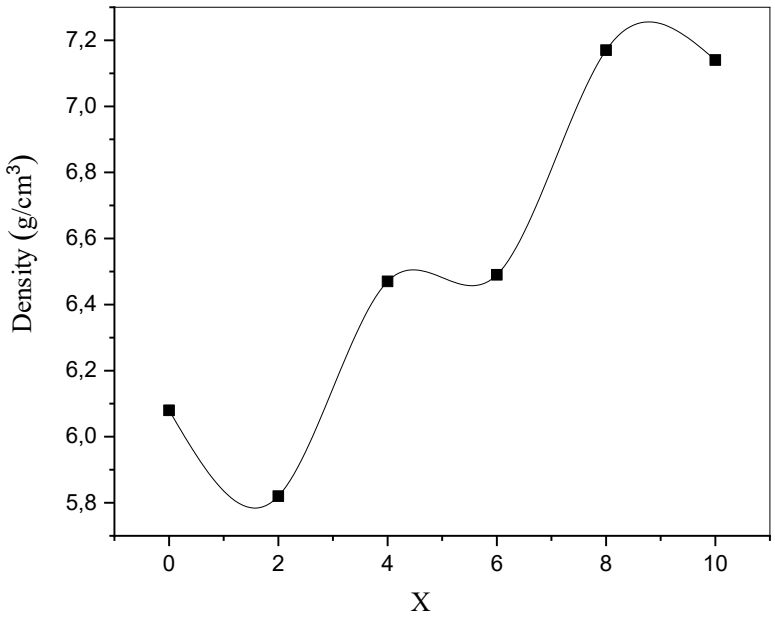

Figure III. 8: Influence of barium substitution on density of $Pb_{1-x}Ba_x(Zr_{0.52}Ti_{0.43}(Al_{0.5}Sb_{0.5})_{0.05})O_3$.

III.8 Microstructural analysis

The size and distribution of the grains can affect properties such as mechanical strength and electrical conductivity. The presence of defects or porosity can influence the reliability and performance of the material under different conditions. Several studies have reported SEM characterization of PZT ceramics. For example, a study by CA Oliveira [146] used SEM to investigate the synthesis and characterization of lead zirconate titanate PZT prepared by different synthesis methods. Figure III.9 represents the SEM micrographs of the specimens sintered at 1220°C, it can be seen that the microstructure of the studied samples is dense and composed of grains having different shapes and relatively small sizes, the sintering temperature, which we have chosen where the density is optimal (see figure III.7) gives us a SEM image which also shows the densification of the materials and therefore less porous. Although the samples are less porous, we do not know if the porosity is zero, which may influence the electrical properties. Image J software was used to approximate the average grain size, it was noticed that the grain size of the compositions x = 0.00, 0.02, 0.04, 0.06, 0.08, and 0.10 are found to be 1.24, 2.84, 2.74, 2.95, 2.14, and 2.75 µm respectively.

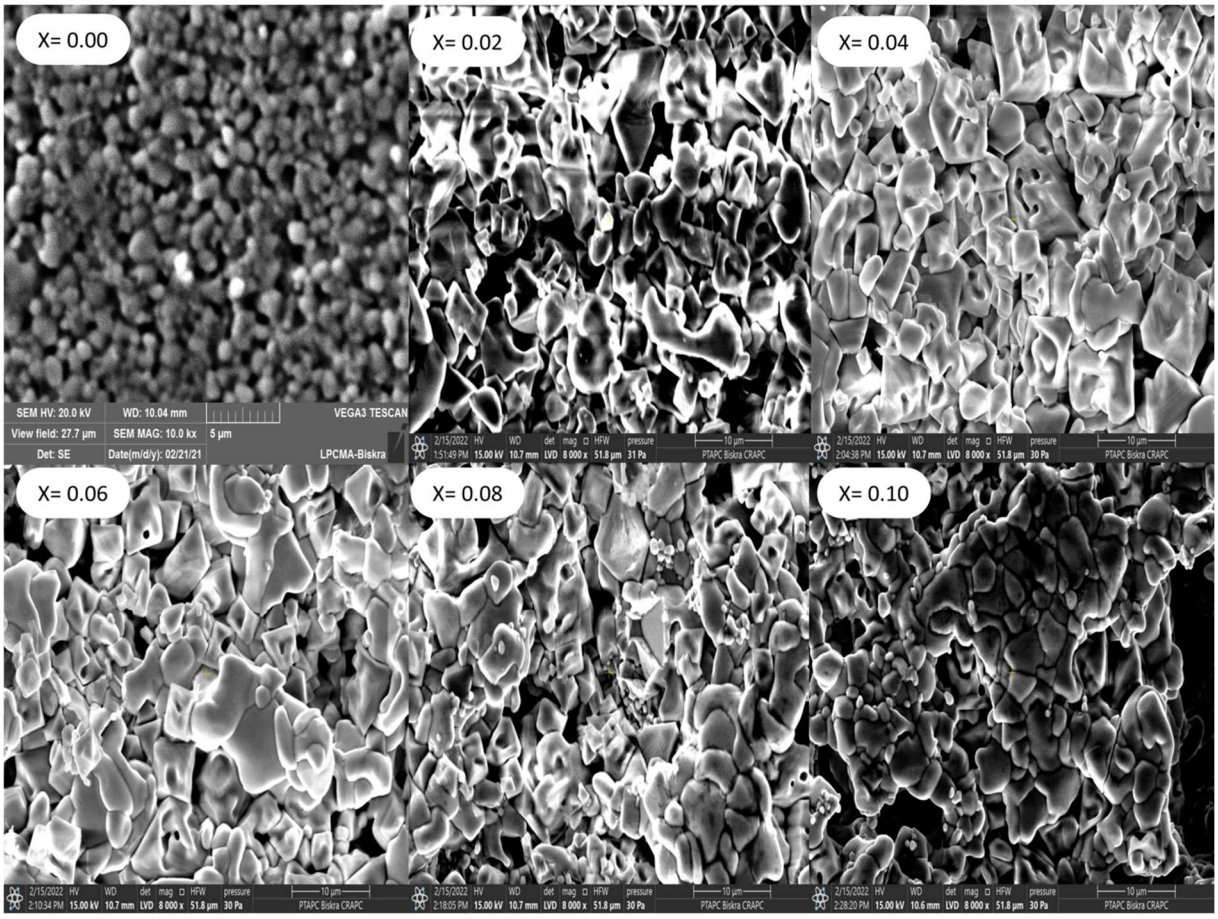

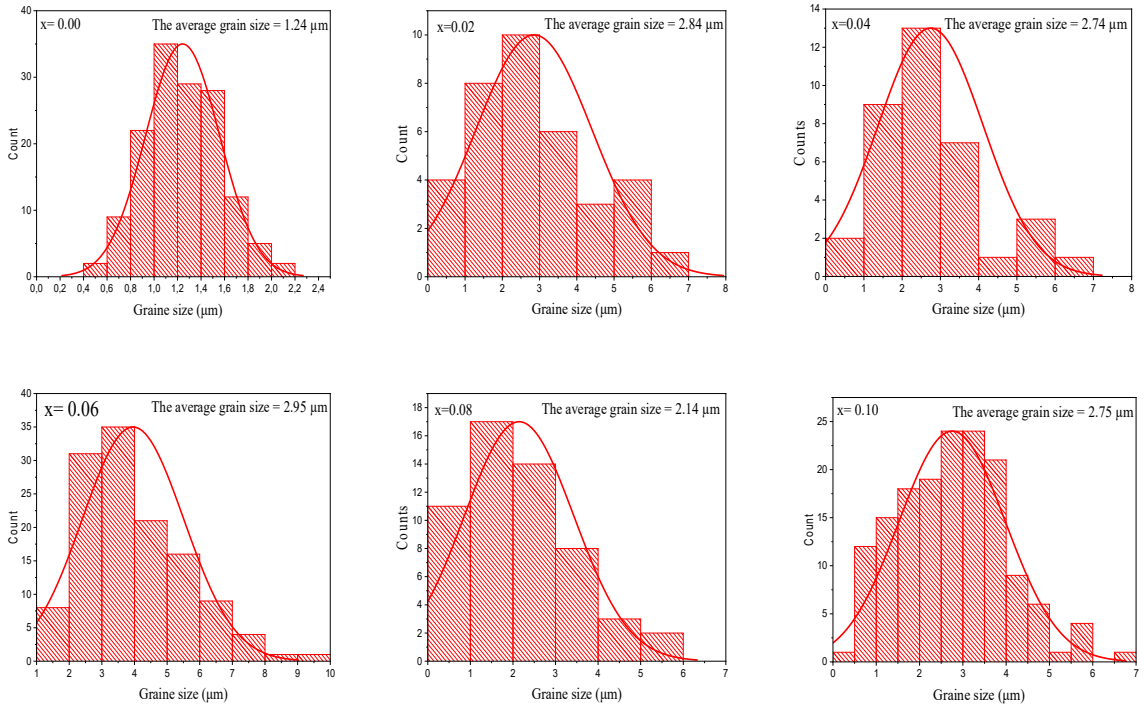

Figure III. 9: SEM images of fracture surface and the average grain size of Pb1-XBaX(Zr0.52Ti0.43(Al0.5Sb0.5)0.05)O3.

III.8.1 Effect of Barium substitution on average grain size

The evolution of the average grain size of specimens sintered at 1220°C as a function of Barium substitution has been shown in Figure III.10. In general, when comparing the base composition (before Barium substitution) with the other compositions, we noticed that the average grain size of the doped composition is very large compared to the basic composition.

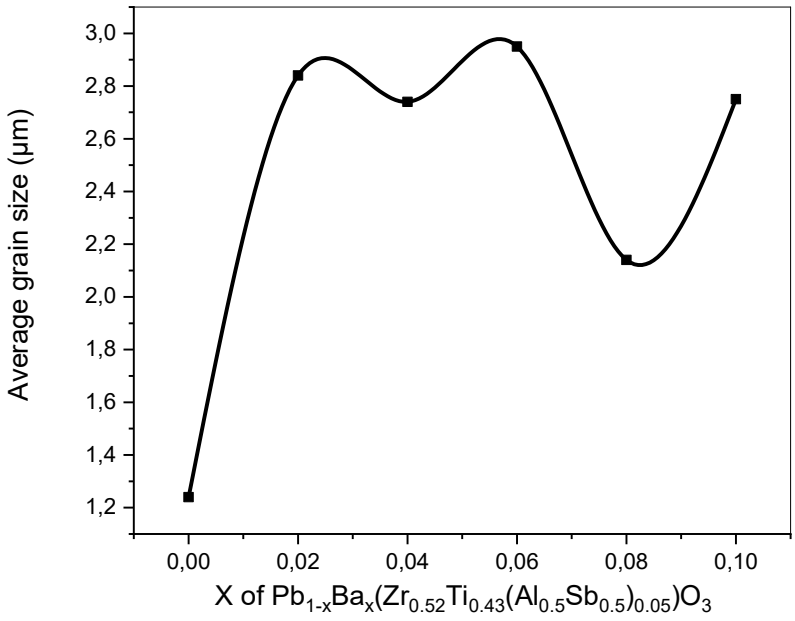

Figure III. 10: The average grain size as a function of Barium substitution

III.9 Energy dispersive spectrometric analysis EDS

Energy dispersive X-ray spectroscopy EDS is a technique commonly used to investigate the chemical composition of ceramics. The results of EDS analysis can be used to interpret the properties and characteristics of the ceramics, such as how impurities may affect their mechanical properties. Figure III.11 shows the analysis we obtained from the EDX instrument for the samples of Barium substitution. From these results we can conclude that all the compositions are clearly pure with no secondary elements or impurities, the chemical elements of our composition are all detected such as Pb, Ba, Zr, Ti, Al, Sb, and O, these results complete the other analyses such as the DRX analysis.

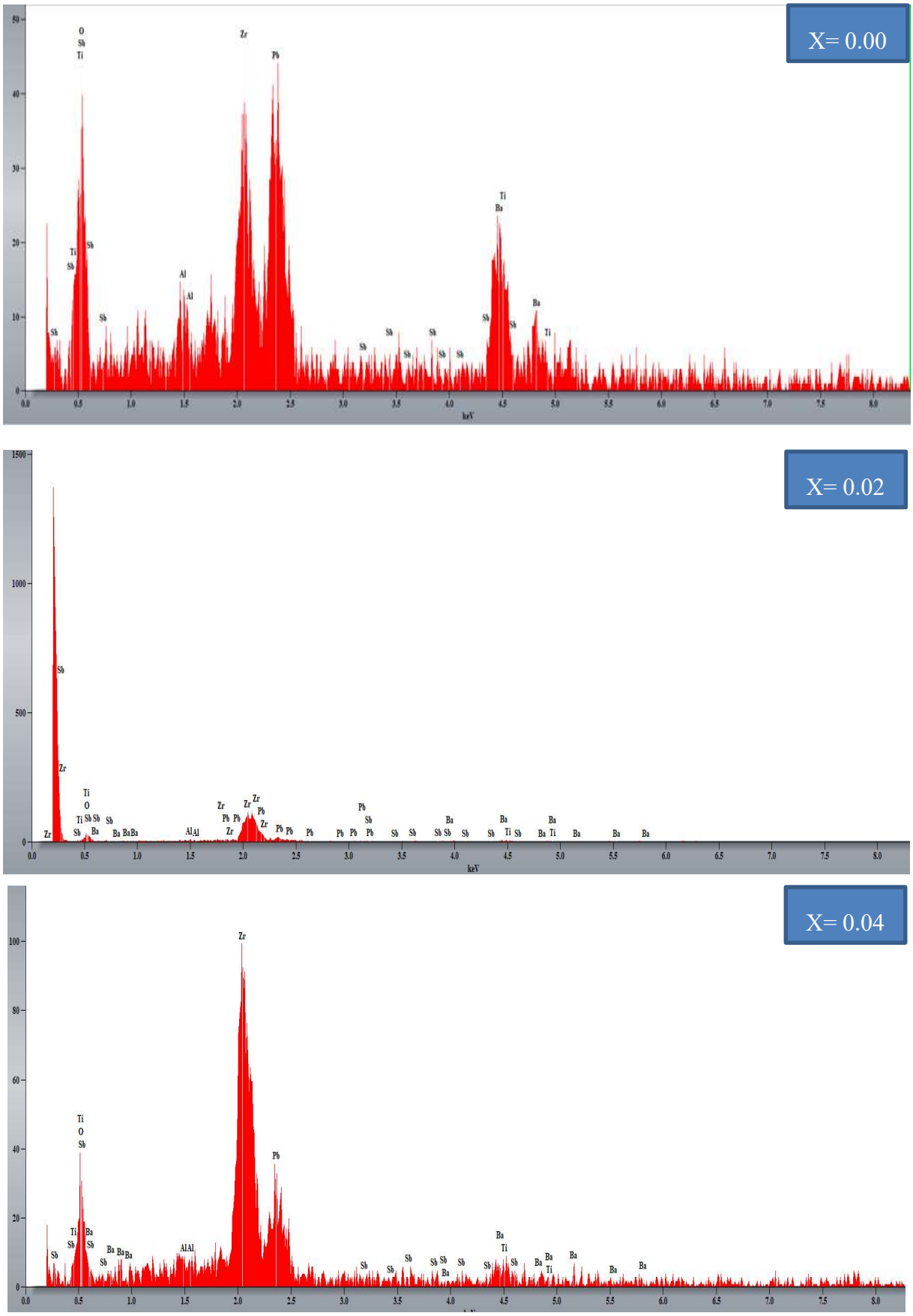

Figure III. 11: X-EDS spectrum for the sample of $Pb_{1-X}Ba_X(Zr_{0.52}Ti_{0.43}(Al_{0.5}Sb_{0.5})_{0.05})O_3$.

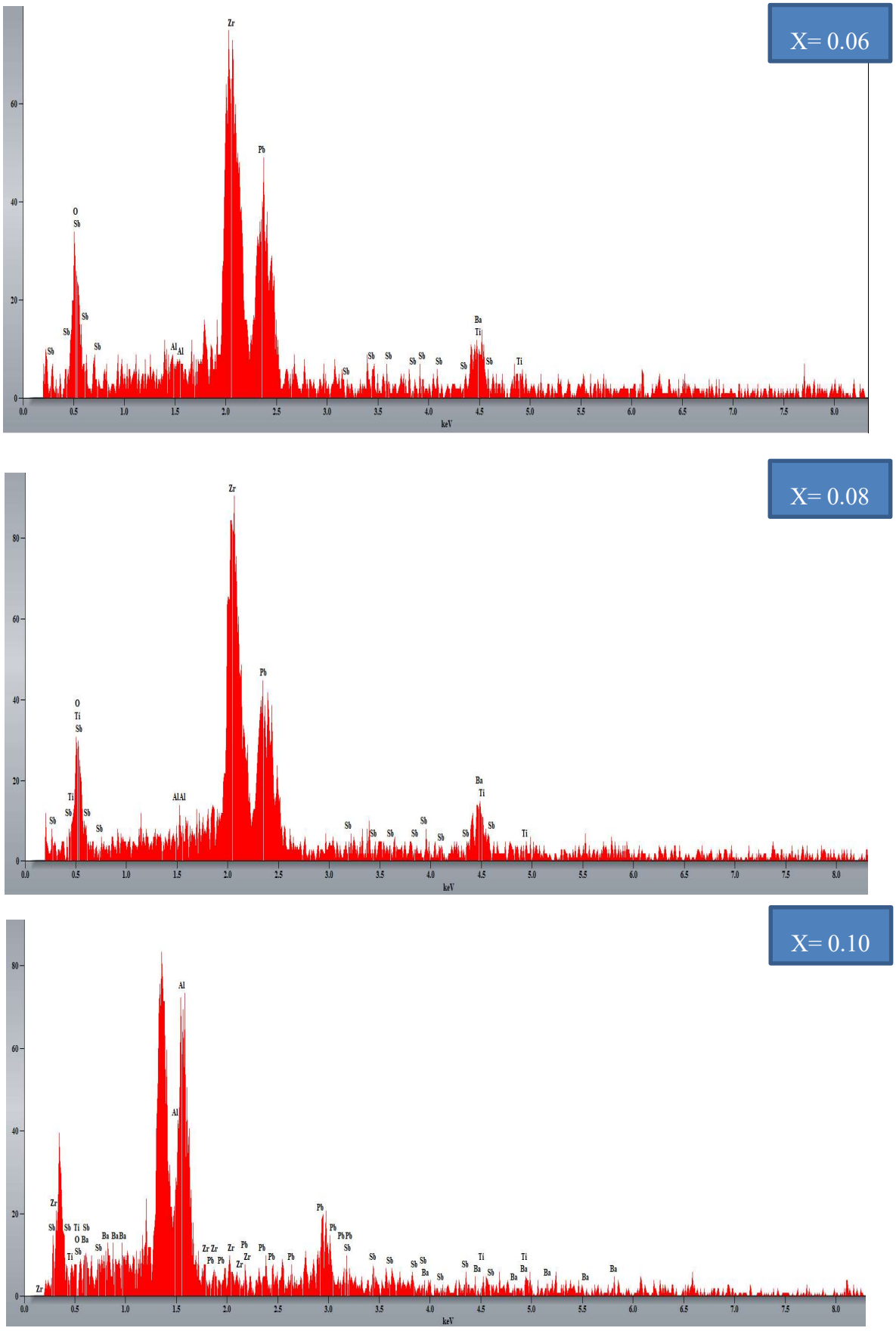

The rest of figure III.11.

III.10 Conclusion

In conclusion, this chapter presented several results related to the structural and morphological properties of the samples. The following techniques were employed:

X-ray Diffraction XRD: XRD analysis confirmed that all the samples were pure. The crystal structure and phase composition of the ceramics were determined using this technique.

Scanning Electron Microscopy SEM: SEM imaging was performed to examine the surface morphology and determine the average grain size of the ceramics; we found that all the samples are homogeneous with a minimum porosity. This analysis provided also the average grain size of our pellets.

Fourier Transform Infrared Spectroscopy FTIR: FTIR spectroscopy was employed to investigate the chemical bonding and functional groups present in the ceramics. This technique has provided us the illustration of all the vibration modes of this type of ceramic.

Morphotropic Phase Boundary: we have discussed the morphotropic phase boundary, which refers to the boundary region between different phases in the material. The effects of composition and processing conditions on the phase boundary were explored.

The impact of temperature and the effect of substituting barium on the density of the pellets was investigated. The variations in density at different temperature ranges and different amounts of Barium compared to pure compositions were showing very interesting results.

The lattice parameters of the ceramics were determined. These parameters provide information about the unit cell dimensions and crystal structure, contributing to the understanding of the material's properties.

The tolerance factor, an important parameter for perovskite structures, was calculated. It helps determine the stability of the crystal lattice in the ceramics. EDS analysis results show that all the compositions are clearly pure with no secondary elements or impurities.

Generally, these results contribute to a comprehensive understanding of the compositional, microstructural, and structural properties of the $Pb_{1-X}Ba_X(Zr_{0.52}Ti_{0.43}(Al_{0.5}Sb_{0.5})_{0.05})O_3$ ceramics. They provide valuable insights for optimizing the materials' performance and tailoring their properties for specific applications.

Chapter IV Effect of Barium substitution and various parameters on impedance spectroscopy and electrical properties of PZT based ceramics

Chapter IV: Effect of Barium substitution and various parameters on impedance spectroscopy and electrical properties of PZT based ceramics

IV.1 Introduction

Dielectric, AC conductivity characteristics and impedance spectroscopy play an important role to understand the electrical behavior and performance of materials. These characteristics are often investigated using impedance spectroscopy, a powerful technique that provides valuable information about electrical properties. In this chapter, we present the interpretation and presentation of the results obtained from impedance spectroscopy measurements, focusing on the effects of barium substitution, temperature, and frequency on AC conductivity and dielectric properties.

Dielectric properties, such as permittivity and dielectric loss, are key parameters that determine the electrical response of materials to an applied electric field. Impedance spectroscopy allows us to measure and analyze the complex impedance, which consists of a real part (resistance) and an imaginary part (reactance). By studying the frequency-dependent behavior of the impedance. The AC conductivity is also an important parameter that characterizes the ability of materials to conduct alternating current. Impedance spectroscopy provides a comprehensive understanding of the frequency-dependent conductivity behavior, revealing insights into charge transport mechanisms and material performance.

The substitution of barium can significantly modify the dielectric response and conductivity behavior. Temperature is a critical parameter that strongly influences the dielectric and AC conductivity characteristics. By studying the temperature dependence of dielectric properties and AC conductivity, we can explore the thermal behavior and phase transitions of the materials. The response of materials to different frequencies reveals information about their polarization mechanisms and relaxation processes. We will examine the frequency dependence of dielectric properties. In this chapter we will analyze how different barium concentrations, temperatures, and frequencies affect the dielectric constant, dielectric loss, and AC conductivity, shedding light on the role of barium in modifying electrical properties.

In summary, this chapter focuses on the interpretation and presentation of dielectric and AC conductivity characteristics obtained through impedance spectroscopy. The effects of barium,

temperature, and frequency on the dielectric constant, dielectric loss, the real part, the imaginary part, and AC conductivity will be thoroughly investigated. These findings will contribute to a deeper understanding of the electrical behavior of $Pb_{1-x}Ba_X(Zr_{0,52}Ti_{0,43}(Al_{0,5}Sb_{0,5})_{0,05})O_3$.

IV.2 Dielectric studies

To get an idea about the electrical properties of materials as a function of temperature and frequency, it is necessary to make the dielectric measurement. The two main electrical characteristics that we can take from the dielectric measurements are the capacity and the conductivity, one which is related to the insulation of materials and the other which is related to the transport of electronic charge, and from this analysis, we can determine the constant and the dielectric loss [147]. The equation in which we can calculate the dielectric constant is the following [105, 131]:

$$\varepsilon_r = \frac{C_p * d}{\varepsilon_0 * A} \qquad (3.5)$$

Where C_p is the parallel capacitance, the thickness of the pellet is denoted by d, A is a ceramic disc area and ε_0 is the free space permittivity ($\varepsilon_0 = 8{,}85*10^{-12}$F/m).

IV.2.1 Dielectric constant and dielectric loss

The dielectric constant and dielectric loss are important parameters that describe the behavior of dielectric materials. These parameters are influenced by various factors, including temperature and frequency. In this explanation, we will discuss the effects of temperature and frequency on the dielectric constant and dielectric loss.

IV.2.1.1 The effect of temperature

Temperature has a significant impact on the dielectric constant and dielectric loss of materials. Typically, The dielectric constant increases with increasing temperature up to the Curie temperature, after which it begins to decrease, while the dielectric loss tangent tan δ usually exhibits an opposite trend. The decrease in the dielectric constant with temperature can be attributed to several factors, such as reduced polarization.

IV.2.1.2 The effect of Frequency

The frequency of the applied electric field also affects the dielectric properties of materials. Dielectric constant and dielectric loss are frequency-dependent and their behavior can be described using frequency response curves.

Figure IV.1 represents the variation of the dielectric constant (ε_r) and dielectric loss (tgδ) of the $Pb_{1-X}Ba_X(Zr_{0,52}Ti_{0,43}(Al_{0,5}Sb_{0,5})_{0,05})O_3$, where x = 0.00, 0.02, 0.04, 0.06, 0.08, and 0.10 sintered at 1220 °C as a function of temperature (300 K–700 K) at several selected frequencies (1, 2, 4, 6, 8, and 10 kHz). It can be seen that the dielectric constant gradually increases with the increase in temperature until the $\varepsilon_{r\ max}$ which corresponds to a specific temperature, after this temperature, the dielectric constant will be strongly decreased which indicate ferroelectric phase transition [148], the temperature where the phase change from ferroelectric to paraelectric (cubic structure) is called the Curie Temperature TC or the phase transition temperature [21].

The highest dielectric constant was found at the Curie temperature ε_{max}, which is probably due to the thermally activated electrons in the system [149]. We can observe also that the curie temperature is not changing as a function of frequency, indicating the normal ferroelectric characteristics [150, 151]. The dielectric constant ε_r drops with increasing frequency which is a general characterization of polar dielectric materials [152], which indicates the presence of all types of polarizations at the same time (dipole, ionic, space charge, electronics, etc.) [119, 138]. Concerning the dielectric loss tgδ, which have very small values, there is decreasing with increasing frequency, also the increase in the dielectric loss at high temperatures could be assigned to the increase in conductivity [153]. the Curie temperature TC, dielectric constant at curie temperature ε_{max}, dielectric constant at room temperature ε_{RT}, dielectric loss at curie temperature $tg\delta_{Tc}$, dielectric loss at room temperature $tg\delta_{RT}$ at a frequency of 1 kHz of PBZTAS with x = 0.00, 0.02, 0.04, 0.06, 0.08, and 0.10 are listed in table IV.I.

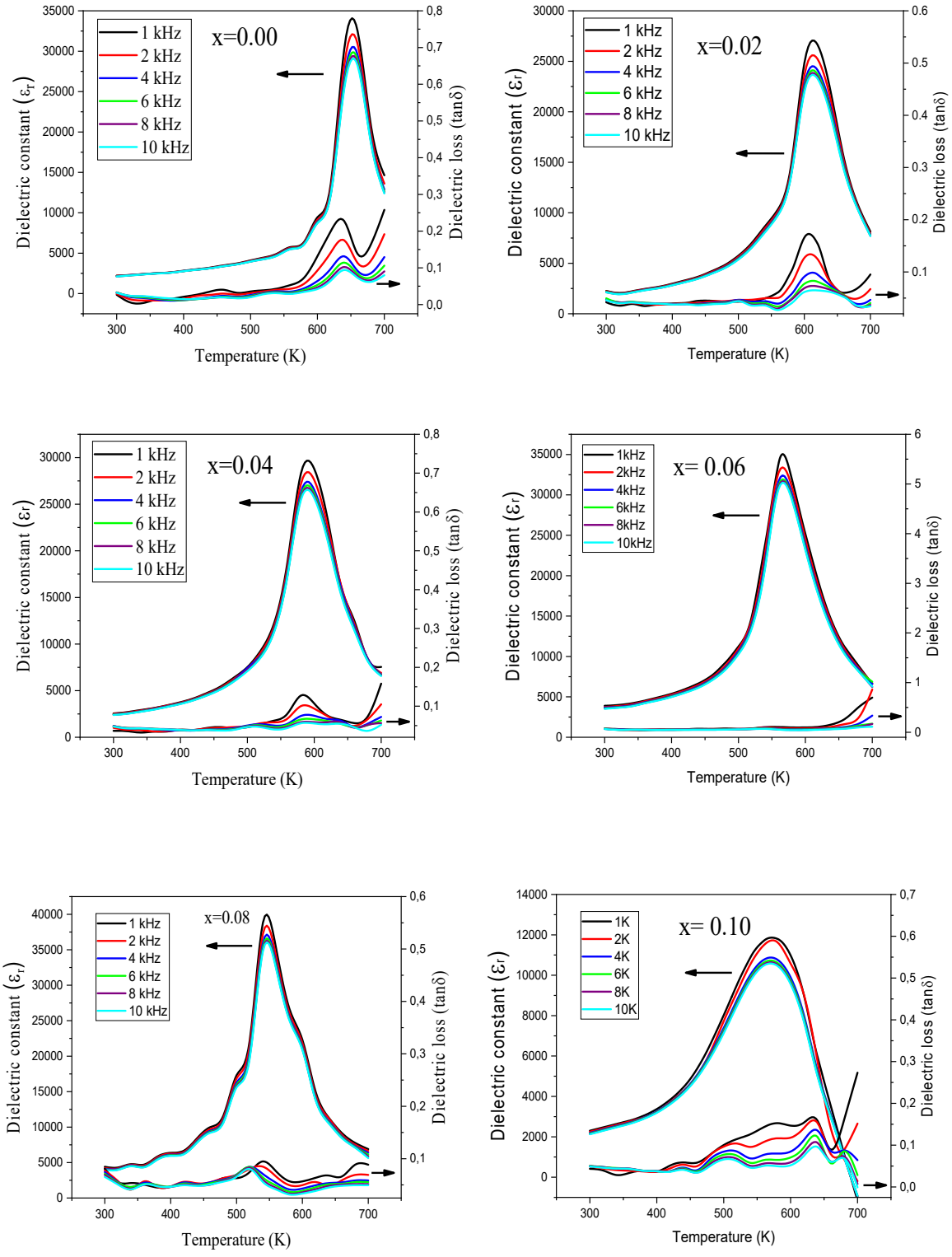

Figure IV. 1: Temperature dependence of Dielectric constant εr and Dielectric loss (tgδ) at different frequencies of Pb1-XBaX(Zr0.52Ti0.43(Al0.5Sb0.5)0.05)O3

Table IV. 1: Variation of TC, εr RT, ε max, Tgδ RT and Tgδ Tc of Pb1-XBaX(Zr0.52Ti0.43(Al0.5Sb0.5)0.05)O3 at 1 kHz.

PBZTAS	TC	ε max	εr RT	Tgδ TC	Tgδ RT
X= 0.00	660	32497	2219	0.138	0.268
X= 0.02	620	26630	2264	0.065	0.046
X= 0.04	600	28787	2557	0.107	0.036
X= 0.06	560	33898	3895	0,070	0,065
X= 0.08	540	38800	4407	0.095	0.081
X= 0.10	560	12657	2313	0,051	0,049

IV.2.1.3 The effect of Barium substitution

Figure IV.2 shows the dielectric constant as a function of temperature at 1 kHz of $Pb_{1-x}Ba_x(Zr_{0.52}Ti_{0.43}(Al_{0.5}Sb_{0.5})_{0.05})O_3$. The compound which corresponds to the strongest dielectric response is that of x= 0.08 (ε_{max}= 38800) which is much higher compared to previous studies [10, 147, 150]. The broadening of the dielectric peaks and the variation of the maximum value of the dielectric constant $\varepsilon_{r\ max}$ with the addition of Ba^{2+} content resulted from the origin of grain size variation and structural disorder [57].

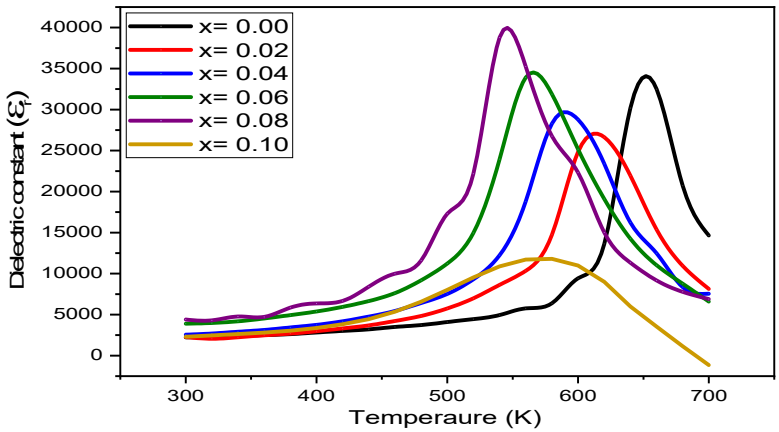

Figure IV. 2: Temperature dependence of Dielectric constant εr at 1 kHz of Pb1-XBaX(Zr0.52Ti0.43(Al0.5Sb0.5)0.05)O3.

IV.3 Curie temperature

One of the aims of this work is to find or determine the effect of the substitution of barium in all the proprieties, and one of these proprieties is the Curie temperature. Figure IV.3 shows the variation of the curie temperature as a function of the barium substitution. It's very clear that the Curie temperature of $Pb_{1-X}Ba_X(Zr_{0.52}Ti_{0.43}(Al_{0.5}Sb_{0.5})_{0.05})O_3$ ceramic decreases from 660 °C to 560 °C with the increase in the barium content, so it can be seen that the no-doped compositions have the highest Curie temperature (TC=660 °C) due to the interaction of the vacancies created by the Ba^{2+} ion and the reduction of the lattice vibrations [19, 154]. Which means that the barium substitution in our composition is not recommended for high-temperature applications [155].

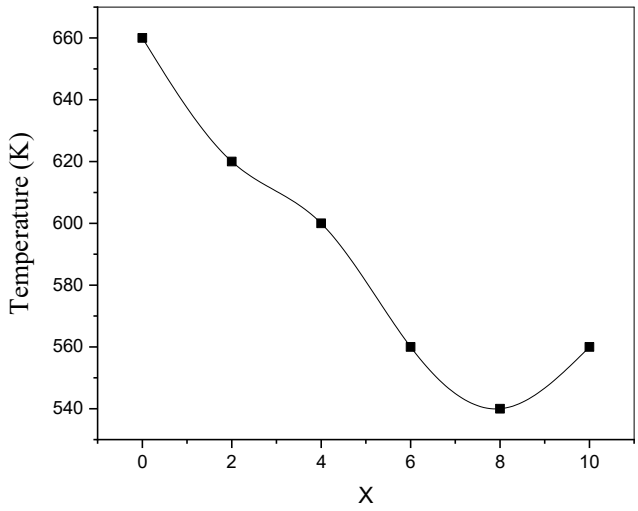

Figure IV. 3: Curie temperature dependent on barium substitution of $Pb_{1-X}Ba_X(Zr_{0.52}Ti_{0.43}(Al_{0.5}Sb_{0.5})_{0.05})O_3$.

IV.4 Impedance spectroscopy

Impedance spectroscopy measurements involve applying an AC voltage to the material and measuring the resulting current as a function of frequency. The resulting impedance spectrum can be analyzed to extract information about the material's electrical properties, such as its capacitance, resistance, and conductivity.

IV.4.1 Nyquist plot

The Nyquist plot can be analyzed using equivalent circuit models to extract the electrical parameters of the material, such as the resistance and capacitance. These parameters can then

be used to model the behavior of the material under different conditions. Several studies have used Nyquist plots to analyze the electrical properties of various materials, including piezoelectric ceramics.

IV.4.1.1 The effect of temperature and frequency on electrical properties

An analysis using the impedance spectroscopy technique was performed for a series of compositions of $Pb_{1-x}Ba_x(Zr_{0.52}Ti_{0.43}(Al_{0.5}Sb_{0.5})_{0.05})O_3$ base matrix ceramics in a frequency range and different temperatures to determine and evaluate the electrical behavior of our materials. Figure IV.4 shows the complex impedance spectra (Nyquist plot Z" VS Z') of the $Pb_{1-x}Ba_x(Zr_{0.52}Ti_{0.43}(Al_{0.5}Sb_{0.5})_{0.05})O_3$ ceramics where x = 0, 0.02, 0.04, 0.06, 0.08, and 0.10 at a frequency range of 0.1 kHz to 1 MHz and at different temperatures. Impedance data for materials are typically plotted with each point representing a specific frequency. These spectra are defined by the presence of a semicircular arc that depends on temperature. From these curves, we have observed a single semi-circle which suggests that the electrical results are homogeneous [156]. We can suggest that the presence of a single depressed semi-circle is due to the mass property of the materials and indicates the existence of a non-Debye type relaxation [157]. Almost all the curves show semicircles, the semi-circles illustrated in the figures give an idea of the impedance properties of materials, which can be evaluated as a function of temperature. It is known that the appearance of two semicircles indicates the contribution of grain and grain boundaries, but when only one semicircle is found (which is what we found in this case) it suggests that the electrical properties of $Pb_{1-x}Ba_x(Zr_{0.52}Ti_{0.43}(Al_{0.5}Sb_{0.5})_{0.05})O_3$ ceramics are mostly determined by the grain [6]. Consequently, the equivalent circuit we have chosen for all samples can be considered as consisting of a bulk resistance Rb and a bulk capacitance Cb connected in parallel [158]. In the case of ceramics and when we have obtained a single semicircle, the intersection of this semicircle with the x-axis which presents the real part of the impedance (Z') is considered as the bulk resistor of the ceramic [159]. It is clear that the diameter of the semicircles is reduced with the increase of the temperature, therefore the resistivity will be increased and consequently the increasing of conductivity. On the other hand, from the point of view of the effect of barium substitution, we observed that each time we increased the quantity of barium the curve took the shape of a semicircle. Several studies have investigated the impedance spectroscopy of PZT ceramics, A Kumari et al.(2021) [160] performed impedance spectroscopy measurements on ferromagnetic ceramics in the frequency range of 100 Hz to 7 MHz. They observed a single semicircle in the impedance spectrum, which they attributed to

the grain boundary contribution. The authors also studied the temperature dependence of the impedance spectra and observed a decrease in the resistance and an increase in the conductivity with increasing temperature. In another study, Pin-Yi Chen et al [161] investigated the impedance spectroscopy of Ferroelectric ceramics in the range of frequency of 0.1 KHz–1 MHz. They found that the impedance spectrum consisted of two semicircles, which could be attributed to the grain and grain boundary contributions. The authors also performed equivalent circuit analysis to extract the electrical parameters of the material, such as the resistance and capacitance. SC PANIGRAHI et al [162]. (2021) used Nyquist plots to investigate the effect of Gd^{+3} doped on the electrical properties of PZT-based ceramics. They found that semicircles are depressed; indicating the presence of non-Debye-type of relaxation, the existence of a single semicircle is related to the mass property of the materials

In a recent study, K. Rama Rao et al.(2021) [163] investigated the impedance spectroscopy of PZT ceramics with varying amounts of Sn^{4+} ion dopant. They show the non-Debye kind of relaxation process. Cole-Cole plots reveal the contribution of grain and grain boundary to the conduction process. The authors also observed a decrease in the resistance and an increase in the capacitance with increasing of Sn^{4+} ion doping.

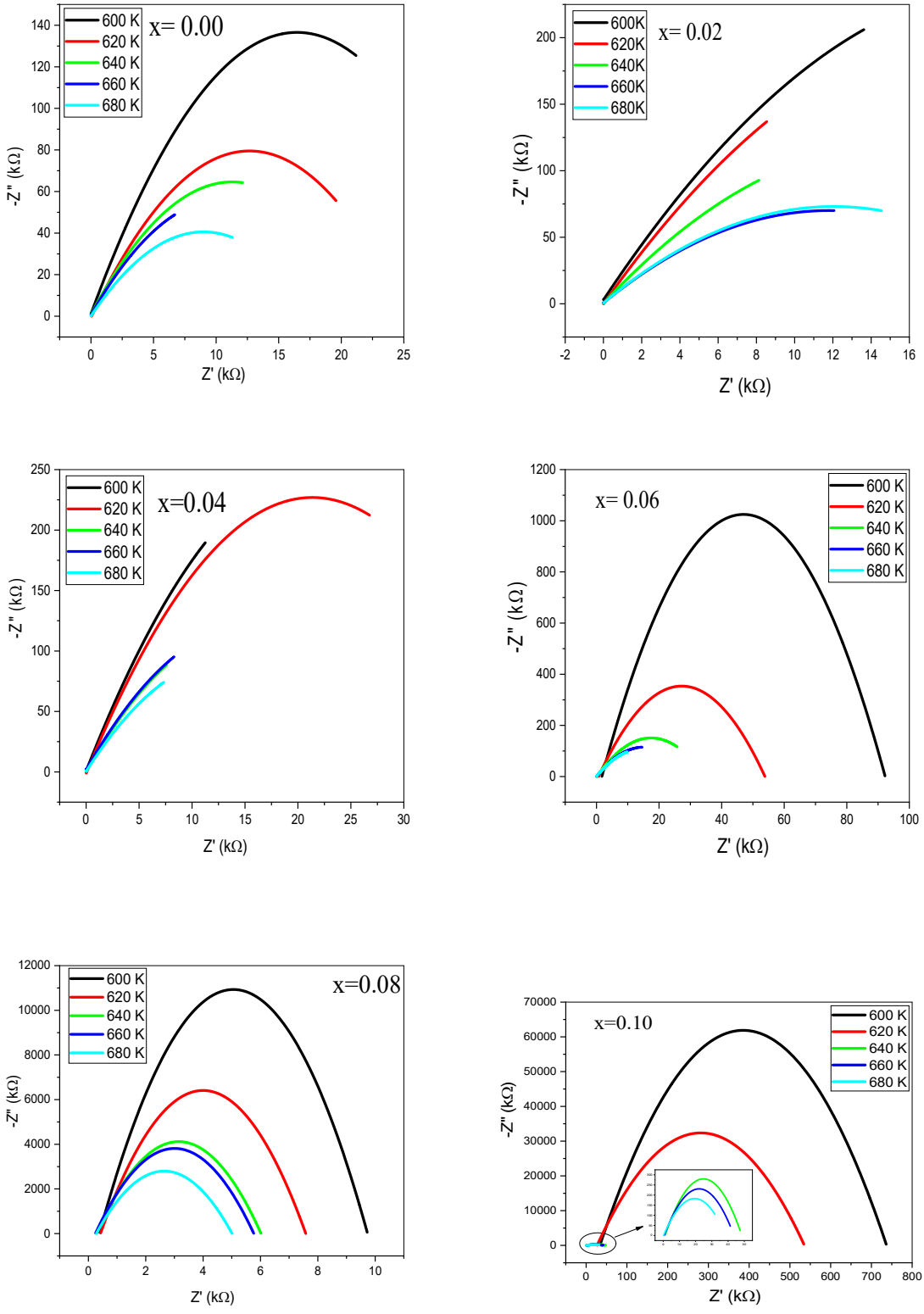

Figure IV. 4: Z'' depending on Z' at different temperatures of $Pb_{1-x}Ba_x(Zr_{0.52}Ti_{0.43}(Al_{0.5}Sb_{0.5})_{0.05})O_3$.

IV.4.2 Bode plots

IV.4.2.1 The Real Part

The variation of the real part of the impedance Z′ depends on the frequency for several temperatures for all compositions has been illustrated in Figure IV.5. It can be seen at low frequencies that the amplitude of Z′ reduces with an increase in temperature, demonstrating negative temperature coefficient of resistance behavior NTCR [158], the negative temperature coefficient of resistance NTCR refers to the variation in resistance of a material as a function of temperature, with an inverse dependency. In other words, as temperature increases, resistance decreases. In an NTCR, the electrical conductivity of the material increases as the temperature rises. This may be due to charge carrier mobility effects or to changes in the crystalline structure of the material. As a result, the electrical resistance of NTCR decreases with increasing temperature. It should be noted that the term 'negative temperature coefficient' can also be applied to other physical quantities, such as thermal conductivity, where an increase in temperature results in a decrease in thermal conductivity [164, 165]. This behavior will change radically at high frequencies, the value of the real part Z' for all temperatures will be completely merged above a specific frequency (f = 30 KHz) which clearly indicates the possibility of the eventual release of the space charge [166], we can consider this phenomenon as an electrical phenomenon that occurs in certain dielectric or insulating materials. When an insulating material is subjected to an external electric field, electric charges can move and accumulate at the interface between the material and the electric field, creating a region known as a "space charge". Furthermore, it is interesting to realize that the value of Z' strongly depends on the Barium content in our composition, it was found that the value of Z' for x=0.00 (without barium doping) at each temperature and frequency is low compared to the other compositions and begins to increase progressively (except x= 0.02 and x=0.08) with increasing barium content.

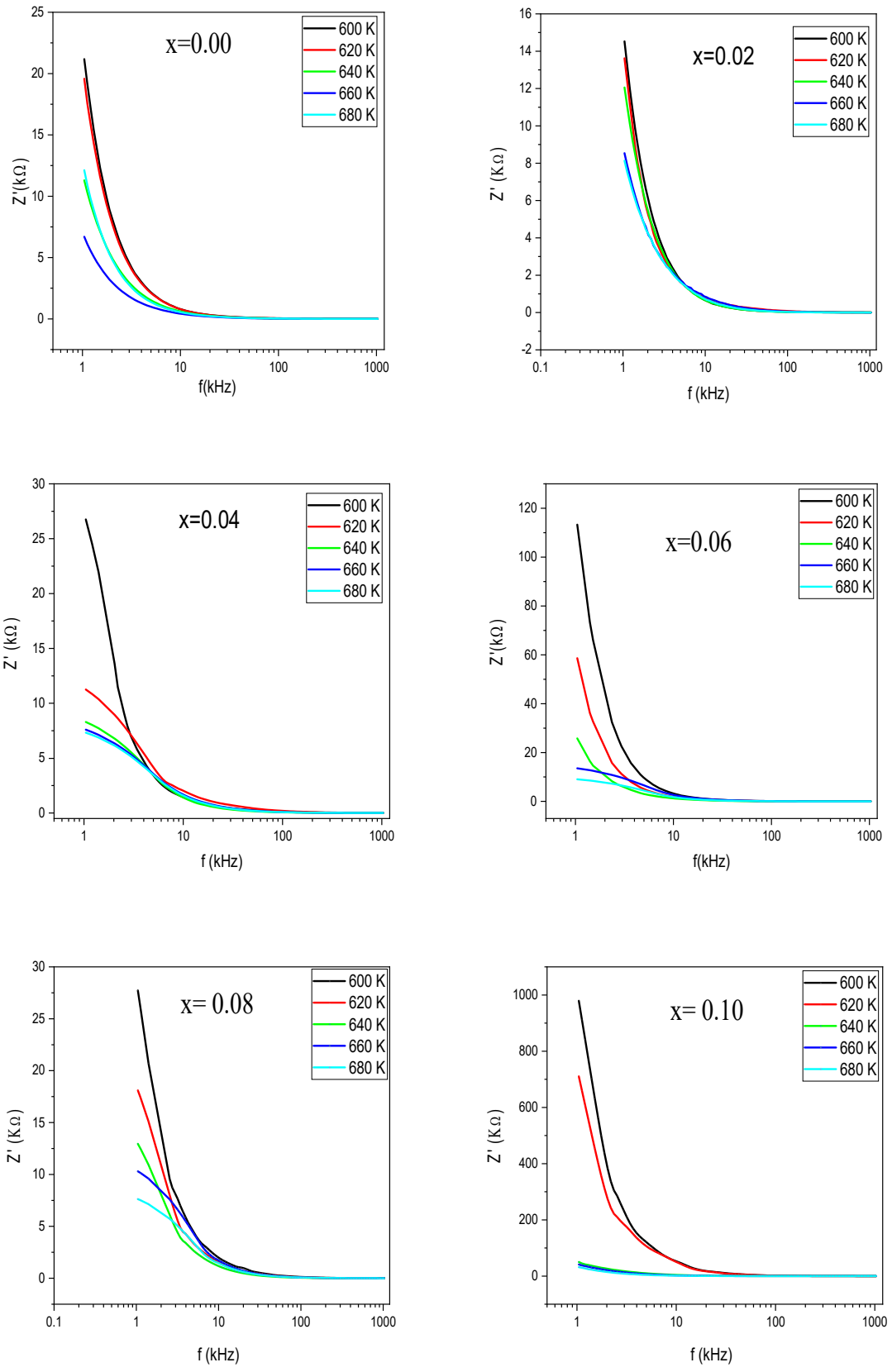

Figure IV. 5: Variation of Z′ with frequency at different temperatures of of Pb1-xBax(Zr0.52Ti0.43(Al0.5Sb0.5)0.05)O3.

IV.4.2.2 The Imaginary Part

Concerning the imaginary part of $Pb_{1-x}Ba_x(Zr_{0.52}Ti_{0.43}(Al_{0.5}Sb_{0.5})_{0.05})O_3$ and their variation as a function of frequency and temperature are illustrated in Figure IV.6. First, we noticed that the imaginary part Z″ decreased with increasing temperature due to the absence of mobile electrons at the examined temperatures [167]. This type of plot gives an idea of the electrical processes involved and the relaxation frequency of the most resistive component. Dispersion at a low frequency and merging at a higher frequency, this is what characterizes this pattern, which is due to the presence of a space charge polarization at a lower frequency and its elimination at a higher frequency [162]. However, it can be said that this style of dispersion and merging of Z" of all compositions at lower and higher frequencies respectively is due to the release of space charges as a result of a reduction in the barrier properties of the material with increasing temperature, can also be seen as an important factor in encouraging temperature-dependent increases in AC conductivity at higher frequencies [168].

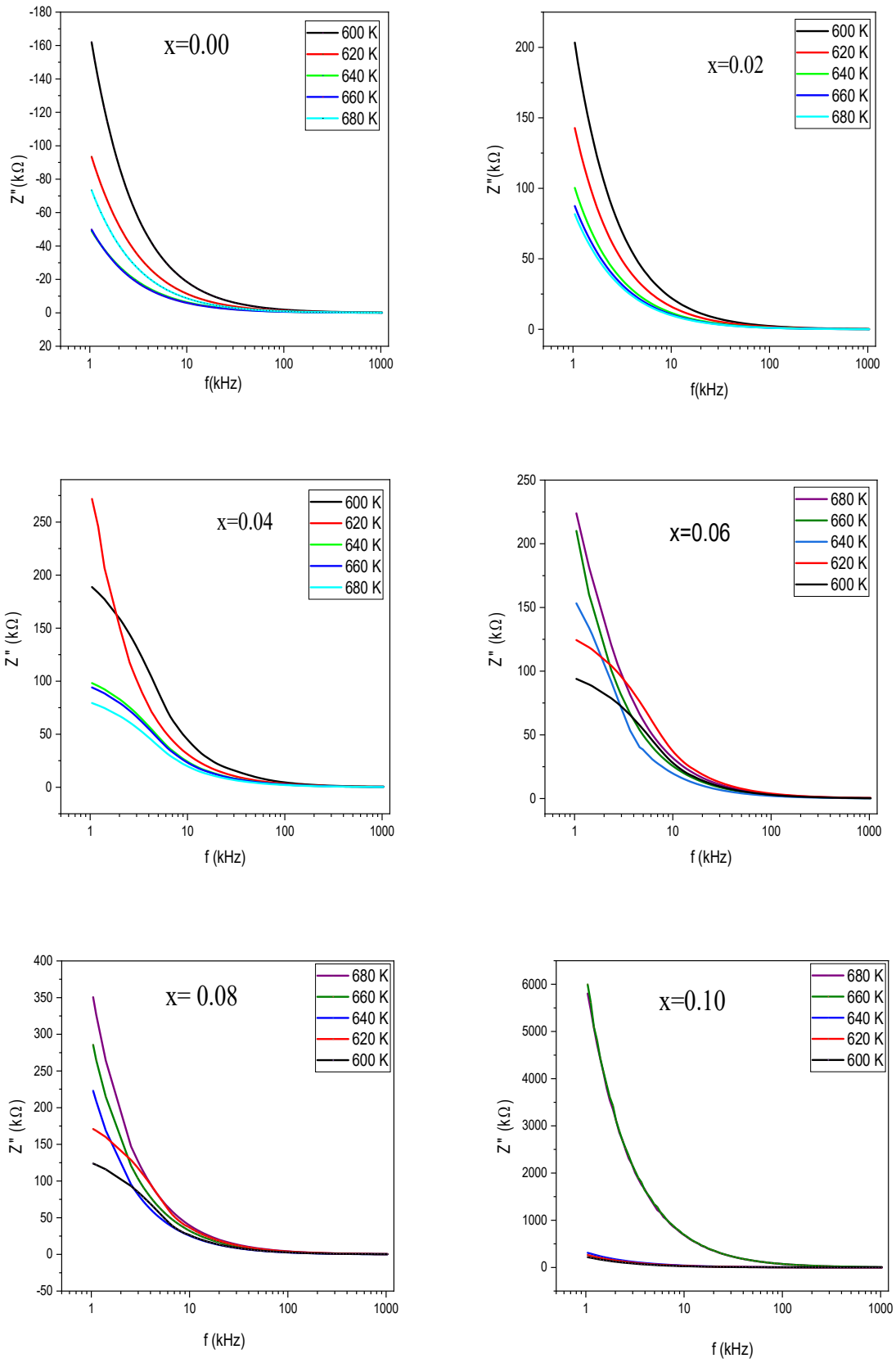

Figure IV. 6: Frequency–temperature dependence of Z” of Pb1-xBax(Zr0.52Ti0.43(Al0.5Sb0.5)0.05)O3.

IV.5 AC conductivity

It is challenging to define the movement of charge carriers in ceramic materials because a variety of complex dynamic processes are involved. However, conductivity can be described as an acceptable proxy for the electrical properties of the materials under study. It is well known that PZT ceramics have a p-type conductivity (hole-type conduction), caused by the loss of Pb due to the high volatility of PbO during the sintering process [115, 169]. The AC conductivity of PZT ceramics refers to their ability to conduct electrical current under the influence of an alternating current (AC) electrical field.

IV.5.1 The evolution of AC conductivity as function of temperature

The AC conductivity of $Pb_{1-x}Ba_x(Zr_{0.52}Ti_{0.43}(Al_{0.5}Sb_{0.5})_{0.05})O_3$ can be influenced by various factors, including temperature, composition, and frequency. Figure IV.7 demonstrates the AC Conductivity σ_{AC} as a function of the inverse of temperature 1000/T at different frequencies for all compositions. Around the Curie temperature, the conductivity increases, indicating an increase in tan δ and the polarizability of the material, which was suggested in the same study that it made by S C PANIGRAHI et al [162], but when the Curie temperature is exceeded, the conductivity takes the form of a straight line, suggesting behavior typical of the DC component of conductivity [119].

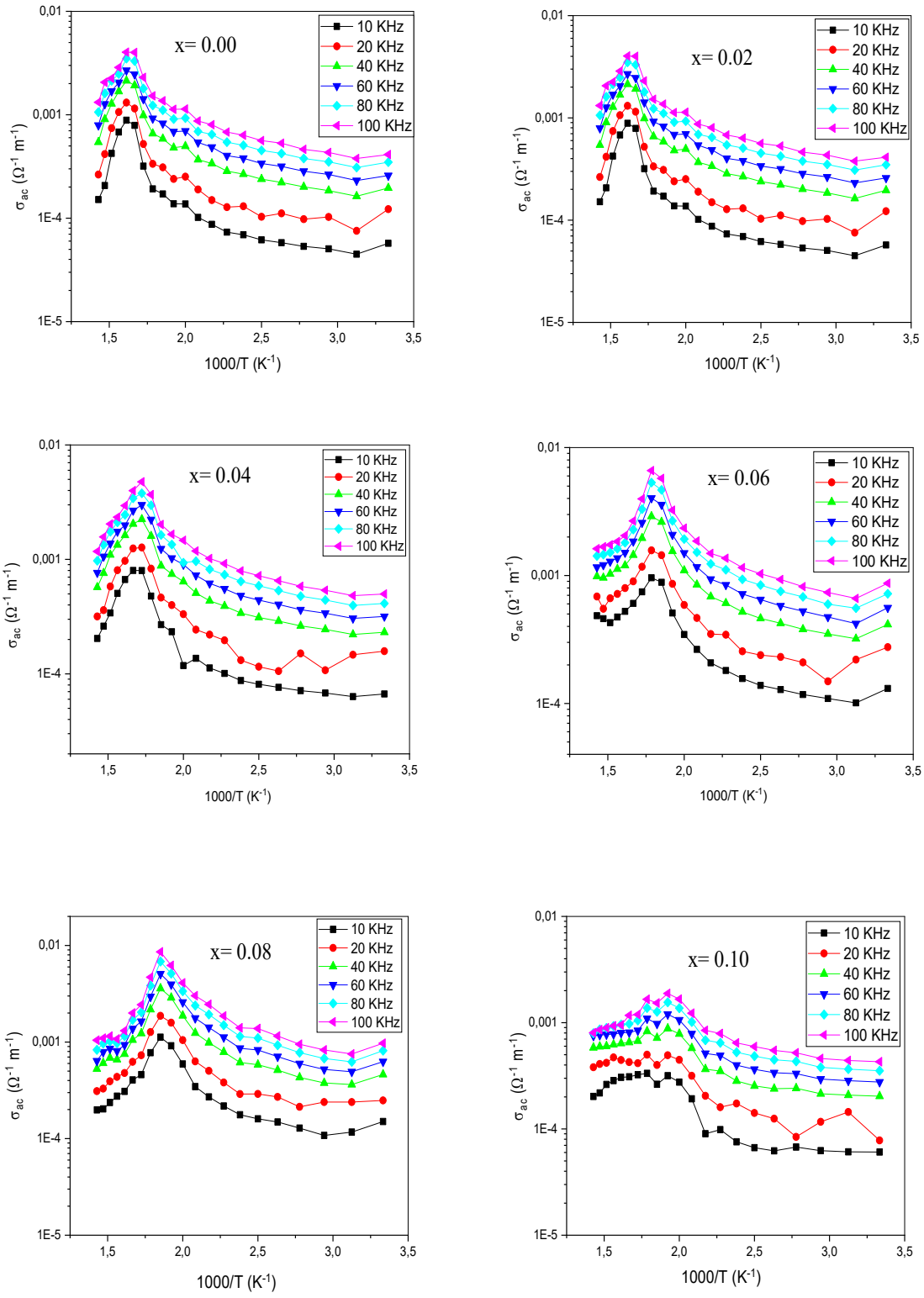

Figure IV. 7: Temperature–frequency dependence of ac conductivity of Pb1-xBax(Zr0.52Ti0.43(Al0.5Sb0.5)0.05)O3.

IV.5.2 The evolution of AC conductivity as function frequency

Figure IV.8 reveals the frequency dependent AC conductivity of $Pb_{1-x}Ba_x(Zr_{0.52}Ti_{0.43}(Al_{0.5}Sb_{0.5})_{0.05})O_3$ at different temperature ranges. AC conductivity σ_{ac} (ω) is related to the total conductivity σ_t (ω) and dc conductivity σ_{dc} according to the relation [170, 171]

$$\sigma_{ac}(\omega) = \sigma_t(\omega) - \sigma_{dc} \qquad \text{IV.2}$$

The AC component is determined by subtracting the dc component from the total conductivity. However, the dc component σ_{dc} is insignificantly small compared to σ_t (ω). Therefore, σ_t (ω) can be considered as σ_{ac}(ω) [172]. In general, the AC conductivity of the dielectric material can be calculated using the following equation [173]:

$$\sigma_{ac} = \omega.C\ tg\delta\ (d/a) \qquad \text{IV.3}$$

where ω represents the angular frequency, C is capacitance, tgδ represents dielectric loss, and d and a denote the thickness and area of the sample, respectively. The equation suggests that the AC conductivity changes slowly at lower frequencies, while at higher frequencies (>100 kHz), the AC conductivity becomes more strongly dependent on the frequency.

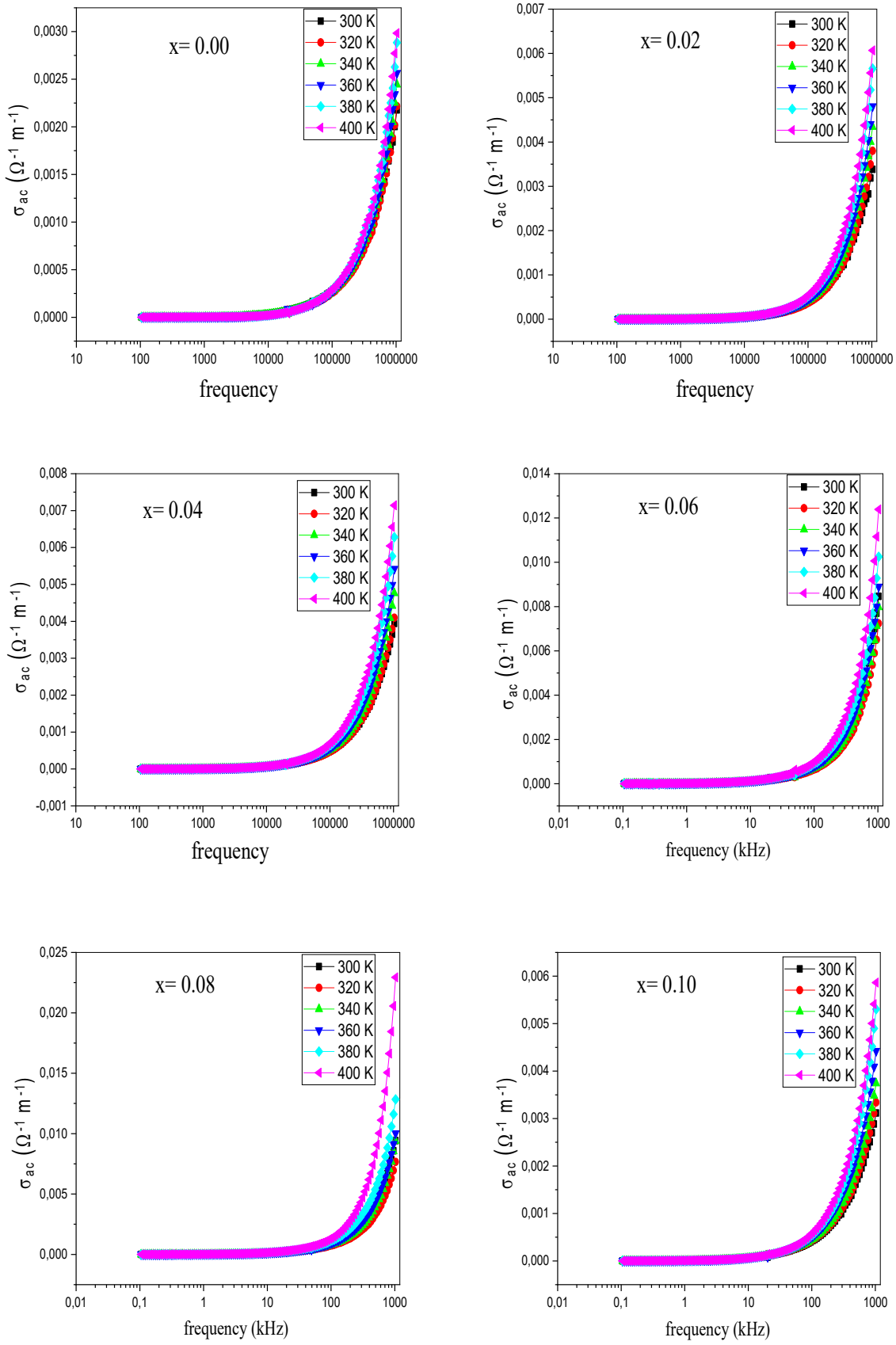

Figure IV. 8: The AC conductivities of Pb1-xBax(Zr0.52Ti0.43(Al0.5Sb0.5)0.05)O3.

IV.5.3 The Barium effect on AC conductivity

Figure IV.9 demonstrate the AC conductivity of $Pb_{1-x}Ba_x(Zr_{0.52}Ti_{0.43}(Al_{0.5}Sb_{0.5})_{0.05})O_3$ as a function of barium concentration, it is clear that the Barium substitution can have a significant effect on their AC conductivity. When barium Ba is substituted for some of the lead Pb, it alters the crystal structure and electrical properties of the material. Barium substitution can modify the oxygen vacancies and defect concentrations in the crystal lattice, thereby affecting the electrical conductivity. The AC conductivity is primarily governed by two conduction mechanisms [174, 175]: electronic conduction and ionic conduction. Electronic conduction involves the movement of free electrons, while ionic conduction involves the migration of charged species, typically oxygen vacancies. So we can suggest that the AC conductivity can be tailored by adjusting the barium content and optimizing the composition to achieve the desired electrical properties [176]. It is worth noting that other factors, such as temperature, sintering conditions, and the presence of dopants, can also influence AC conductivity. Therefore, comprehensive experimental studies [177, 178] and characterization techniques are typically necessary to understand and quantify the specific impact of barium substitution on the AC conductivity of $Pb_{1-x}Ba_x(Zr_{0.52}Ti_{0.43}(Al_{0.5}Sb_{0.5})_{0.05})O_3$ ceramics.

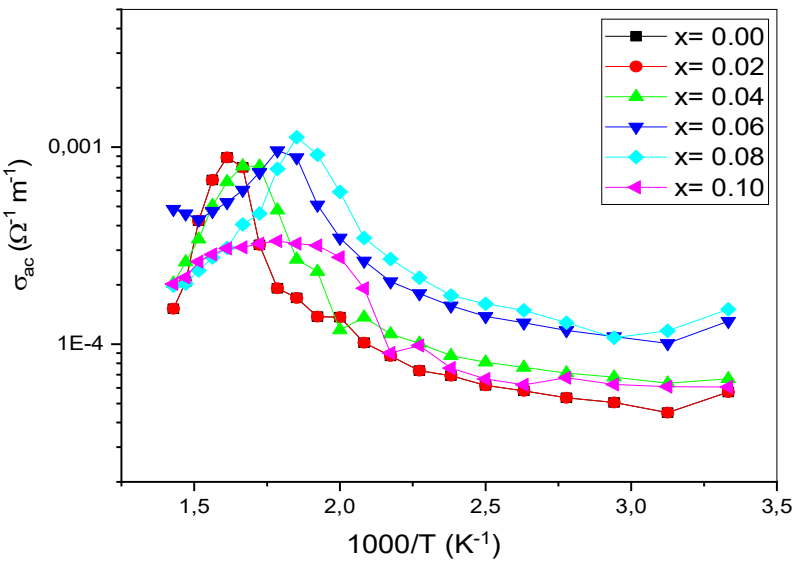

Figure IV. 9: Barium amount dependence of AC conductivity of Pb1-xBax(Zr0.52Ti0.43(Al0.5Sb0.5)0.05)O3 ceramics.

IV.6 Conclusion

In conclusion, this chapter presented an in-depth analysis of the dielectric and AC conductivity characteristics using impedance spectroscopy. The following key results were obtained:

Bode and Nyquist diagrams were utilized to visualize the impedance behavior. The Nyquist diagram provided information on the complex impedance and allowed the determination of the material's electrical properties. The real and imaginary parts of impedance were investigated as a function of temperature and frequency. At low frequencies the amplitude of Z' reduces with an increase in temperature, demonstrating a negative temperature coefficient of resistance behavior NTCR, and this behavior will change radically at high frequencies, the value of the real part Z' for all temperatures will be completely merged above a specific frequency (f = 30 KHz) which clearly indicates the possibility of the eventual release of the space charge. We also noticed that the imaginary part Z'' decreased with increasing temperature due to the absence of mobile electrons at the examined temperatures. The permittivity and dielectric loss were calculated from the impedance measurements. The permittivity represented the material's ability to store electrical energy.

Finally, the results presented in this chapter provided a comprehensive understanding of the dielectric and AC conductivity characteristics of $Pb_{1-x}Ba_x(Zr_{0.52}Ti_{0.43}(Al_{0.5}Sb_{0.5})_{0.05})O_3$ ceramics. The temperature and frequency dependencies, as well as the effects of barium substitution, were thoroughly analyzed. These findings contribute to the broader knowledge of impedance spectroscopy and its application in characterizing dielectric materials.

General conclusion

General conclusion

This doctoral thesis, the $Pb_{1-X}Ba_X(Zr_{0,52}Ti_{0,43}(Al_{0,5}Sb_{0,5})_{0,05})O_3$ ceramics where (x = 0.00, 0.02, 0.04, 0.06, 0.08, and 0.10) have been successfully prepared using the solid-state reaction method, we successfully investigated the characteristics of this type of ceramic and providing valuable insights into their, dielectric, and AC conductivity behavior. The combination of extensive literature research and practical experimentation allowed for a comprehensive understanding the electrical behavior.

The main results and objectives we were hoping to achieve include:

XRD results show all the peaks are corresponding to perovskite structures, so we conclude that the perovskite structure was successfully formed for each composition studied without any detectable secondary phase, so the indication of the Ba^{2+} ions are well incorporated in the crystal lattice. The deconvolution of the peaks situated between 42° and 47° by using the Gaussian function which helps us to observe three small peaks corresponding to the (002) and (200) of the Tetragonal phase T and (200) of the Rhombohedral phase R, suggesting the coexistence of two phases T+R at the same time, meaning that we are in the region of the MPB. The FTIR results are consistent with the XRD results above and confirmed that the perovskite structure was successfully formed.

The results of the tolerance factor are in the range of 0.9968 and 1.0001 which indicate the stability of the perovskite structure, in addition, the increase of Ba^{+2} amounts brings the tolerance factor close to 1, which makes the perovskite structure more stable. The effect of Barium substitution on density is significantly clear, in that the density of the pellets increases with increasing Barium content, reaching up to 7.17 g/cm^3. The SEM micrographs of the specimens sintered demonstrate that the microstructure of the studied samples is dense and composed of grains of different shapes and relatively small sizes, showing that the samples are denser and therefore less porous.

The variation of the dielectric constant εr and dielectric loss tgδ demonstrate that the dielectric constant gradually increases with an increase in temperature until the TC after that the dielectric constant will be strongly decreased which indicates ferroelectric phase transition, The highest dielectric constant was found at the Curie temperature ε max, which is probably due to the thermally activated electrons in the system. The dielectric constant εr

drops with increasing frequency which is a general characterization of polar dielectric materials which indicates the presence of all types of polarizations. Concerning the dielectric loss tgδ, which has very small values, there is decreasing with increasing frequency, also the increase in the dielectric loss at high temperatures could be assigned to the increase in conductivity. It is very clear that the Curie temperature ceramic decreases from 660 °C to 560 °C with the increase in the barium content, which means that the barium substitution in our composition is not recommended for high-temperature applications.

From the Nyquist plot, we can suggest from the presence of a single depressed semi-circle is due to the mass property of the materials and indicates the existence of a non-Debye type relaxation. It can be seen from the variation of the real part of the impedance Z′ depends on the frequency for several temperatures, that at low frequencies the amplitude of Z′ reduces with an increase in temperature, demonstrating a negative temperature coefficient of resistance behavior NTCR, this behavior will change radically at high frequencies, the value of the real part Z' for all temperatures will be completely merged which clearly indicates the possibility of the eventual release of the space charge.

We noticed too that the imaginary part Z″ decreased with increasing temperature due to the absence of mobile electrons at the examined temperatures. Around the Curie temperature, the conductivity increases, indicating an increase in tan δ and the polarizability of the material. The effect of barium substitution on AC conductivity depends on the concentration of barium and the specific composition of our material. In general, increasing barium content can lead to changes in the AC conductivity

In conclusion, our research work has yielded significant results, and we have successfully achieved our research objectives. The results obtained in this study provide valuable insights into the characteristics of barium-doped PZT ceramics and contribute to the existing knowledge base in this field of research. Extensive analysis and experimental research have concluded that barium has a major influence on the various properties and characteristics of $Pb_{1-X}Ba_X(Zr_{0,52}Ti_{0,43}(Al_{0,5}Sb_{0,5})_{0,05})O_3$ ceramics, these results underscore the importance and highlight its potential applications in various fields.

Additionally, our research work has addressed several research gaps and generated new perspectives for future investigations. Overall, this study significantly advances our understanding of PZT-based materials and their properties and sets the stage for further research and development in this area." We therefore hope also that every researcher in this

field will benefit from this modest work, so that it will provide at least a small helping hand to develop and give a new idea in this specialization of scientific research.

References

[1] S. Yan, C. Sun, Q. Cui, M. He, R. Wang, J. Hao, X. Chu, Dielectric, piezoelectric and dc bias characteristics of Bi-doped PZT multilayer ceramic actuator, Mater. Chem. Phys. 255 (2020) 123605. https://doi.org/https://doi.org/10.2298/PAC1603175M.

[2] M.D. Durruthy-Rodríguez, J. Portellez-Rodríguez, J.F. Bentancourt, M. Hernández-García, M.A. Hernández-Landaverde, F. Rodríguez-Melgarejo, J.M. Yañez-Limón, Ferroelastic and ferroelectric phase transition in bulk Pb1-xLax (Zr0. 53Ti0. 47) O3, Appl. Phys. A 127 (2021) 1-8. https://doi.org/https://doi.org/10.1007/s00339-021-04829-7.

[3] F. Guo, S. Zhang, W. Long, P. Fang, X. Li, Z. Xi, SnO2 modified PNN-PZT ceramics with ultra-high piezoelectric and dielectric properties, Ceram. Int. (2022). https://doi.org/https://doi.org/10.1016/j.ceramint.2022.04.308.

[4] H. Chen, T. Pu, S. Fan, H. Liu, J. Zhu, Q. Chen, Enhanced electrical properties in low-temperature sintering PNN–PMW–PZT ceramics by Yb2O3 doping, Mater. Res. Bull. 146 (2022) 111576. https://doi.org/https://doi.org/10.1016/j.materresbull.2021.111576.

[5] T. Rashid, Z.A. Ahmad, H. Mohamad, Influence of sintering parameters on structural, dielectric and piezoelectric properties of Ca, La and Sr-doped PZT (PCLSZT) electroceramics, J. Mater. Sci. - Mater. Electron. 32 (2021) 18095-18107. https://doi.org/https://doi.org/10.1007/s10854-021-06354-y.

[6] B. Tiwari, C. RNP, Electrical Impedance and Modulus Characteristics of Bulk PZT Ceramics Modified by Mn and Ce, International Research Journal on Advanced Science Hub 2 (2020) 44-48.

[7] P. Panda, B. Sahoo, PZT to lead free piezo ceramics: a review, Ferroelectrics 474 (2015) 128-143.

[8] V. Pal, O. Thakur, R. Dwivedi, Investigation of MPB region in lead free BLNT-BCT system through XRD and Raman spectroscopy, J. Phys. D: Appl. Phys. 48 (2015) 055301. https://doi.org/https://doi.org/10.1088/0022-3727/48/5/055301.

[9] S. Sen, R. Choudhary, A. Tarafdar, P. Pramanik, Impedance spectroscopy study of strontium modified lead zirconate titanate ceramics, J. Appl. Phys. 99 (2006) 124114. https://doi.org/https://doi.org/10.1063/1.2206850.

[10] R. Pandey, M. Bhatnagar, P. Kumar, R.K. Malik, C. Prakash, Improved dielectric and energy storage properties in (1-x) BaTi0. 80Zr0. 20O3-xBa0. 70Ca0. 30Ti0. 99Fe0. 01O3 ceramics near morphotropic phase boundary, Mater. Lett. 318 (2022) 132126. https://doi.org/https://doi.org/10.1016/j.matlet.2022.132126.

[11] Z. Huang, Y. Lai, W. Guan, Y. Zeng, Y. Wei, S. Wu, J. Han, Y. Mao, Y. Xiang, Structure, dielectric and ferroelectric properties of lead-free (1− x)(Ba0. 85Ca0. 15)(Ti0. 9Zr0. 1) O3-xBa (Mg1/3Nb2/3) O3 ceramics, Mater. Lett. 178 (2016) 163-165. https://doi.org/https://doi.org/10.1016/j.matlet.2016.05.010.

[12] B. Sahoo, P.K. Panda, Ferroelectric, dielectric and piezoelectric properties of Pb1− x Ce x (Zr0. 60Ti0. 40) O3, 0≤ x≤ 0.08, J. Mater. Sci. 42 (2007) 9684-9688. https://doi.org/https://doi.org/10.1007/s10853-007-1948-4.

[13] Z. Xu, X. Zeng, Z. Cao, L. Ling, P. Qiu, X. He, Effects of barium substitution on the optical and electrical properties of PLZT transparent electro-optical ceramics, Ceramics International 45 (2019) 17890-17897.

[14] K. Ramam, M. Lopez, Effect of strontium doping on dielectric, ferroelectric and piezoelectric properties of PLZTN ceramics, Mater Sci Eng B 145 (2007) 41-47. https://doi.org/https://doi.org/10.1016/j.mseb.2007.09.085.

[15] L. Hamzioui, F. Kahoul, A. Boutarfaia, A. Guemache, M. Aillerie, Structure, dielectric and piezoelectric properties of Pb [(Zr0. 45, Ti0. 5)(Mn0. 5, Sb0. 5) 0.05] O3 ceramics, Process. Appl. Ceram 14 (2020) 19-24. https://doi.org/https://doi.org/10.2298/PAC2001019H.

[16] R. Rai, S. Sharma, R. Choudhary, Effect of Al doping on structural and dielectric properties of PLZT ceramics, J. Mater. Sci. 41 (2006) 4259-4265. https://doi.org/https://doi.org/10.1007/s10853-005-5455-1.

[17] Q. Zhang, X. Liu, Y. Zhang, X. Song, J. Zhu, I. Baturin, J. Chen, Effect of barium content on dielectric and energy storage properties of (Pb, La, Ba)(Zr, Sn, Ti) O3 ceramics, Ceram. Int. 41 (2015) 3030-3035. https://doi.org/https://doi.org/10.1016/j.ceramint.2014.10.139. .

[18] B.P. Kumar, S. Sangawar, H. Kumar, Structural and electrical properties of double doped (Fe3+ and Ba2+) PZT electroceramics, Ceram. Int. 40 (2014) 3809-3812. https://doi.org/https://doi.org/10.1016/j.ceramint.2013.08.014.

[19] K. Ramam, M. Lopez, Ferroelectric and piezoelectric properties of Ba modified lead zirconium titanate ceramics, J. Phys. D: Appl. Phys. 39 (2006) 4466. https://doi.org/https://doi.org/10.1088/0022-3727/39/20/025.

[20] X. Wang, W. Cai, Z. Xiao, X. Yu, J. Chen, T. Yang, Enhanced dielectric and tunable properties of Ba-doped (Pb, La)(Zr, Sn, Ti) O3 antiferroelectric ceramics, J. Mater. Sci. - Mater. Electron. 31 (2020) 17013-17017. https://doi.org/https://doi.org/10.1007/s10854-020-04258-x.

[21] J. Juneja, S. Singh, K. Raina, C. Prakash, Study on structural, dielectric, ferroelectric and piezoelectric properties of Ba doped Lead Zirconate Titanate Ceramics, Phys. B: Condens. Matter 431 (2013) 109-114. https://doi.org/https://doi.org/10.1016/j.physb.2013.09.011.

[22] P. Boch, J.-C. Ni, Ceramic materials: Processes, properties, and applications, John Wiley & Sons2010.

[23] W. Ching, Theoretical studies of the electronic properties of ceramic materials, Journal of the American Ceramic Society 73 (1990) 3135-3160.

[24] S. Swartz, Topics in electronic ceramics, IEEE Transactions on Electrical Insulation 25 (1990) 935-987.

[25] E. Boucher, Elaboration et caractérisation de céramiques PZT bi-substituees et modélisation non-linéaire de leur comportement en contrainte et en champ électrique, Lyon, INSA, 2002.

[26] A. Benayad, Matériaux monocristallins à forte activité piézoélectrique: élaboration, caractérisation et application, INSA de Lyon (2005).

[27] H. Stoyanov, Soft nanocomposites with enhanced electromechanical response for dielectric elastomer actuators, Universität Potsdam, 2011.

[28] L. Hamzioui, Etude des propriétés diélectriques et piézoélectriques dans le système ternaire: Pb0. 98Ca0. 02 [(Zr0. 52Ti0. 48) 0.98 (Cr3+ 0.5, Ta5+ 0.5) 0.02] O3 effet du dopage, (2013).

[29] S.R. Moheimani, A.J. Fleming, Piezoelectric transducers for vibration control and damping, Springer2006.

[30] J. Fernandez Lopez, Modeling and optimization of ultrasonic linear motors, EPFL, 2006.

[31] K. Ralls, T.H. Courtney, J. Wulff, Introduction to materials science and engineering, John Wiley & Sons, Inc.1976.

[32] A. Kumar, V. Pal, S. Mishra, Preparation, microstructure, dielectric and electrical analysis of Fe-modified PZT piezoceramics, Journal of Materials Science: Materials in Electronics 32 (2021) 2946-2952.

[33] A. Sharma, K.M. Batoo, O.M. Aldossary, S. Jindal, N. Aggarwal, G. Kumar, Investigation of dielectric, electrical and optical properties of copper substituted Mn-Zn nanoferrites, Journal of Materials Science: Materials in Electronics 32 (2021) 313-322.

[34] C. Huber, Synthèse et caractérisation de nouveaux matériaux ferroélectriques accordables pour applications hyperfréquences, Université Sciences et Technologies-Bordeaux I, 2003.

[35] S. Orlowska, Conception and Prediction of Dielectric Characteristics of Two- and Three-Phase Composite Materials Through Modeling and Experimental Validation

Conception et prédiction des caractéristiques diélectriques des matériaux composites à deux et trois phases par la modélisation et la validation expérimentale, Ecole Centrale de Lyon, 2003. https://theses.hal.science/tel-00144550.

[36] R. Coelho, Les diélectriques : propriétés diélectriques des matériaux isolants, Hermes Science Publications, Paris: Hermes, 1993.

[37] C. Huber, synthesis and characterisation of new tunable ferroelectic materials for hyperfrequency applications

Synthèse et caractérisation de nouveaux matériaux ferroélectriques accordables pour applications hyperfréquences, Université Sciences et Technologies - Bordeaux I, 2003. https://theses.hal.science/tel-00203599.

[38] A. Boudefel, Propriétés diélectriques de polymères composites et leurs applications en microélectronique, Université Badji Mokhtar Annaba,Faculté des Sciences de l' IngénieurAnnaba, 2009, pp. 113.

[39] Z.G. Ye, Handbook of Advanced Dielectric, Piezoelectric and Ferroelectric Materials: Synthesis, Properties and Applications, Elsevier Science2008.

[40] M. Frey, Z. Xu, P. Han, D. Payne, The role of interfaces on an apparent grain size effect on the dielectric properties for ferroelectric barium titanate ceramics, Ferroelectrics 206 (1998) 337-353.

[41] K. Kinoshita, A. Yamaji, Grain-size effects on dielectric properties in barium titanate ceramics, Journal of applied physics 47 (1976) 371-373.

[42] G. Arlt, D. Hennings, G. De With, Dielectric properties of fine-grained barium titanate ceramics, Journal of applied physics 58 (1985) 1619-1625.

[43] S. Sarraute, Pb5Al3F19 : Relationships between structures, ferroic properties and phase transitions

Pb5Al3F19 : relation entre structures, propriétés ferroiques et transitions de phases, Université Sciences et Technologies - Bordeaux I, 1995. https://theses.hal.science/tel-00148834.

[44] G.-T. Joo, Nouvelles phases ferroélectriques non stoechiométriques de type perovskite ou LiTaO3, Université Sciences et Technologies - Bordeaux I, 1986. https://theses.hal.science/tel-00203505.

[45] M.A. Hentati, Effects of local inhomogeneities and external constraints on dielectric and structural properties of PZN-x% PT single crystals

Effets des inhomogénéités locales et des contraintes extérieures sur les propriétés diélectriques et structurales des monocristaux PZN-x%PT, Ecole Centrale Paris, 2013. https://theses.hal.science/tel-01003354.

[46] M. MME SAIDI, Effet des conditions de synthèse sur les propriétés diélectriques, ferroélectrique et piézoélectriques de la composition [(Na0. 535 K 0.480) 0.966 Li0. 058](Nb0. 90Ta 0.10) O3, Université de Tizi Ouzou-Mouloud Mammeri.

[47] C. Millon, Contribution à l'étude de procédés de réalisation de structures métal/PZT/métal sur silicium pour microsystèmes piézoélectriques, Lyon, INSA, 2003.

[48] G. Lippmann, Principe de la conservation de l'électricité, ou second principe de la théorie des phénomènes électriques, Journal de Physique Théorique et Appliquée 10 (1881) 381-394.

[49] V. Kovacova, Etude des corrélations entre la microstructure et les propriétés piézoélectriques des films minces Pb (ZrTi) O3, Université Grenoble Alpes (ComUE), 2015.

[50] J.P. Glusker, M. Lewis, M. Rossi, Crystal structure analysis for chemists and biologists, John Wiley & Sons1996.

[51] B. Jaffe, R. Roth, S. Marzullo, Piezoelectric properties of lead zirconate-lead titanate solid-solution ceramics, Journal of Applied Physics 25 (1954) 809-810.

[52] S.L.d. Santos e Lucato, Constraint-Induced Crack Initiation and Crack Growth at Electrode Edges in Piezoelectric Ceramics, Technische Universität.

[53] H.D. Megaw, Origin of ferroelectricity in barium titanate and other perovskite-type crystals, Acta Crystallographica 5 (1952) 739-749.

[54] A. Von Hippel, Piezoelectricity, ferroelectricity, and crystal structure, Zeitschrift für Physik A Hadrons and nuclei 133 (1952) 158-173.

[55] D. Kobor, Synthèse, dopage et caractérisation de monocristaux ferroélectriques type PZN-PT par la méthode du flux, 2005.

[56] A. Meklid, Elaboration, caractérisation et étude des propriétés diélectriques et électromécaniques d'un nouveau matériau de céramique de type Zirconate-Titanate de plomb (PZT), UNIVERSITE MOHAMED KHIDER-BISKRA, 2018.

[57] M.E. Lines, A.M. Glass, Principles and applications of ferroelectrics and related materials, Oxford university press2001.

[58] J. Dygas, G. Fafilek, M. Breiter, Study of grain boundary polarization by two-probe and four-probe impedance spectroscopy, Solid State Ionics 119 (1999) 115-125.

[59] H.T. Langhammer, D. Makovec, Y. Pu, H.-P. Abicht, M. Drofenik, Grain boundary reoxidation of donor-doped barium titanate ceramics, Journal of the European Ceramic Society 26 (2006) 2899-2907.

[60] N. Zidi, A. Chaouchi, S. d'Astorg, M. Rguiti, C. Courtois, Dielectric and impedance spectroscopy characterizations of CuO added (Na0. 5Bi0. 5) 0.94 Ba0. 06TiO3 lead-free piezoelectric ceramics, Journal of alloys and compounds 590 (2014) 557-564.

[61] G. Galicia Aguilar, Corrosion study of magnesium and AZ91 magnesium alloys by EIS and LEIS techniques

Etude par spectroscopie d'impédance globale et locale de la corrosion du magnésium et des alliages de magnésium AZ91, Université Paris 6 - Pierre et Marie Curie, 2006. https://theses.hal.science/tel-01378620.

[62] A. Ziani, Etude de nouveaux matériaux : Films minces perovskites oxynitrures, de la photocatalyse à la microélectronique, Université Européenne de Bretagne, 2009. https://theses.hal.science/tel-00441375.

[63] E.A. Katz, Perovskite: name puzzle and German-Russian odyssey of discovery, Helvetica Chimica Acta 103 (2020) e2000061.

[64] H.-R. Wenk, A. Bulakh, Minerals: their constitution and origin, Cambridge University Press2016.

[65] B. Saparov, D.B. Mitzi, Organic–inorganic perovskites: structural versatility for functional materials design, Chemical reviews 116 (2016) 4558-4596.

[66] M. O'keeffe, B. Hyde, Some structures topologically related to cubic perovskite (E21), ReO3 (D09) and Cu3Au (L12), Acta Crystallographica Section B: Structural Crystallography and Crystal Chemistry 33 (1977) 3802-3813.

[67] S. Sasaki, C.T. Prewitt, J.D. Bass, W. Schulze, Orthorhombic perovskite CaTiO3 and CdTiO3: structure and space group, Acta Crystallographica Section C: Crystal Structure Communications 43 (1987) 1668-1674.

[68] Y. Dang, D. Ju, L. Wang, X. Tao, Recent progress in the synthesis of hybrid halide perovskite single crystals, CrystEngComm 18 (2016) 4476-4484.

[69] R. Roukos, Phases transitions in complexe oxides with perovskite structure : case system (1-x)Na0,5Bi0,5TiO3 - xCaTiO3

Transitions de phases dans des oxydes complexes de structure pérovskite : cas du système (1-x)Na0,5Bi0,5TiO3 - xCaTiO3, Université de Bourgogne, 2015. https://theses.hal.science/tel-01562679.

[70] L. Pauling, The nature of the chemical bond, 3rd ed., Cornell University Press1960.

[71] H.D. Megaw, Crystal structure of double oxides of the perovskite type, Proceedings of the Physical Society 58 (1946) 133.

[72] V.M. Goldschmidt, Die gesetze der krystallochemie, Naturwissenschaften 14 (1926) 477-485.

[73] Z. Dai, W. Liu, D. Lin, X. Ren, Electrical properties of zirconium-modified BiScO3-PbTiO3 piezoelectric ceramics at re-designed phase boundary, Materials Letters 215 (2018) 46-49.

[74] S.E. Park, K. Markowski, S. Yoshikawa, L.E. Cross, Effect on electrical properties of barium and strontium additions in the lead lanthanum zirconate stannate titanate system, Journal of the American Ceramic Society 80 (1997) 407-412.

[75] L. Viciu, V.O. Golub, J.B. Wiley, Structural, thermal and magnetic characterization of the manganese oxyhalide layered perovskite,(MnCl) LaNb2O7, Journal of Solid State Chemistry 175 (2003) 88-93.

[76] Y. Mao, S. Banerjee, S.S. Wong, Large-scale synthesis of single-crystalline perovskite nanostructures, Journal of the American Chemical Society 125 (2003) 15718-15719.

[77] R. Zhang, B. Jiang, W. Cao, Elastic, piezoelectric, and dielectric properties of multidomain 0.67 Pb (Mg 1/3 Nb 2/3) O 3–0.33 PbTiO 3 single crystals, Journal of Applied Physics 90 (2001) 3471-3475.

[78] S.J. Skinner, Recent advances in Perovskite-type materials for solid oxide fuel cell cathodes, International Journal of Inorganic Materials 3 (2001) 113-121.

[79] A. Kojima, K. Teshima, Y. Shirai, T. Miyasaka, Organometal halide perovskites as visible-light sensitizers for photovoltaic cells, Journal of the american chemical society 131 (2009) 6050-6051.

[80] E.H. Anaraki, A. Kermanpur, L. Steier, K. Domanski, T. Matsui, W. Tress, M. Saliba, A. Abate, M. Grätzel, A. Hagfeldt, Highly efficient and stable planar perovskite solar cells by solution-processed tin oxide, Energy & Environmental Science 9 (2016) 3128-3134.

[81] G. Shirane, A. Takeda, Phase transitions in solid solutions of PbZrO3 and PbTiO3 (I) small concentrations of PbTiO3, Journal of the Physical Society of Japan 7 (1952) 5-11.

[82] E. Sawaguchi, Ferroelectricity versus antiferroelectricity in the solid solutions of PbZrO3 and PbTiO3, Journal of the physical society of Japan 8 (1953) 615-629.

[83] M. Shuaib, D. Hall, Influence of atmospheric annealing on the conductivity of Mn-doped PZT ceramics, Key Engineering Materials, Trans Tech Publ, 2010, pp. 415-421.

[84] B. Jaffe, R. Roth, S. Marzullo, Properties of piezoelectric ceramics in the solid-solution series lead titanate-lead zirconate-lead oxide: tin oxide and lead titanate-lead hafnate, Journal of research of the National Bureau of Standards 55 (1955) 239-254.

[85] P.G. Lucuta, F. Constantinescu, D. Barb, Structural dependence on sintering temperature of lead zirconate-titanate solid solutions, Journal of the American Ceramic Society 68 (1985) 533-537.

[86] W. Cao, L.E. Cross, Theoretical model for the morphotropic phase boundary in lead zirconate–lead titanate solid solution, Physical Review B 47 (1993) 4825.

[87] A.S. Bhalla, R. Guo, E.F. Alberta, Some comments on the morphotropic phase boundary and property diagrams in ferroelectric relaxor systems, Materials Letters 54 (2002) 264-268.

[88] V. Isupov, Phases in the PZT ceramics, Ferroelectrics 266 (2002) 91-102.

[89] H. Jaffe, Piezoelectric ceramics, Journal of the American Ceramic Society 41 (1958) 494-498.

[90] D. Berlincourt, Piezoelectric ceramic compositional development, The Journal of the Acoustical Society of America 91 (1992) 3034-3040.

[91] B. Sahoo, P.K. Panda, Effect of lanthanum, neodymium on piezoelectric, dielectric and ferroelectric properties of PZT, Journal of Advanced Ceramics 2 (2013) 37-41.

[92] L. Wu, S. Kim, C. Moriyoshi, Y. Kuroiwa, M. Suzuki, K. Shinoda, R. Aoyagi, J. Akedo, Synthesis of Pb (Zr, Ti) O3 fine ceramic powder at room temperature by dry mechanochemical solid-state reaction evaluated using synchrotron radiation X-ray diffraction, Japanese Journal of Applied Physics 60 (2021) SFFA02.

[93] D. Wang, S. Rocks, R. Dorey, Electrohydrodynamic atomization deposition of PZT sol–gel slurry and sol infiltration on the films, Journal of the European Ceramic Society 32 (2012) 1651-1658.

[94] Y. Deng, L. Liu, Y. Cheng, C.-W. Nan, S.-j. Zhao, Hydrothermal synthesis and characterization of nanocrystalline PZT powders, Materials Letters 57 (2003) 1675-1678.

[95] B.D. Cullity, S.R. Stock, Elements of X-ray Diffraction, Prentice Hall2001.

[96] C.N.R. Rao, J. Gopalakrishnan, New directions in solid state chemistry, Cambridge University Press1997.

[97] R.A. Bapat, H.J. Yang, T.V. Chaubal, S. Dharmadhikari, A.M. Abdulla, S. Arora, S. Rawal, P. Kesharwani, Review on synthesis, properties and multifarious therapeutic applications of nanostructured zirconia in dentistry, RSC advances 12 (2022) 12773-12793.

[98] A.D. Racovita, Titanium Dioxide: Structure, Impact, and Toxicity, International Journal of Environmental Research and Public Health 19 (2022) 5681. https://doi.org/10.3390/ijerph19095681. https://dx.doi.org/10.3390/ijerph19095681.

[99] N. Vargas-Martínez, Á.d.J. Ruíz-Baltazar, N.A. Medellín-Castillo, S.Y. Reyes-López, Synthesis of α-alumina nano-onions by thermal decomposition of aluminum formate, Journal of Nanomaterials 2018 (2018).

[100] D.R. Lide, CRC handbook of chemistry and physics, CRC press2004.

[101] N.C.f.B. Information, Barium Carbonate, PubChem Compound Summary for CID 10563, 2023.

[102] S.F.Z. Chegar Nadjah, Effet De La Substitution Du Plomb Par Le Baryum Sur La Structure Pérovskite Des Solutions Solide : Pb1-x Bax (zr0.52 Ti0.43 Al0.025 Sb0.025) O3, Université Mohamed Khider - Biskra, Université Mohamed Khider, Biskra, Algeria, 2021.

[103] F. Kahoul, L. Hamzioui, A. Guemache, M. Aillerie, A. Boutarfaia, Study of Dielectric and Piezoelectric Properties of (1-x) PZT-xSFN Ceramics Prepared by Conventional Solid State Reaction Method, Journal of the Chemical Society of Pakistan 42 (2020).

[104] D. Bernache-Assollant, J.-P. Bonnet, Frittage: aspects physico-chimiques Partie 2: frittage en phase liquide, Techniques de l'ingénieur. Sciences fondamentales (2005) AF6621. 6621-AF6621. 6614.

[105] A. Kumar, V. Pal, S. Mishra, Preparation, microstructure, dielectric and electrical analysis of Fe-modified PZT piezoceramics, J. Mater. Sci. - Mater. Electron. 32 (2021) 2946-2952. https://doi.org/https://doi.org/10.1007/s10854-020-05046-3.

[106] B. Cullity, S. Stock, Elements of X-ray Diffraction, 3rd edn Prentice Hall, New York (2001) 174-177.

[107] W.L. Bragg, The structure of some crystals as indicated by their diffraction of X-rays, Proceedings of the Royal Society of London. Series A, Containing papers of a mathematical and physical character 89 (1913) 248-277.

[108] A.A. Bunaciu, E.G. UdriŞTioiu, H.Y. Aboul-Enein, X-ray diffraction: instrumentation and applications, Critical reviews in analytical chemistry 45 (2015) 289-299.

[109] J.I. Goldstein, D.E. Newbury, J.R. Michael, N.W. Ritchie, J.H.J. Scott, D.C. Joy, Scanning electron microscopy and X-ray microanalysis, Springer2017.

[110] L. Reimer, Scanning electron microscopy: physics of image formation and microanalysis, Measurement Science and Technology 11 (2000) 1826-1826.

[111] B.A. CARTER, D.B. Williams, C.B. Carter, D.B. Williams, Transmission electron microscopy: a textbook for materials science. Diffraction. II, Springer Science & Business Media1996.

[112] C.M. Simonescu, Application of FTIR spectroscopy in environmental studies, Advanced aspects of spectroscopy 29 (2012) 77-86.

[113] J.R. Ferraro, L.J. Basile, Fourier transform infrared spectra: applications to chemical systems, Academic press2012.

[114] A. Dutta, Fourier transform infrared spectroscopy, Spectroscopic methods for nanomaterials characterization (2017) 73-93.

[115] E.A. Neppiras, Piezoelectric ceramics 1971: B. Jaffe, W. R. Cook Jr and H. Jaffe. London and New York: Academic Press. 317 pp., £5.50, 1972.

[116] B.P. Kumar, H. Kumar, D. Kharat, Effect of porosity on dielectric properties and microstructure of porous PZT ceramics, Materials Science and Engineering: B 127 (2006) 130-133.

[117] F. Kremer, A. Schönhals, Broadband dielectric spectroscopy, Springer Science & Business Media2002.

[118] E. Barsoukov, J.R. Macdonald, Impedance spectroscopy theory, experiment, and, Applications, 2nd ed.(Hoboken, NJ: John Wiley &Sons, Inc., 2005) (2005).

[119] R. Ranjan, R. Kumar, R. Choudhary, Effect of Sm substitution on structural, dielectric, and transport properties of PZT ceramics, Phys. Res. Int. 2009 (2009). https://doi.org/https://doi:10.1155/2009/382578.

[120] M. Ahart, M. Somayazulu, R. Cohen, P. Ganesh, P. Dera, H.-k. Mao, R.J. Hemley, Y. Ren, P. Liermann, Z. Wu, Origin of morphotropic phase boundaries in ferroelectrics, Nature 451 (2008) 545-548.

[121] H. Chen, J. Long, Z. Meng, Effect of Zr/Ti ratio on the properties of PMMN–PZT ceramics near the morphotropic phase boundary, Materials Science and Engineering: B 99 (2003) 433-436.

[122] K.A. Schönau, L.A. Schmitt, M. Knapp, H. Fuess, R.-A. Eichel, H. Kungl, M.J. Hoffmann, Nanodomain structure of Pb [Zr 1− x Ti x] O 3 at its morphotropic phase boundary: Investigations from local to average structure, Physical Review B 75 (2007) 184117.

[123] X. Huang, J. Zeng, X. Ruan, L. Zheng, G. Li, Structure, electrical, and thermal expansion properties of PZ nTe–PZT ternary system piezoelectric ceramics, J. Am. Ceram. Soc. 101 (2018) 274-282. https://doi.org/https://doi.org/10.1111/jace.15179.

[124] Y. Luo, T. Pu, S. Fan, H. Liu, J. Zhu, Enhanced piezoelectric properties in low-temperature sintering PZN-PZT ceramics by adjusting Zr/Ti ratio, J. Adv. Dielectr 12 (2022) 2250001. https://doi.org/https://dx.doi.org/10.1142/S2010135X22500011.

[125] C.-C. Tsai, S.-Y. Chu, J.-S. Jiang, C.-S. Hong, Y.-F. Chiu, The phase structure, electrical properties, and correlated characterizations of (Mn, Sb) co-tuned PZMnNS–PZT ceramics with relaxation behavior near the morphotropic phase boundary, Ceram. Int. 40 (2014) 11713-11725. https://doi.org/https://doi.org/10.1016/j.ceramint.2014.03.185.

[126] Z. Xia, Q. Li, Phase transformation in (0.90− x) Pb (Mg1/3Nb2/3) O3–xPbTiO3–0.10 PbZrO3 piezoelectric ceramic: X-ray diffraction and Raman investigation, Solid State Commun. 142 (2007) 323-328. https://doi.org/https://doi.org/10.1016/j.ssc.2007.03.004.

[127] Z. Gao, H. Ning, C. Chen, R. Wilson, B. Shi, H. Ye, H. Yan, M.J. Reece, The effect of barium substitution on the ferroelectric properties of Sr 2 Nb 2 O 7 ceramics, Journal of the American Ceramic Society 96 (2013) 1163-1170.

[128] M.S. Silva, G.F. Teixeira, G.F. Cavenago, L.L. da Silva, R.G. Dias, M.A. Zaghete, M. Cilense, E. Longo, A.A. Cavalheiro, Effects of The Addition of Ions Barium on The Structural and Electrical Properties of PZT Ceramic, Materials Science Forum, Trans Tech Publ, 2014, pp. 199-204.

[129] K.M. Batoo, R. Verma, A. Chauhan, R. Kumar, M. Hadi, O.M. Aldossary, Y. Al-Douri, Improved room temperature dielectric properties of Gd3+ and Nb5+ co-doped Barium Titanate ceramics, J. Alloys Compd. 883 (2021) 160836. https://doi.org/https://doi.org/10.1016/j.jallcom.2021.160836.

[130] M. Anupama, B. Rudraswamy, N. Dhananjaya, Investigation on impedance response and dielectric relaxation of Ni-Zn ferrites prepared by self-combustion technique, J. Alloys Compd. 706 (2017) 554-561. https://doi.org/https://doi.org/10.1016/j.jallcom.2017.02.241.

[131] A. Sharma, K.M. Batoo, O.M. Aldossary, S. Jindal, N. Aggarwal, G. Kumar, Investigation of dielectric, electrical and optical properties of copper substituted Mn-Zn nanoferrites, J. Mater. Sci. - Mater. Electron. 32 (2021) 313-322. https://doi.org/https://doi.org/10.1007/s10854-020-04782-w.

[132] P. Kour, P. Kumar, S. Sinha, M. Kar, Electrical properties of calcium modified PZT (52/48) ceramics, Solid State Commun. 190 (2014) 33-39. https://doi.org/https://doi.org/10.1016/j.ssc.2014.03.025.

[133] Q. Peng, W. Jin-Feng, M. Bao-Quan, W. Chun-Ming, L. Xing-Hua, Phase transition and high piezoactivity of Sb doped (Na0. 53K0. 435Li0. 035) Nb0. 94Ta0. 06O3 lead-free ceramics, Chin. Phys. Lett 24 (2007) 3535. https://doi.org/https://doi.org/10.1088/0256-307X/24/12/067.

[134] T.-F. Cao, J.-Q. Dai, X.-W. Wang, Physical properties of Al doped BiFeO3 obtained by sol-gel route and two-step sintering process, Ceram. Int. 46 (2020) 7954-7960. https://doi.org/https://doi.org/10.1016/j.ceramint.2019.12.016.

[135] A. Meklid, S.E. Hachani, Z. Necira, H. Menasra, M. Abba, A. Boutarfaia, Phase structure, microstructure and electrical properties of PCNS–PZ–PT ternary ceramics near the morphotropic phase boundary, Appl. Phys. A 126 (2020) 1-7. https://doi.org/https://doi.org/10.1007/s00339-019-3209-1.

[136] W.-C. Lee, C.-Y. Huang, L.-K. Tsao, Y.-C. Wu, Chemical composition and tolerance factor at the morphotropic phase boundary in (Bi0. 5Na0. 5) TiO3-based piezoelectric ceramics, J. Eur. Ceram. Soc. 29 (2009) 1443-1448. https://doi.org/https://doi.org/10.1016/j.jeurceramsoc.2008.08.028.

[137] C. Perry, B. Khanna, G. Rupprecht, Infrared studies of perovskite titanates, Phys. Rev. 135 (1964) A408. https://doi.org/https://doi.org/10.1103/PhysRev.135.A408.

[138] S. Revathi, L.J. Kennedy, S. Basha, R. Padmanabhan, Synthesis, structural, optical and dielectric properties of nanostructured 0–3 PZT/PVDF composite films, J. Nanosci. Nanotechnol 18 (2018) 4953-4962. https://doi.org/https://doi.org/10.1166/jnn.2018.15336.

[139] P.K. Panda, B. Sahoo, V. Sureshkumar, E.D. Politova, Effect of Zr 4+ on piezoelectric, dielectric and ferroelectric properties of barium calcium titanate lead-free ceramics, Journal of Advanced Dielectrics 11 (2021) 2150024.

[140] P. Kour, S. Pradhan, P. Kumar, S. Sinha, M. Kar, Study of ferroelectric and piezoelectric properties on Ca doped PZT ceramics, Mater. Today: Proc 4 (2017) 5727-5733. https://doi.org/https://doi.org/10.1016/j.matpr.2017.06.037.

[141] G. Pecchi, C. Campos, O. Peña, L.E. Cadus, Structural, magnetic and catalytic properties of perovskite-type mixed oxides LaMn1− yCoyO3 (y= 0.0, 0.1, 0.3, 0.5, 0.7, 0.9, 1.0), J. Mol. Catal. A: Chem. 282 (2008) 158-166. https://doi.org/https://doi.org/10.1016/j.molcata.2007.12.022.

[142] D. Sun, X. Jin, H. Liu, J. Zhu, Y. Zhu, Y. Zhu, Investigation on FTIR spectrum of barium titanate ceramics doped with alkali ions, Ferroelectrics 355 (2007) 145-148. https://doi.org/https://doi.org/10.1080/00150190701517630.

[143] A. Mirzaei, M. Bonyani, S. Torkian, Effect of Nb doping on sintering and dielectric properties of PZT ceramics, Process. Appl. Ceram 10 (2016) 175-182. https://doi.org/https://doi.org/10.2298/PAC1603175M.

[144] B. Kalisky, E.M. Spanton, H. Noad, J.R. Kirtley, K.C. Nowack, C. Bell, H.K. Sato, M. Hosoda, Y. Xie, Y. Hikita, Locally enhanced conductivity due to the tetragonal domain structure in LaAlO3/SrTiO3 heterointerfaces, Nature materials 12 (2013) 1091-1095.

[145] N. Zidi, A. Chaouchi, M. Rguiti, Y. Lorgouilloux, C. Courtois, Study of structural, impedance spectroscopy and dielectric properties of Li and Al co-doped Ba0. 85Ca0. 15Ti0. 9Zr0. 1O3 ceramics, J. Mater. Sci. - Mater. Electron. (2022) 1-20. https://doi.org/https://doi.org/10.1007/s10854-022-08369-5.

[146] C. Oliveira, E. Longo, J.A. Varela, M. Zaghete, Synthesis and characterization of lead zirconate titanate (PZT) obtained by two chemical methods, Ceramics International 40 (2014) 1717-1722.

[147] N. Sahu, S. Panigrahi, M. Kar, Structural investigation and dielectric studies on Mn substituted Pb (Zr0. 65Ti0. 35) O3 perovskite ceramics, Ceram. Int. 38 (2012) 1549-1556. https://doi.org/https://doi.org/10.1016/j.ceramint.2011.09.040.

[148] D. Mahato, R. Chaudhary, S. Srivastava, Dielectric behaviour of spray dried Pb sub (0. 98)(La sub (1-x/3) Na sub (x)) sub (0. 02)(Zr sub (0. 53) Ti sub (0). 47) sub (0. 9950) O sub (3) system, J. Mater. Sci. 40 (2005) 381-386. https://doi.org/https://doi.org/10.1007/s10853-005-6094-2.

[149] M. Arshad, H. Du, M.S. Javed, A. Maqsood, I. Ashraf, S. Hussain, W. Ma, H. Ran, Fabrication, structure, and frequency-dependent electrical and dielectric properties of Sr-doped BaTiO3 ceramics, Ceram. Int. 46 (2020) 2238-2246. https://doi.org/https://doi.org/10.1016/j.ceramint.2019.09.208.

[150] P. Singh, S. Singh, J. Juneja, C. Prakash, Effect of Samarium substitution on dielectric properties of (Pb)(Zr, Ti, Fe, Nb) O3 type ceramic system, Ceram. Int. 35 (2009) 3335-3338. https://doi.org/https://doi.org/10.1016/j.ceramint.2009.05.036.

[151] Y. Xu, Ferroelectric materials and their applications, Elsevier2013.

[152] F. Kahoul, L. Hamzioui, A. Guemache, M. Aillerie, A. Boutarfaia, Phase structure, microstructure, and dielectric properties of (1–x) Pb (Zr0. 50 Ti0. 50) O3–x Ba (W2/3 Mn1/3) O3 ceramics, Ferroelectrics 572 (2021) 229-237. https://doi.org/https://doi.org/10.1080/00150193.2020.1868885.

[153] O. Thakur, C. Prakash, Dielectric properties of samarium substituted barium strontium titanate, Ph. Transit. 76 (2003) 567-574. https://doi.org/https://doi.org/10.1080/01411590290030708.

[154] K. Ramam, V. Miguel, Microstructure, dielectric and ferroelectric characterization of Ba doped PLZT ceramics, EPJ Appl. Phys. 35 (2006) 43-47. https://doi.org/https://doi.org/10.1051/epjap:2006065.

[155] C. Shi, J. Ma, J. Wu, X. Wang, F. Miao, Y. Huang, K. Chen, W. Wu, B. Wu, Coexistence of excellent piezoelectric performance and high Curie temperature in KNN-based lead-free piezoelectric ceramics, Journal of Alloys and Compounds 846 (2020) 156245.

[156] X. Wang, P. Liang, X. Chao, Z. Yang, Dielectric properties and impedance spectroscopy of MnCO3-modified (Ba0. 85Ca0. 15)(Zr0. 1Ti0. 9) O3 lead-free ceramics, Journal of the American Ceramic Society 98 (2015) 1506-1514.

[157] P. Das, P. Chakraborty, B. Behera, R. Choudhary, Electrical properties of Li2BiV5O15 ceramics, Physica B: Condensed Matter 395 (2007) 98-103.

[158] S. Pradhan, S. Das, S. Bhuyan, C. Behera, R. Padhee, R. Choudhary, Structural, dielectric and impedance characteristics of lanthanum-modified BiFeO 3–PbTiO 3 electronic system, Applied Physics A 122 (2016) 1-9.

[159] Z. Zeng, Q. Wu, M. Hao, W. Lu, G. Fan, M. Yuchi, M. Ding, Impedance spectroscopy and piezoelectric property of LiF-doped PZN–PZT low-temperature sintering piezoelectric ceramics, Journal of Materials Science: Materials in Electronics 29 (2018) 8279-8286.

[160] A. Kumari, S. Sanghi, A. Agarwal, O. Singh, Investigation of crystal structure, dielectric properties, impedance spectroscopy and magnetic properties of (1-x) BaTiO3–(x) Ba0. 9Ca0. 1 Fe12O19 multiferroic composites, Ceramics International 47 (2021) 23088-23100.

[161] P.-Y. Chen, C.-C. Chou, T.-Y. Tseng, H. Chen, Correlation of microstructures and conductivities of ferroelectric ceramics using complex impedance spectroscopy, Japanese Journal of Applied Physics 49 (2010) 061505.

[162] S. Panigrahi, P.R. Das, R. Padhee, Electrical properties of Gd-modified PZT (MPB) ceramics, Pramana 95 (2021) 70.

[163] K.R. Rao, M. Ramesh, M.C. Varma, Raman, impedance spectroscopy and ferroelectric studies of Sn4+ doped PbZr0. 52Ti0. 48O3 ceramics, Ferroelectrics 583 (2021) 51-66.

[164] O.S. Aleksić, P.M. Nikolić, Recent advances in NTC thick film thermistor properties and applications, Facta universitatis-series: Electronics and Energetics 30 (2017) 267-284.

[165] A. Feteira, Negative temperature coefficient resistance (NTCR) ceramic thermistors: an industrial perspective, Journal of the American Ceramic Society 92 (2009) 967-983.

[166] J. Suchanicz, The low-frequency dielectric relaxation Na0. 5Bi0. 5TiO3 ceramics, Materials Science and Engineering: B 55 (1998) 114-118.

[167] P. Sharma, S. Hajra, S. Sahoo, P.K. Rout, R.N.P. Choudhary, Structural and electrical characteristics of gallium modified PZT ceramics, Processing and Application of Ceramics 11 (2017) 171-176.

[168] N. Prasad, J. Subrahmanyam, P. Narayana Murty, S. Karmakar, S. Gupta, Impedance measurements on PZT and La 0.75 Bi 3.25 Ti 3 O 12 ceramics, International Journal of Modern Physics B 23 (2009) 3881-3893.

[169] C. Stenger, A. Burggraaf, Study of phase transitions and properties of tetragonal (Pb, La)(Zr, Ti) O3 ceramics—II: Diffuse phase transitions and thermodynamics, Journal of physics and chemistry of solids 41 (1980) 25-30.

[170] M. Afifi, M. El-Nahass, A. Bekheet, I. Zedan, Dc and ac electrical conductivity of bulk CdSexTe1− x (0⩽ x⩽ 0.4), Physica B: Condensed Matter 400 (2007) 248-251.

[171] N. Hegab, M. Afifi, H. Atyia, A. Farid, ac conductivity and dielectric properties of amorphous Se80Te20− xGex chalcogenide glass film compositions, Journal of Alloys and Compounds 477 (2009) 925-930.

[172] N. Hegab, H. El-Mallah, AC Conductivity and Dielectric Properties of Amorphous Te_42As_36Ge_10Si_12 Glass, Acta Physica Polonica A 116 (2009) 1048-1052.

[173] S.-H. Kim, J.-H. Koh, Dielectric properties and AC conduction of 5 wt% ZnBO doped (Ba, Sr) TiO3 ceramics for low temperature Co-fired ceramics applications, Japanese Journal of Applied Physics 48 (2009) 041407.

[174] J. Owen, 21-Ionic Conductivity, Comprehensive Polymer Science and Supplements, Pergamon, Amsterdam (1989) 669-686.

[175] B.A. Boukamp, M.T. Pham, D.H. Blank, H.J. Bouwmeester, Ionic and electronic conductivity in lead–zirconate–titanate (PZT), Solid State Ionics 170 (2004) 239-254.

[176] J. Daniels, H. Kh, ELECTRICAL CONDUCTIVITY AT HIGH TEMPERATURES OF DONOR-DOPED BARIUM TITANATE CERAMICS. I, (1976).

[177] P. Nayak, S. Mohapatra, P. Kumar, S. Panigrahi, Effect of Ba2+ substitution on the structural and electrical properties of SrBi4Ti4O15 ceramic, Ceramics International 41 (2015) 9361-9372.

[178] M. Rawat, K. L Yadav, A. Kumar, P. Kumar Patel, N. Adhlakha, J. Rani, Structural, dielectric and conductivity properties of Ba2+ doped (Bi0. 5Na0. 5) TiO3 ceramic, Advanced Materials Letters 3 (2012) 286-292.

Annexes

Dielectric constant (εr) of $Pb_{1-x}Ba_x(Zr_{0.52}Ti_{0.43}(Al_{0.5}Sb_{0.5})_{0.05})O_3$ were x = 0.00

	1 kHz	2 kHz	4 kHz	6 kHz	8 kHz	10 kHz
300	2218,5	2196,06	2157,3	2138,94	2124,66	2113,44
320	2290,92	2293,98	2278,68	2262,36	2250,12	2241,96
340	2409,24	2423,52	2403,12	2388,84	2379,66	2367,42
360	2503,08	2518,38	2514,3	2503,08	2492,88	2483,7
380	2621,4	2605,08	2593,86	2591,82	2588,76	2583,66
400	2817,24	2791,74	2786,64	2782,56	2777,46	2770,32
420	3011,04	2985,54	2967,18	2962,08	2956,98	2949,84
440	3209,94	3172,2	3150,78	3141,6	3134,46	3126,3
460	3491,46	3450,66	3410,88	3396,6	3388,44	3379,26
480	3729,12	3689,34	3649,56	3634,26	3625,08	3618,96
500	4100,4	4055,52	4001,46	3982,08	3966,78	3957,6
520	4455,36	4390,08	4323,78	4291,14	4267,68	4249,32
540	4954,14	4874,58	4790,94	4753,2	4725,66	4703,22
560	5757,9	5672,22	5587,56	5545,74	5517,18	5495,76
580	6385,2	6273	6172,02	6127,14	6092,46	6066,96
600	9437,04	9131,04	8902,56	8813,82	8754,66	8709,78
620	13617	13035,6	12597	12444	12321,6	12250,2
640	30181,8	28152	26622	26010	25591,8	25296
660	32497,2	30906	29549,4	28957,8	28539,6	28233,6
680	20716,2	19839	19176	18910,8	18727,2	18584,4
700	14647,2	13606,8	12892,8	12648	12495	12393

Dielectric constant (εr) of $Pb_{1-x}Ba_x(Zr_{0.52}Ti_{0.43}(Al_{0.5}Sb_{0.5})_{0.05})O_3$ were x = 0.02

	1 kHz	2 kHz	4 kHz	6 kHz	8 kHz	10 kHz
300	2264,46	2227,96	2178,32	2159,34	2130,14	2121,38
320	2057,14	2026,48	1984,14	1963,7	1949,1	1935,96
340	2235,26	2203,14	2157,88	2135,98	2118,46	2105,32
360	2477,62	2445,5	2398,78	2373,96	2354,98	2340,38
380	2683,48	2639,68	2591,5	2568,14	2547,7	2533,1
400	2976,94	2922,92	2876,2	2849,92	2828,02	2811,96
420	3314,2	3254,34	3198,86	3168,2	3146,3	3127,32
440	3687,96	3619,34	3555,1	3524,44	3501,08	3482,1
460	4223,78	4144,94	4063,18	4023,76	3996,02	3974,12
480	4839,9	4743,54	4644,26	4597,54	4563,96	4537,68
500	5752,4	5638,52	5511,5	5450,18	5402	5365,5
520	6986,1	6831,34	6670,74	6602,12	6555,4	6521,82
540	8631,52	8427,12	8227,1	8139,5	8082,56	8041,68
560	10339,72	10123,64	9938,22	9855	9798,06	9755,72
580	14746	14289,02	13957,6	13848,1	13753,2	13671,44
600	24820	23593,6	22703	22352,6	22119	21943,8
620	26630,4	25214,2	24119,2	23725	23462,2	23272,4
640	21943,8	21170	20396,2	20016,6	19768,4	19578,6
660	15359,2	15038	14687,6	14493,42	14321,14	14210,18
680	10951,46	10766,04	10612,74	10549,96	10493,02	10446,3
700	8135,12	7951,16	7811	7758,44	7720,48	7689,82

Dielectric constant (εr) of $Pb_{1-x}Ba_x(Zr_{0.52}Ti_{0.43}(Al_{0.5}Sb_{0.5})_{0.05})O_3$ were x = 0.04

	1 kHz	2 kHz	4 kHz	6 kHz	8 kHz	10 kHz
300	2556,68	2519,65	2455,25	2431,1	2405,34	2387,63
320	2695,14	2643,62	2580,83	2555,07	2532,53	2514,82
340	2917,32	2854,53	2806,23	2774,03	2749,88	2728,95
360	3133,06	3100,86	3039,68	3007,48	2981,72	2960,79
380	3427,69	3397,1	3332,7	3298,89	3273,13	3252,2
400	3756,13	3704,61	3649,87	3616,06	3588,69	3566,15
420	4184,39	4116,77	4049,15	4015,34	3987,97	3965,43
440	4762,38	4673,83	4585,28	4546,64	4516,05	4488,68
460	5440,19	5324,27	5229,28	5184,2	5148,78	5121,41
480	6407,8	6269,34	6129,27	6068,09	6023,01	5989,2
500	7521,92	7401,17	7422,1	7172,55	7261,1	7092,05
520	9300,97	9073,96	8816,36	8700,44	8615,11	8553,93
540	12240,83	11896,29	11585,56	11458,37	11368,21	11305,42
560	18804,8	18257,4	17758,3	17532,9	17388	17275,3
580	28287,7	27160,7	26243	25888,8	25647,3	25454,1
600	28786,8	27595,4	26532,8	26162,5	25888,8	25663,4
620	23393,3	22652,7	21847,7	21525,7	21284,2	21091
640	16228,8	16325,4	16033,99	15634,71	15464,05	15304,66
660	12469,45	12155,5	11886,63	11627,42	11558,19	11439,05
680	8354,29	8431,57	8405,81	8246,42	8227,1	8151,43
700	7546,07	6903,68	6731,41	6671,84	6634,81	6573,63

Dielectric constant (εr) of $Pb_{1-x}Ba_x(Zr_{0.52}Ti_{0.43}(Al_{0.5}Sb_{0.5})_{0.05})O_3$ were x = 0.06

	1 kHz	2 kHz	4 kHz	6 kHz	8 kHz	10 kHz
300	3895	3740,84	3675,24	3588,32	3567	3524,36
320	3986,84	3862,2	3768,72	3706,4	3675,24	3645,72
340	4190,2	4070,48	3954,04	3885,16	3857,28	3827,76
360	4528,04	4446,04	4331,24	4259,08	4234,48	4206,6
380	4934,76	4819,96	4696,96	4634,64	4598,56	4564,12
400	5379,2	5267,68	5126,64	5062,68	5016,76	4985,6
420	5943,36	5803,96	5654,72	5577,64	5543,2	5497,28
440	6650,2	6481,28	6307,44	6215,6	6169,68	6120,48
460	7617,8	7414,44	7232,4	7122,52	7070,04	7017,56
480	9190,56	8828,12	8596,88	8454,2	8378,76	8316,44
500	11225,8	10979,8	10653,44	10445,16	10356,6	10274,6
520	14960,08	14538,6	14056,44	13779,28	13641,52	13493,92
540	23960,4	22992,8	21992,4	21484	21254,4	21041,2
560	33898,8	32750,8	31684,8	31192,8	30963,2	30750
580	31881,6	30946,8	30110,4	29700,4	29520	29356
600	25174	24534,4	23829,2	23501,2	23337,2	23189,6
620	19089,6	18532	17990,8	17695,6	17580,8	17449,6
640	14253,24	13972,8	13564,44	13329,92	13228,24	13111,8
660	11029	10722,32	10438,6	10277,88	10207,36	10131,92
680	8772,36	8544,4	8386,96	8229,52	8163,92	8101,6
700	6597,6	6691,6	6616,8	6869,96	6209,04	6272

Dielectric constant (εr) of $Pb_{1-x}Ba_x(Zr_{0.52}Ti_{0.43}(Al_{0.5}Sb_{0.5})_{0.05})O_3$ were x = 0.08

	1 kHz	2 kHz	4 kHz	6 kHz	8 kHz	10 kHz
300	4406,67	4230,54	4115,97	4052,7	4013,37	3963,78
320	4298,94	4182,66	4102,29	4040,73	4001,4	3968,91
340	4770,9	4697,37	4618,71	4555,44	4516,11	4481,91
360	4719,6	4606,74	4487,04	4423,77	4377,6	4341,69
380	5849,91	5747,31	5586,57	5511,33	5454,9	5407,02
400	6362,91	6255,18	6121,8	6038,01	5988,42	5945,67
420	6672,42	6503,13	6349,23	6267,15	6209,01	6164,55
440	8414,91	8226,81	8021,61	7915,59	7843,77	7785,63
460	9986,4	9705,96	9468,27	9345,15	9263,07	9187,83
480	11604,06	11274,03	10957,68	10798,65	10684,08	10598,58
500	17305,2	16841,79	16262,1	15974,82	15755,94	15588,36
520	22178,7	21460,5	20622,6	20195,1	19870,2	19630,8
540	38799,9	37226,7	35927,1	35397	35037,9	34781,4
560	35260,2	34131,6	33208,2	32832	32558,4	32387,4
580	26761,5	26163	25615,8	25376,4	25239,6	25102,8
600	22315,5	21836,7	21340,8	21152,7	20998,8	20879,1
620	15003,54	14521,32	14146,83	13992,93	13890,33	13801,41
640	11333,88	11229,57	10860,21	10711,44	10602	10528,47
660	9158,76	8926,2	8710,74	8603,01	8512,38	8449,11
680	7777,08	7525,71	7317,09	7217,91	7154,64	7093,08
700	6893,01	6639	6384,76	6130,48	5874,83	5630,93

Dielectric constant (εr) of $Pb_{1-x}Ba_x(Zr_{0.52}Ti_{0.43}(Al_{0.5}Sb_{0.5})_{0.05})O_3$ were x = 0.10

	1 kHz	2 kHz	4 kHz	6 kHz	8 kHz	10 kHz
300	2297,40661	2253,70434	2192,66129	2164,08798	2141,8601	2123,64691
320	2464,59224	2418,8898	2366,16086	2338,15736	2315,72001	2297,55577
340	2633,25301	2590,06891	2540,3109	2512,95254	2490,35458	2472,263
360	2803,88799	2766,49495	2716,5205	2689,76112	2667,08416	2649,09925
380	3039,02535	2957,62225	2946,12392	2919,27937	2896,65312	2878,76106
400	3374,38255	3251,09637	3261,92872	3233,01024	3209,67292	3190,91327
420	3833,69551	3721,05163	3689,53149	3656,65443	3631,36702	3611,47416
440	4456,55748	4281,71557	4258,46448	4216,27725	4185,2978	4161,85816
460	5353,29376	5031,22876	5047,13716	4983,58733	4938,14206	4905,47465
480	6579,78825	6197,73744	6112,27022	6019,22193	5953,64496	5908,21024
500	8020,9209	7726,58639	7391,29711	7270,69264	7188,24362	7130,35272
520	9538,67838	9174,15563	8785,58664	8649,77271	8559,54477	8495,57236
540	10885,31854	10550,78727	10031,06401	9888,8198	9798,99996	9735,17094
560	11704,46838	11488,62083	10769,54458	10626,53549	10539,29532	10479,02265
580	11801,28482	11642,21407	10777,0657	10625,20553	10533,4907	10472,30043
600	10983,76035	10582,12212	9900,44309	9731,8195	9630,11791	9565,33541
620	8995,13426	9023,75083	8013,00124	7848,99234	7745,45488	7682,62195
640	5992,86527	5791,715	5289,24137	5161,11937	5078,04588	5029,55753
660	3530,68108	2417,69611	3122,71652	3046,44344	2995,1077	2966,40813
680	1140,20697	886,75307	1028,20993	1005,56876	987,932	979,6993
700	-1156,61133	-193,34299	-976,79086	-945,19298	-928,19255	-915,87424

AC conductivity of $Pb_{1-x}Ba_x(Zr_{0.52}Ti_{0.43}(Al_{0.5}Sb_{0.5})_{0.05})O_3$ were x = 0.00

1000/T	10 kHz	20 kHz	40 kHz	60 kHz	80 kHz	100 kHz
3,33333	5,71E-05	1,22E-04	1,96E-04	2,58E-04	3,48E-04	4,12E-04
3,125	4,49E-05	7,55E-05	1,63E-04	2,31E-04	3,09E-04	3,78E-04
2,94118	5,06E-05	1,03E-04	1,85E-04	2,65E-04	3,51E-04	4,32E-04
2,77778	5,34E-05	9,78E-05	2,01E-04	2,84E-04	3,78E-04	4,63E-04
2,63158	5,80E-05	1,11E-04	2,22E-04	3,17E-04	4,23E-04	5,31E-04
2,5	6,18E-05	1,03E-04	2,38E-04	3,38E-04	4,52E-04	5,63E-04
2,38095	6,91E-05	1,31E-04	2,67E-04	3,80E-04	5,07E-04	6,34E-04
2,27273	7,33E-05	1,28E-04	2,85E-04	4,02E-04	5,43E-04	6,80E-04
2,17391	8,72E-05	1,50E-04	3,38E-04	4,87E-04	6,45E-04	8,02E-04
2,08333	1,02E-04	1,90E-04	3,69E-04	5,40E-04	6,90E-04	8,70E-04
2	1,37E-04	2,52E-04	4,96E-04	6,97E-04	9,28E-04	0,00113
1,92308	1,38E-04	2,40E-04	4,81E-04	6,85E-04	9,09E-04	0,00113
1,85185	1,72E-04	3,10E-04	5,86E-04	8,24E-04	0,00111	0,00136
1,78571	1,92E-04	3,35E-04	6,58E-04	9,22E-04	0,00123	0,00152
1,72414	3,19E-04	5,21E-04	9,88E-04	0,00142	0,00179	0,0023
1,66667	7,90E-04	0,00115	0,00192	0,00246	0,00331	0,00401
1,6129	8,87E-04	0,00131	0,00214	0,00269	0,00349	0,00403
1,5625	6,81E-04	0,00106	0,00168	0,00205	0,00248	0,00287
1,51515	4,23E-04	7,44E-04	0,00128	0,00169	0,00213	0,00225
1,47059	2,07E-04	4,17E-04	9,05E-04	0,00127	0,00161	0,00206
1,42857	1,51E-04	2,64E-04	5,44E-04	7,93E-04	0,00106	0,00132

AC conductivity of $Pb_{1-x}Ba_x(Zr_{0.52}Ti_{0.43}(Al_{0.5}Sb_{0.5})_{0.05})O_3$ were x = 0.02

1000/T	10 kHz	20 kHz	40 kHz	60 kHz	80 kHz	100 kHz
3,33333	5,71E-05	1,22E-04	1,96E-04	2,58E-04	3,48E-04	4,12E-04
3,125	4,49E-05	7,55E-05	1,63E-04	2,31E-04	3,09E-04	3,78E-04
2,94118	5,06E-05	1,03E-04	1,85E-04	2,65E-04	3,51E-04	4,32E-04
2,77778	5,34E-05	9,78E-05	2,01E-04	2,84E-04	3,78E-04	4,63E-04
2,63158	5,80E-05	1,11E-04	2,22E-04	3,17E-04	4,23E-04	5,31E-04
2,5	6,18E-05	1,03E-04	2,38E-04	3,38E-04	4,52E-04	5,63E-04
2,38095	6,91E-05	1,31E-04	2,67E-04	3,80E-04	5,07E-04	6,34E-04
2,27273	7,33E-05	1,28E-04	2,85E-04	4,02E-04	5,43E-04	6,80E-04
2,17391	8,72E-05	1,50E-04	3,38E-04	4,87E-04	6,45E-04	8,02E-04
2,08333	1,02E-04	1,90E-04	3,69E-04	5,40E-04	6,90E-04	8,70E-04
2	1,37E-04	2,52E-04	4,96E-04	6,97E-04	9,28E-04	0,00113
1,92308	1,38E-04	2,40E-04	4,81E-04	6,85E-04	9,09E-04	0,00113
1,85185	1,72E-04	3,10E-04	5,86E-04	8,24E-04	0,00111	0,00136
1,78571	1,92E-04	3,35E-04	6,58E-04	9,22E-04	0,00123	0,00152
1,72414	3,19E-04	5,21E-04	9,88E-04	0,00142	0,00179	0,0023
1,66667	7,90E-04	0,00115	0,00192	0,00246	0,00331	0,00401
1,6129	8,87E-04	0,00131	0,00214	0,00269	0,00349	0,00403
1,5625	6,81E-04	0,00106	0,00168	0,00205	0,00248	0,00287
1,51515	4,23E-04	7,44E-04	0,00128	0,00169	0,00213	0,00225
1,47059	2,07E-04	4,17E-04	9,05E-04	0,00127	0,00161	0,00206
1,42857	1,51E-04	2,64E-04	5,44E-04	7,93E-04	0,00106	0,00132

AC conductivity of $Pb_{1-x}Ba_x(Zr_{0.52}Ti_{0.43}(Al_{0.5}Sb_{0.5})_{0.05})O_3$ were x = 0.04

1000/T	10 kHz	20 kHz	40 kHz	60 kHz	80 kHz	100 kHz
3,33333	6,67E-05	1,58E-04	2,31E-04	3,18E-04	4,12E-04	4,99E-04
3,125	6,33E-05	1,47E-04	2,21E-04	3,05E-04	3,96E-04	4,83E-04
2,94118	6,80E-05	1,08E-04	2,45E-04	3,39E-04	4,41E-04	5,38E-04
2,77778	7,14E-05	1,51E-04	2,62E-04	3,64E-04	4,77E-04	5,82E-04
2,63158	7,62E-05	1,06E-04	2,89E-04	4,04E-04	5,34E-04	6,51E-04
2,5	8,10E-05	1,15E-04	3,11E-04	4,41E-04	5,88E-04	7,21E-04
2,38095	8,74E-05	1,32E-04	3,40E-04	4,82E-04	6,42E-04	7,93E-04
2,27273	1,01E-04	1,96E-04	3,92E-04	5,54E-04	7,35E-04	9,20E-04
2,17391	1,13E-04	2,20E-04	4,35E-04	6,17E-04	8,20E-04	1,02E-03
2,08333	1,37E-04	2,43E-04	5,09E-04	7,26E-04	9,63E-04	1,18E-03
2	1,18E-04	3,32E-04	6,40E-04	9,02E-04	9,37E-04	0,00147
1,92308	2,33E-04	3,99E-04	7,45E-04	1,03E-03	1,35E-03	0,00166
1,85185	2,69E-04	4,64E-04	8,81E-04	1,24E-03	0,00163	0,00202
1,78571	4,78E-04	8,31E-04	1,60E-03	2,23E-03	0,00297	0,00368
1,72414	7,98E-04	1,27E-03	2,24E-03	0,00299	0,00378	0,00476
1,66667	8,01E-04	0,00125	0,00204	0,00268	0,00342	0,00399
1,6129	6,67E-04	9,71E-04	0,00163	0,00199	0,00245	0,00295
1,5625	5,05E-04	8,04E-04	0,00134	0,00175	0,00211	0,00234
1,51515	3,41E-04	5,81E-04	0,0011	0,00138	0,00174	0,00204
1,47059	2,61E-04	3,60E-04	7,60E-04	0,00106	0,00134	0,00157
1,42857	2,04E-04	3,18E-04	5,71E-04	7,65E-04	9,73E-04	0,00117

AC conductivity of $Pb_{1-x}Ba_x(Zr_{0.52}Ti_{0.43}(Al_{0.5}Sb_{0.5})_{0.05})O_3$ were x = 0.04

1000/T	10 kHz	20 kHz	40 kHz	60 kHz	80 kHz	100 kHz
3,33333	6,67E-05	1,58E-04	2,31E-04	3,18E-04	4,12E-04	4,99E-04
3,125	6,33E-05	1,47E-04	2,21E-04	3,05E-04	3,96E-04	4,83E-04
2,94118	6,80E-05	1,08E-04	2,45E-04	3,39E-04	4,41E-04	5,38E-04
2,77778	7,14E-05	1,51E-04	2,62E-04	3,64E-04	4,77E-04	5,82E-04
2,63158	7,62E-05	1,06E-04	2,89E-04	4,04E-04	5,34E-04	6,51E-04
2,5	8,10E-05	1,15E-04	3,11E-04	4,41E-04	5,88E-04	7,21E-04
2,38095	8,74E-05	1,32E-04	3,40E-04	4,82E-04	6,42E-04	7,93E-04
2,27273	1,01E-04	1,96E-04	3,92E-04	5,54E-04	7,35E-04	9,20E-04
2,17391	1,13E-04	2,20E-04	4,35E-04	6,17E-04	8,20E-04	1,02E-03
2,08333	1,37E-04	2,43E-04	5,09E-04	7,26E-04	9,63E-04	1,18E-03
2	1,18E-04	3,32E-04	6,40E-04	9,02E-04	9,37E-04	0,00147
1,92308	2,33E-04	3,99E-04	7,45E-04	1,03E-03	1,35E-03	0,00166
1,85185	2,69E-04	4,64E-04	8,81E-04	1,24E-03	0,00163	0,00202
1,78571	4,78E-04	8,31E-04	1,60E-03	2,23E-03	0,00297	0,00368
1,72414	7,98E-04	1,27E-03	2,24E-03	0,00299	0,00378	0,00476
1,66667	8,01E-04	0,00125	0,00204	0,00268	0,00342	0,00399
1,6129	6,67E-04	9,71E-04	0,00163	0,00199	0,00245	0,00295
1,5625	5,05E-04	8,04E-04	0,00134	0,00175	0,00211	0,00234
1,51515	3,41E-04	5,81E-04	0,0011	0,00138	0,00174	0,00204
1,47059	2,61E-04	3,60E-04	7,60E-04	0,00106	0,00134	0,00157
1,42857	2,04E-04	3,18E-04	5,71E-04	7,65E-04	9,73E-04	0,00117

AC conductivity of $Pb_{1-x}Ba_x(Zr_{0.52}Ti_{0.43}(Al_{0.5}Sb_{0.5})_{0.05})O_3$ were x = 0.06

1000/T	10 kHz	20 kHz	40 kHz	60 kHz	80 kHz	100 kHz
3,33333	1,31E-04	2,76E-04	4,14E-04	5,60E-04	7,20E-04	8,70E-04
3,125	1,01E-04	2,20E-04	3,20E-04	4,21E-04	5,56E-04	6,62E-04
2,94118	1,09E-04	1,49E-04	3,49E-04	4,74E-04	5,97E-04	7,38E-04
2,77778	1,17E-04	2,09E-04	3,80E-04	5,26E-04	6,81E-04	8,19E-04
2,63158	1,28E-04	2,31E-04	4,24E-04	5,79E-04	7,52E-04	9,31E-04
2,5	1,38E-04	2,38E-04	4,62E-04	6,48E-04	8,42E-04	1,03E-03
2,38095	1,57E-04	2,56E-04	5,20E-04	7,17E-04	9,33E-04	1,15E-03
2,27273	1,81E-04	3,44E-04	6,08E-04	8,44E-04	1,11E-03	1,36E-03
2,17391	2,08E-04	3,49E-04	6,84E-04	9,36E-04	1,23E-03	1,49E-03
2,08333	2,64E-04	4,66E-04	8,48E-04	1,16E-03	1,52E-03	1,86E-03
2	3,46E-04	5,89E-04	1,10E-03	1,50E-03	1,93E-03	0,00235
1,92308	5,09E-04	8,60E-04	1,55E-03	2,08E-03	2,68E-03	0,00324
1,85185	8,85E-04	1,44E-03	2,62E-03	3,58E-03	0,00467	0,00574
1,78571	9,60E-04	1,57E-03	2,90E-03	4,03E-03	0,00533	0,00661
1,72414	7,45E-04	1,17E-03	1,96E-03	0,00259	0,0033	0,00397
1,66667	6,05E-04	9,00E-04	0,00144	0,00185	0,00228	0,00267
1,6129	5,24E-04	7,97E-04	0,0012	0,00151	0,00181	0,00205
1,5625	4,73E-04	7,18E-04	0,00112	0,00137	0,00162	0,00184
1,51515	4,28E-04	6,64E-04	0,00103	0,00129	0,00151	0,00174
1,47059	4,60E-04	5,49E-04	9,59E-04	0,00121	0,00146	0,00168
1,42857	4,85E-04	6,85E-04	9,85E-04	1,16E-03	1,42E-03	0,00162

AC conductivity of $Pb_{1-x}Ba_x(Zr_{0.52}Ti_{0.43}(Al_{0.5}Sb_{0.5})_{0.05})O_3$ were x = 0.08

1000/T	10 kHz	20 kHz	40 kHz	60 kHz	80 kHz	100 kHz
3,33333	1,50E-04	2,49E-04	4,62E-04	6,27E-04	8,15E-04	9,72E-04
3,125	1,17E-04	2,39E-04	3,63E-04	4,93E-04	6,24E-04	7,53E-04
2,94118	1,08E-04	2,39E-04	3,78E-04	5,21E-04	6,76E-04	8,30E-04
2,77778	1,29E-04	2,14E-04	4,31E-04	5,98E-04	7,77E-04	9,49E-04
2,63158	1,49E-04	2,70E-04	5,13E-04	7,07E-04	9,26E-04	1,15E-03
2,5	1,60E-04	2,90E-04	5,83E-04	8,27E-04	1,10E-03	1,38E-03
2,38095	1,76E-04	2,89E-04	6,14E-04	8,61E-04	1,14E-03	1,40E-03
2,27273	2,18E-04	3,81E-04	7,88E-04	1,12E-03	1,49E-03	1,86E-03
2,17391	2,71E-04	5,03E-04	9,88E-04	1,42E-03	1,93E-03	2,46E-03
2,08333	3,46E-04	6,30E-04	1,24E-03	1,77E-03	2,39E-03	3,02E-03
2	5,93E-04	1,05E-03	1,88E-03	2,59E-03	3,37E-03	0,0041
1,92308	9,15E-04	1,59E-03	2,88E-03	3,95E-03	5,12E-03	0,00622
1,85185	1,12E-03	1,87E-03	3,59E-03	5,09E-03	0,00682	0,00859
1,78571	7,75E-04	1,27E-03	2,18E-03	2,96E-03	0,00384	0,00469
1,72414	4,60E-04	7,31E-04	1,23E-03	0,00164	0,00204	0,00244
1,66667	4,05E-04	6,24E-04	0,00105	0,00138	0,0017	0,002
1,6129	3,08E-04	4,79E-04	7,52E-04	9,33E-04	0,00115	0,00131
1,5625	2,75E-04	4,36E-04	6,60E-04	8,08E-04	9,72E-04	0,00108
1,51515	2,37E-04	3,93E-04	6,88E-04	8,55E-04	0,00102	0,00115
1,47059	2,03E-04	3,29E-04	6,06E-04	7,88E-04	9,66E-04	0,0011
1,42857	1,98E-04	3,10E-04	5,28E-04	6,38E-04	8,31E-04	0,00105

AC conductivity of $Pb_{1-x}Ba_x(Zr_{0.52}Ti_{0.43}(Al_{0.5}Sb_{0.5})_{0.05})O_3$ were x = 0.10

1000/T	10 kHz	20 kHz	40 kHz	60 kHz	80 kHz	100 kHz
3,33333	6,06E-05	7,80E-05	2,03E-04	2,76E-04	3,53E-04	4,29E-04
3,125	6,08E-05	1,45E-04	2,08E-04	2,84E-04	3,66E-04	4,41E-04
2,94118	6,25E-05	1,17E-04	2,14E-04	2,95E-04	3,80E-04	4,61E-04
2,77778	6,75E-05	8,42E-05	2,42E-04	3,32E-04	4,32E-04	5,20E-04
2,63158	6,22E-05	1,25E-04	2,39E-04	3,38E-04	4,48E-04	5,49E-04
2,5	6,66E-05	1,41E-04	2,54E-04	3,64E-04	4,84E-04	5,96E-04
2,38095	7,56E-05	1,74E-04	2,83E-04	3,98E-04	5,27E-04	6,46E-04
2,27273	9,85E-05	1,60E-04	3,50E-04	4,91E-04	6,47E-04	7,92E-04
2,17391	9,02E-05	2,05E-04	3,65E-04	5,13E-04	6,85E-04	8,48E-04
2,08333	1,92E-04	3,16E-04	5,76E-04	7,87E-04	1,02E-03	1,23E-03
2	2,76E-04	4,47E-04	7,85E-04	1,06E-03	1,37E-03	0,00167
1,92308	3,17E-04	4,94E-04	8,80E-04	1,20E-03	1,56E-03	0,00188
1,85185	2,63E-04	4,00E-04	7,19E-04	9,74E-04	0,00127	0,00153
1,78571	3,33E-04	4,99E-04	8,31E-04	1,09E-03	0,00138	0,00166
1,72414	3,23E-04	4,16E-04	6,74E-04	8,43E-04	0,00105	0,00119
1,66667	3,10E-04	4,26E-04	6,53E-04	8,10E-04	9,75E-04	0,00117
1,6129	3,06E-04	4,45E-04	6,40E-04	8,02E-04	9,59E-04	9,53E-04
1,5625	2,85E-04	4,71E-04	6,22E-04	7,80E-04	9,28E-04	9,32E-04
1,51515	2,62E-04	4,19E-04	6,01E-04	7,76E-04	8,90E-04	8,93E-04
1,47059	2,18E-04	4,09E-04	5,95E-04	7,66E-04	8,64E-04	8,59E-04
1,42857	2,02E-04	3,81E-04	5,82E-04	7,52E-04	7,96E-04	8,04E-04